MINIMALLY INVASIVE DETECTION OF EOSINOPHILIC ESOPHAGITIS-ASSOCIATED INFLAMMATION

by

Hedieh Saffari

A dissertation submitted to the faculty of
The University of Utah
in partial fulfillment of the requirements for the degree of

Doctor of Philosophy

Department of Chemical Engineering

The University of Utah

December 2013

The University of Utah Graduate School

STATEMENT OF DISSERTATION APPROVAL

The dissertation of **Hedieh Saffari**

has been approved by the following supervisory committee members:

Leonard F. Pease III	, Chair	**10/22/2013** Date Approved
John Mclennan	, Member	**10/22/2013** Date Approved
Swomitra Mohanty	, Member	**10/22/2013** Date Approved
Gerald J. Gleich	, Member	**10/22/2013** Date Approved
Kathryn A. Peterson	, Member	**10/22/2013** Date Approved

and by **Milind Deo** , Chair/Dean of

the Department/College/School of **Chemical Engineering**

and by David B. Kieda, Dean of The Graduate School.

ABSTRACT

Eosinophilic esophagitis (EoE) is an inflammatory disease characterized by infiltration of eosinophils into the esophageal wall. Current diagnosis requires analysis of small biopsy samples, leading to possible misdiagnosis if the tissue is sampled insufficiently. Here we develop a minimally invasive imaging method for the detection and mapping of eosinophil degranulation in EoE. The idea is to have patients swallow a radiolabeled contrast agent specific to eosinophil granule proteins and image the full length of the esophagus with single-photon emission computer tomography (SPECT/CT) imaging.

First, we studied the patchiness of the disease by mapping an esophagectomy sample from a known EoE patient and found a significant variation in eosinophil distribution. Second, we determined and quantified eosinophil degranulation by electron microscopy from 9 randomly selected EoE patients and showed that the majority of eosinophils were associated with the release of intact granules into the epithelium. Third, we developed a radiolabeled contrast agent specific to eosinophil granule proteins. We synthesized Technetium-99m labeled heparin (^{99m}Tc-heparin) and studied the binding of the radiolabeled heparin to *ex vivo* biopsy tissues from patients. To evaluate the organ distribution, the dose assessment of orally administered ^{99m}Tc-heparin was studied in healthy mice. These findings suggest that ^{99m}Tc-heparin can be used as a targeting agent to detect the eosinophils-associated inflammation.

TABLE OF CONTENTS

ACKNOWLEDGEMENTS

This work has been supported by financial supports from a University of Utah TCG grant, TCIP grants from the Utah Governor's Office of Economic Development, the American Partnership for Eosinophilic Disorders (APFED), and NSF CBET (CBET-1125490).

I would like to specifically acknowledge my research team, Leonard F. Pease III, Gerald J. Gleich, Kathryn A. Peterson, and Kristin M. Leiferman, for all of their guidance and support. I am very grateful to my committee members, John McLennan and Swomitra Mohanty for their support and helpful comments. I truly acknowledge the help of Russell Condie, and Laura Hoffman in running the experiments.

I would also like to thank all of our collaborators who were involved or are currently involved in this project. I appreciate the advice and assistance from Peter Jenkins at Department of Radiology, Jeffrey Krstyen and Farand Smith at Intermountain Radiopharmacy, Brian Watson at the Small Animal Imaging Facility, Delynn Strate at Nuclear Medicine, Dr. Anne Kennedy at Department of Clinical Radiology, Dr. Frederic Clayton at Department of Pathology, and Nancy Chandler at the University of Utah Core Facility.

CHAPTER 1

INTRODUCTION

Eosinophilic esophagitis (EoE) is an inflammatory disease affecting over 300,000 patients per year that is caused by the infiltration of eosinophils into the esophagus. EoE has become increasingly prominent over the past two decades [1-6]. This disease, which commonly affects children, adolescents, and young adults as well as senior citizens, presents with difficulty or painful swallowing (dysphagia), food impaction, heartburn, and chest burn [7-9]. Esophagogastroduodenoscopy (EGD) is performed, in which a small probe with a camera at its distal end passes into the esophagus, stomach, and small intestine to visualize the tissue surface of the gastrointestinal organs. EoE also affects the esophageal wall caliber and phenotypic appearance of the esophagus, such as rings or furrows, which can further develop into strictures that close off the esophagus, resulting in dysphagia, food impaction, and emergency hospital visits [10-12].

The criteria for diagnosing EoE in a biopsy specimen is the presence of eosinophils. Normal esophageal tissue does not contain eosinophils. The diagnosis of eosinophilic esophagitis is made by obtaining a medical history evaluating for dysphagia and performing EGD to obtain esophageal biopsies. EGD remains invasive and requires anesthesia with pharmaceutical agents that induce conscious sedation. The

disease affects the esophagus in a spotty manner, such that at least 5, and preferably a greater number of, biopsies should be obtained. Biopsies are examined by a pathologist, and inflammation associated with 15 or greater eosinophils per high power field (hpf, microscopic view equal to 0.23 mm^2) satisfies diagnostic guidelines [6, 13]. Figure 1.1 shows the hematoxylin and eosin stain (H&E stain, a typical staining method in histology) of a patient diagnosed with EoE versus a normal patient (absence of eosinophils). When clinical suspicion for EoE is high, consensus practice requires sampling at 4-5 sites throughout the esophagus [14-16]. However, five 2 mm by 2 mm biopsies represent less than 0.7% of the 20-25 cm long esophageal mucosa and may result in underdiagnosis of EoE if mucosal eosinophilia is particularly patchy [16].

Several studies showed that food allergies are the main culprit of EoE. EoE symptoms can be resolved and the inflammation in the esophagus eventually heals when these allergenic foods are removed from the patient's diet [17]. A variety of allergy tests including blood test for IgE-mediated allergies and skin tests are used to identify underlying food allergies that are associated with EoE [18]. A six food elimination diet, which involves removing the six most common foods, that is milk, egg, soy, wheat, nuts, and fish, is the most common allergy diet used to treat EoE [19]. Also, a common drug therapy to treat EoE is budesonide, a glucocorticoid (i.e., a steroid).

A distinctive characteristic of eosinophils is their granules, which comprise markedly cationic proteins, each of which is composed of a core and a matrix. The core consists primarily of major basic protein 1 (MBP-1); the matrix consists of eosinophil peroxidase (EPO), eosinophil cationic protein (ECP), and eosinophil derived neurotoxin

(EDN) [20-24]. MBP-1 is a highly basic protein with the molecular weight of approximately 14 kDa and isoelectric point approaching 12 [25, 26]. It is a member of the C-type lectin family (lectins bind sugars) and has the highest concentration in the eosinophil granule on a per molecule basis. EPO has the highest concentration in the granule per mass basis [27].

At the molecular level, eosinophils degranulate, releasing intact granules and individual granule proteins into both epithelial and submucosal layers. Evidence of eosinophil degranulation includes expression of membrane markers (such as eotaxin-3, IL-5), formation of vesicles, and changes in the eosinophil granule matrix. In EoE, eosinophil granule proteins including major basic protein (MBP-1), eosinophil derived neurotoxin (EDN) (an RNase2), eosinophil peroxidase (EPO), and eosinophil cationic protein (ECP) (an RNase3) are localized on esophageal epithelial cells [24, 28]. Remarkably, EDN is extensively deposited on the diseased esophagus implying eosinophil activation and release of EDN from its storage site in the granule matrix. Extracellular deposition of MBP-1 is observed during eosinophil degranulation (see Figure 1.2). These eosinophilic granule proteins act as inflammatory mediators and may cause tissue damage.

Secretion of eosinophil granule proteins occurs by eosinophil cytolysis and release of intact granules or by piecemeal degranulation (PMD), a unique secretory process characterized by transport of vesicles to the cell surface [21, 29]. Large vesiculotubular carriers, referred to as sombrero vesicles, because of their resemblance to the well-known Mexican hat, have been identified as playing a key role for moving eosinophil proteins from granules to the plasma membrane for extracellular release [29].

During secretion, the eosinophil sombrero vesicles are actively formed. Figure 1.3a shows a typical normal eosinophil with intact individual granule proteins (dark core and light matrix) with an intact cellular membrane. As eosinophils degranulate, they release their granule protein, from both the core and matrix, into the tissue and piecemeal degranulation occurs as judged by reversal of staining (see Figure 1.3b).

Currently, as symptoms are unable to predict the severity of eosinophilic involvement, the only way to adequately monitor the severity of the disease is through EGD and obtaining biopsy samples, which is invasive. Patients may often need to have several upper endoscopies per year for food re-introduction and therapeutic evaluations [30]. Some patients may become noncompliant because of the cost and discomfort due to the method of monitoring. Additionally, there is a lack of sensitivity of biopsies in detecting and understanding such a patchy disease because histologically biopsy samples only characterize a small portion of the entire esophagus [16].

Despite the rapidly growing incidence of EoE, state-of-the-art diagnostic techniques remain inadequate to fully characterize this disease. As such, there is a need to develop a precise and comprehensive technique to image and map the distribution of eosinophils and deposition of eosinophil granule proteins. Such techniques will provide a tool to diagnose EoE and detect the eosinophil's associated inflammation, track disease activity in response to various treatment regimens, and obtain previously unreachable insight into disease pathophysiology.

The overall objective of this research study is to develop a minimally invasive technique to diagnose EoE and detect eosinophil-associated inflammation. The infiltration of eosinophils and deposition of the eosinophil's cationic proteins into the

esophageal wall often leads to esophageal inflammation in EoE patients (including increase in pain, loss of function, and swelling of esophagus, which are classic signs of acute inflammation). In addition to release of eosinophil-associated products, other markers of inflammation include the changes in extracellular spaces, and phenotypic features of esophageal tissue. By eosinophil-associated inflammation, here we refer specifically to distinct eosinophils markers such as major basic protein, leading to possibility of inflammatory processes in diseased esophagi. Therefore, in this dissertation, we mainly focused on minimally invasive detection of the eosinophil's granule protein degranulation, as part of the eosinophil's associated inflammation.

Current diagnostic methods are invasive, costly, and limited by the number of biopsies, leading to possible underdiagnosis of the disease. In this research study, with the help of radiology imaging techniques, such as single-photon emission computed tomography (SPECT), we hypothesize that eosinophil-rich tissue can be distinguished from eosinophil-free tissue using ^{99m}Tc-heparin. To enable our goal, we will synthesize the radiolabeled conjugate, test the binding on human biopsy tissue, and determine radiological safety in animals. If successful, we can monitor the severity of degranulation in diseased esophagi by having the patient swallow a radiolabeled conjugate specific to eosinophil's granule proteins. This project takes advantage of this possibility by developing a novel way to image EoE on a molecular level, which could potentially provide less invasive diagnostic tools to gain insight into the disease's inflammation.

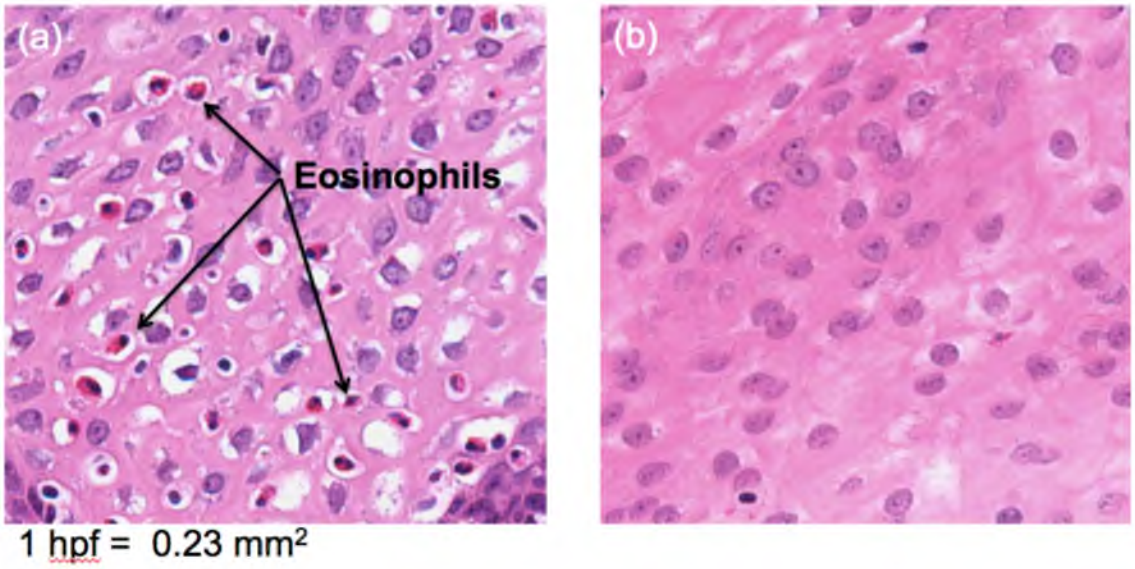

Figure 1.1. Light microscopy images after H&E staining. (a) EoE tissue (presence of numerous eosinophils greater than 15 per hpf in peak areas). (b) Normal tissue (no evidence of eosinophils) [16].

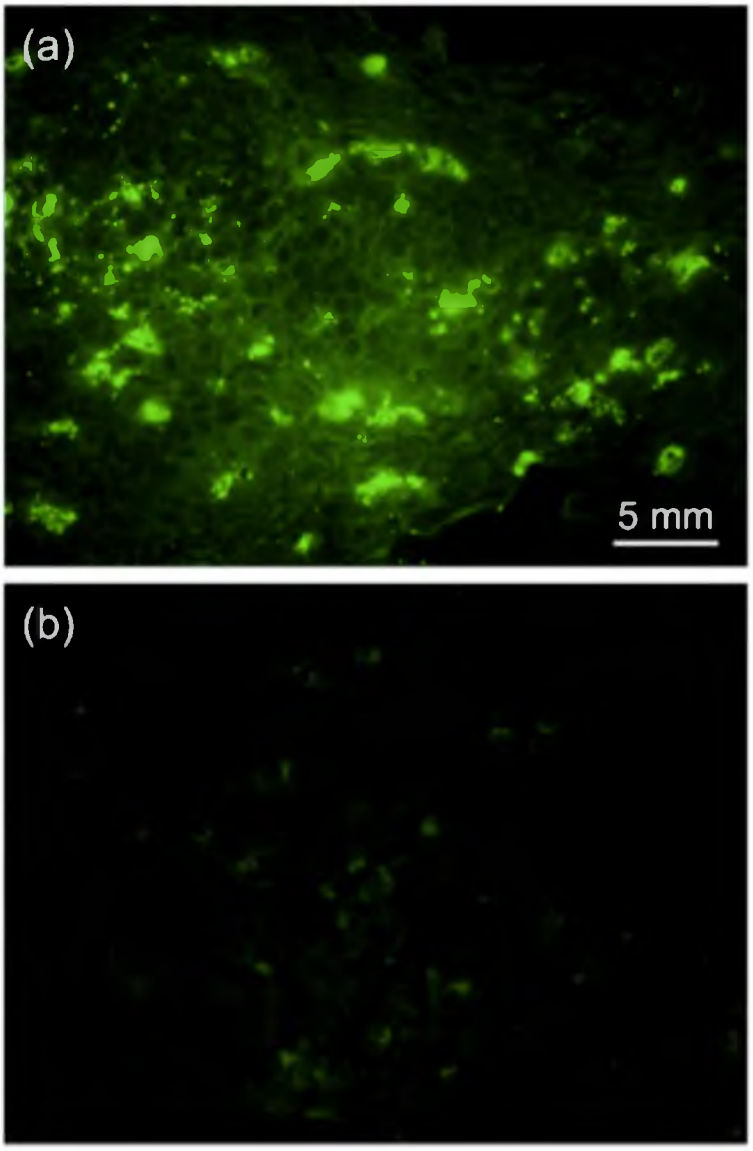

Figure 1.2. Fluorescently stained (a) EoE tissue and (b) control using antibodies to MBP-1 indicating that this granule protein is released in the disease state. Images courtesy of Dr. Kirstin Leiferman, Immunodermatology Lab at the University of Utah Hospital.

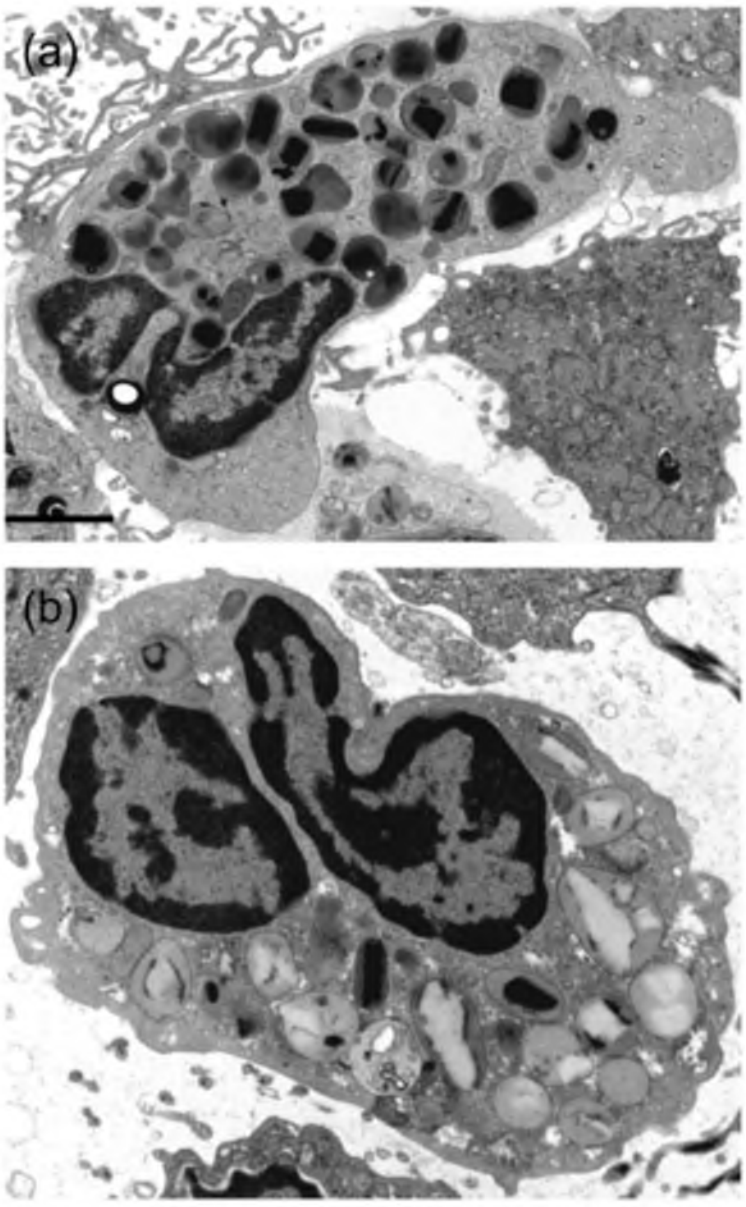

Figure 1.3. Electron microscopy image of (a) Normal eosinophil with intact membrane and intact granule proteins. (b) Degranulating eosinophil with release of granule protein into the cytoplasm as seen as by the reversal of staining (light core and dark matrix; see Chapter 3 for further details).

References

1. Fox, V.L., S. Nurko, and G.T. Furuta, *Eosinophilic esophagitis: it's not just kid's stuff* Gastrointest Endosc, 2002. **56**(2): p. 260-70.

2. Noel, R.J., P.E. Putnam, and M.E. Rothenberg, *Eosinophilic esophagitis.* N Engl J Med, 2004. **351**(9): p. 940-1.

3. Furuta, G.T., et al., *Eosinophilic esophagitis in children and adults: a systematic review and consensus recommendations for diagnosis and treatment.* Gastroenterology, 2007. **133**(4): p. 1342-63.

4. Gleich, G.J., et al., *Eosinophils and human disease.* Int Arch Allergy Appl Immunol, 1989. **88**(1-2): p. 59-62.

5. Liacouras, C.A., *Eosinophilic esophagitis in children and adults.* J Pediatr Gastroenterol Nutr, 2003. **37 Suppl 1**: p. S23-8.

6. Liacouras, C.A., et al., *Eosinophilic esophagitis: updated consensus recommendations for children and adults.* J Allergy Clin Immunol, 2011. **128**(1): p. 3-20 e6; quiz 21-2.

7. Gonsalves, N. and P.J. Kahrilas, *Eosinophilic oesophagitis in adults.* Neurogastroenterol Motil, 2009. **21**(10): p. 1017-26.

8. Gonsalves, N., et al., *Histopathologic variability and endoscopic correlates in adults with eosinophilic esophagitis.* Gastrointest Endosc, 2006. **64**(3): p. 313-9.

9. Riou, P.J., A.G. Nicholson, and U. Pastorino, *Esophageal rupture in a patient with idiopathic eosinophilic esophagitis.* Ann Thorac Surg, 1996. **62**(6): p. 1854-6.

10. Attwood, S.E., et al., *Esophageal eosinophilia with dysphagia. A distinct clinicopathologic syndrome.* Dig Dis Sci, 1993. **38**(1): p. 109-16.

11. Mackenzie, S.H., et al., *Eosinophilic oesophagitis in patients presenting with dysphagia--a prospective analysis.* Aliment Pharmacol Ther, 2008. **28**(9): p. 1140-6.

12. Potter, J.W., et al., *Eosinophilic esophagitis in adults: an emerging problem with unique esophageal features.* Gastrointest Endosc, 2004. **59**(3): p. 355-61.

13. Rodrigo, S., et al., *High intraepithelial eosinophil counts in esophageal squamous epithelium are not specific for eosinophilic esophagitis in adults.* Am J Gastroenterol, 2008. **103**(2): p. 435-42.

14. Shah, A., et al., *Histopathologic variability in children with eosinophilic esophagitis.* Am J Gastroenterol, 2009. **104**(3): p. 716-21.

15. Dellon, E.S., et al., *Variability in diagnostic criteria for eosinophilic esophagitis: a systematic review.* Am J Gastroenterol, 2007. **102**(10): p. 2300-13.

16. Saffari, H., et al., *Patchy eosinophil distributions in an esophagectomy specimen from a patient with eosinophilic esophagitis: Implications for endoscopic biopsy.* J Allergy Clin Immunol, 2012. **130**(3): p. 798-800.

17. Markowitz, J.E., et al., *Elemental diet is an effective treatment for eosinophilic esophagitis in children and adolescents.* Am J Gastroenterol, 2003. **98**(4): p. 777-82.

18. Leiferman, K.M., et al., *Extracellular deposition of eosinophil and neutrophil granule proteins in the IgE-mediated cutaneous late phase reaction.* Lab Invest, 1990. **62**(5): p. 579-89.

19. Gonsalves, N., et al., *Elimination diet effectively treats eosinophilic esophagitis in adults; food reintroduction identifies causative factors.* Gastroenterology, 2012. **142**(7): p. 1451-9 e1; quiz e14-5.

20. Peters, M.S., M. Rodriguez, and G.J. Gleich, *Localization of human eosinophil granule major basic protein, eosinophil cationic protein, and eosinophil-derived neurotoxin by immunoelectron microscopy.* Lab Invest, 1986. **54**(6): p. 656-62.

21. Melo, R.C., et al., *Vesicle-mediated secretion of human eosinophil granule-derived major basic protein.* Lab Invest, 2009. **89**(7): p. 769-81.

22. Peters, M.S., A.L. Schroeter, and G.J. Gleich, *Immunofluorescence identification of eosinophil granule major basic protein in the flame figures of Wells' syndrome.* Br J Dermatol, 1983. **109**(2): p. 141-8.

23. Plager, D.A., et al., *Eosinophil ribonucleases and their cutaneous lesion-forming activity.* J Immunol, 2009. **183**(6): p. 4013-20.

24. Kephart, G.M., et al., *Marked deposition of eosinophil-derived neurotoxin in adult patients with eosinophilic esophagitis.* Am J Gastroenterol, 2010. **105**(2): p. 298-307.

25. Gleich, G.J., et al., *Biochemical and functional similarities between human eosinophil-derived neurotoxin and eosinophil cationic protein: homology with ribonuclease.* Proc Natl Acad Sci U S A, 1986. **83**(10): p. 3146-50.

26. Gleich, G.J., et al., *Comparative properties of the Charcot-Leyden crystal protein and the major basic protein from human eosinophils.* J Clin Invest, 1976. **57**(3): p. 633-40.

27. Gleich, G.J., et al., *Physiochemical and biological properties of the major basic protein from guinea pig eosinophil granules.* J Exp Med, 1974. **140**(2): p. 313-32.

28. Justinich, C.J., et al., *Activated eosinophils in esophagitis in children: a transmission electron microscopic study.* J Pediatr Gastroenterol Nutr, 1997. **25**(2): p. 194-8.

29. Erjefalt, J.S., et al., *Cytolysis and piecemeal degranulation as distinct modes of activation of airway mucosal eosinophils.* J Allergy Clin Immunol, 1998. **102**(2): p. 286-94.

30. Henderson, C.J., et al., *Comparative dietary therapy effectiveness in remission of pediatric eosinophilic esophagitis.* J Allergy Clin Immunol, 2012. **129**(6): p. 1570-8.

CHAPTER 2

PATCHY EOSINOPHIL DISTRIBUTIONS IN AN EOSINOPHILIC ESOPHAGITIS ESOPHAGECTOMY SPECIMEN: IMPLICATIONS FOR ENDOSCOPIC BIOPSY[1]

2.1 Abstract

The eosinophil infiltration in eosinophilic esophagitis (EoE) is known to be patchy, but detailed spatial knowledge of eosinophil distributions within the esophageal lumen and their implications for accurate diagnosis remain unclear. We analyzed full circumferential cross-sections of a several centimeter long esophagectomy specimen from a known EoE patient and mapped eosinophil density in the lumenal epithelium. We applied a statistical (Monte Carlo) model to predict the minimum number of biopsies that would be required to make a diagnosis of EoE in areas with low, intermediate, and high eosinophil density in this patient. Eosinophil density shows a nonuniform distribution in the lumenal epithelium. Within a given cross-section, 1 to 14 Gaussian regions or patches contained an eosinophil density above the diagnostic threshold for EoE (≥15eos/hpf), typically between lumenal folds. Overall, 31.5% of the total lumenal epithelium contains eosinophil counts above the threshold for disease.

[1] The material provided in this chapter is available at: J. Allergy Clin. Immunol. 2012; 130:798-800. Reprinted and adapted with permission from Elsevier.

This data set indicates an average probability of detecting EoE as low as 62% in at least one out of 4-5 biopsies. Our analysis suggests that the standard protocol of 4-5 biopsies may result in underdiagnosis of EoE in areas of low eosinophil density. EoE patients would require ≥31, ≥12, or ≥4 random biopsies to detect the disease with 95% confidence from low, average, and high eosinophil density regions, respectively. The Gaussian distribution of eosinophil density suggests that eosinophils infiltrate from specific localized points in the esophagus.

2. 2 Introduction and Background

Eosinophilic esophagitis (EoE) is characterized by patchy infiltration of the esophagus by eosinophils, inflammatory leukocytes which are not found in the healthy esophagus [1-4]. The diagnosis of EoE is established through correlation of clinical presentation (typically a child or young male with dysphagia or food impaction) with endoscopic and pathologic findings [5]. The pathologic diagnosis can be difficult since the degree of eosinophil infiltration varies greatly within the esophagus, leading to a possibility of underdiagnosis if the tissue is sampled insufficiently. When clinical suspicion for EoE is high, consensus practice requires sampling at 4-5 sites throughout the esophagus [5-8]. However, five 2 mm biopsies represent less than 0.7% of the 20-25 cm long esophageal mucosa and may result in underdiagnosis of EoE if mucosal eosinophilia is particularly patchy [9]. The distribution of eosinophils in EoE is thought to be patchy based on small biopsy samples, but a rigorous mapping study to determine the characteristic size and frequency of diagnostic patches of enriched eosinophil density requires a large tissue specimen from an esophagectomy or autopsy. Since EoE patients are typically (but not exclusively) young and otherwise healthy, opportunities

to obtain this type of specimen are rare [10-12]. Here we report the analysis of a unique full circumferential esophagectomy specimen from a known EoE patient who underwent partial esophagectomy for a concomitant early-stage esophageal adenocarcinoma. We obtained serial cross-sections of the esophagus and mapped eosinophil density across the entire esophageal epithelium. We performed statistical analysis of the data with a Monte Carlo simulation to predict the number of biopsies required to make a diagnosis of EoE in patients with different eosinophil densities.

2.3 Methods

2.3.1 Esophagectomy. With approval from the University of Utah IRB, an esophagectomy specimen from a 68-year-old patient with known EoE was obtained at time of surgery for early-stage T1N0M0 esophageal adenocarcinoma. He presented with food impaction in 2008 and was found to have both nondysplastic Barrett's esophagus and eosinophilic esophagitis [13]. He reported a several-year history of solid food dysphagia as well as seasonal allergies, but no food allergies, asthma, or eczema. He was treated with high-dose protein pump inhibitor (PPI) therapy. Subsequent biopsies performed 6 months after initial presentation demonstrated a short distal esophageal stricture and short-segment nondysplastic Barrett's disease. Follow up biopsy in 2009 revealed invasive intramucosal adenocarcinoma in the setting of short segment Barrett's esophagus. In addition, greater than 100 eosinophils (eos)/high power field (hpf) were seen in the surrounding benign squamous mucosa, consistent with persistent eosinophilic esophagitis. The patient then underwent distal esophagectomy without prior adjuvant or radiation treatment. After removing routine segments for

cancer diagnosis and staging, four addition tissue segments were removed and fixed in formalin. The more proximal of two segments available for analysis, obtained from the proximal esophagus, was 2.6 cm long and 1.5 cm in diameter, and labeled by surgical pathology as segment 3. They reported up to 30 eos/hpf, consistent with the earlier diagnosis of EoE. The second esophageal segment, obtained from the distal portion of the esophagus beginning at the gastroesophageal junction, was 9.0 cm long and 2.0 cm in diameter, and was labeled as segment 2. Pathology observed eosinophilic abscesses and reported up to 40 intraepithelial eos/hpf in this segment. The esophagus was later sectioned horizontally (i.e., traverse to the esophageal longitudinal axis) at 3 mm to 5 mm intervals to yield pairs of tissue slices separated by 3 μm to 5 μm (see Figure 2.1a for section ordering and approximate intervals). Each of the 17 sections was designated by surgical pathology with a number and letter representing the segment and section, respectively (see Table 2.1).

2.3.2 Histology, mapping, and data analysis. Each section was stained with hematoxylin and eosin (H&E) (see Figure 2.1b). Tissue was imaged using an Olympus microscope at 400x magnification. Each microscopic site or circular field of view had a diameter of 0.54 mm, representing 0.23 mm^2 of tissue. The eosinophil count for each 400x field was performed manually one hpf at a time all the way around the entire perimeter (Figure 2.1c and Table 2.1). In this study, we only counted the eosinophils in epithelium layer and did not map the eosinophil density in deeper tissue layers in the esophagus. The number of sites containing a "diagnostic" level of eosinophils [either 15 eos/hpf (65 eos/mm^2, clinically recommended criteria) or 20 eos/hpf (87 eos/mm^2,

research purposes criteria)] was determined for each of the 17 circumferential sections (see Appendix A for additional information).

2.3.3 Monte Carlo simulation and statistical analysis. A Monte Carlo method was used to evaluate the relationship between eosinophil density and the number of biopsies required to make a diagnosis of eosinophilic esophagitis [14]. This simulation mimics the random process of selecting a biopsy site during endoscopy by using a random number generator to select a site from the esophagectomy map. A "biopsy" is defined in the simulation as four adjacent 0.54 mm fields of view, since a typical endoscopic esophageal biopsy specimen measures approximately 2 mm [9]. The biopsy was considered "positive" if at least one of the four adjacent fields of view contained at least 15 eosinophils. The simulation was coded in Visual Basic for Applications (VBA) in MS Excel 2003. The simulation was repeated two to forty times to represent multiple biopsies per endoscopy [5]. The average, μ, and standard deviation, σ, were calculated over the 10,000 endoscopies simulated for each scenario considered (see Appendix B for additional information).

The simulations were summarized by reporting either a probability of detection (μ) or the number of biopsies required to obtain at least one biopsy specimen meeting the diagnostic threshold of $\geq$15 eosinophils/hpf with a confidence level of 95% or 99%. The number of biopsies required was calculated for three different eosinophil densities: low (average of 5.7% of sites $\geq$15 eos/hpf from three lowest density sections, one from each of 3C, 3D, and 3E in Table 2.1), average (31.5% of sites $\geq$15 eos/hpf across all sections), and high (average of 79.3% of sites $\geq$15 eos/hpf from three highest density sections, one from 2W and both of 2U). For each eosinophil density, the 95% and 99%

confidence levels for EoE diagnosis (i.e., number of biopsies required to obtain a diagnostic tissue fragment) were determined. These were calculated by μ-1.96σ and μ-2.58σ, respectively, from a singled tailed normal distribution.

To determine whether two consecutive biopsies will produce the same result, pairs of consecutively simulated biopsies were selected and classified as "positive" or "negative." If both were negative, then the pair was designated as a "double miss" because the tissue is from a known EoE patient. If both were positive, the pair was designated as a "double hit." Disparate results were classified as a "miss-hit" or "hit-miss." Because the order of endoscopy remains arbitrary in the simulation, differences between the latter two classifications reflect numerical uncertainty.

2.4 Results

The tissue sections, summarized in Figure 2.1 and Table 2.1, show the eosinophil density to be highly variable in this EoE patient both axially and circumferentially. Figure 2.1b shows a typical 360° H&E-stained cross-section. By methodically counting the intraepithelial eosinophil number in each sequential 0.54 mm field of view, eosinophil density was mapped for the entire perimeter of each tissue section (Figure 2.1c and Table 2.1). The greatest peak eosinophil count was 176 eosinophils/hpf (770 eosinophils/mm^2), the average eosinophil density was approximately 14.8 eosinophils/hpf (64 eosinophils/mm^2), and some fields of view did not contain any eosinophils. Figure 2.1c shows an example of eosinophil density variation per high power field of view (hpf on left axis) or per square millimeter (right axis). The histograms for all circumferential sections are provided in the Supporting

Information. Each section contains 1 to 14 areas or patches comprised of one or more sites exceeding the diagnostic threshold of 15 eosinophils/hpf. These diagnostic areas or patches were separated by regions of lower (nondiagnostic) eosinophil density, which ranged from 0.5 mm to 38.3 mm in length (see Table 2.2). Correlation of eosinophil density in Figure 2.1c with the topology of Figure 2.1b indicates that eosinophil peak counts appear to cluster between lumenal folds and associate with locally increased vasculature.

Figure 2.1d shows a representation of eosinophil density in each tissue section, shaded for infiltration intensity. The greatest percentage of areas with high eosinophil density was seen in the distal esophagus (segment 2). In total, 31.5% of the high power fields contained eosinophil densities $\geq$15 eosinophils/hpf. When using the more stringent threshold of $\geq$ 20 eosinophils/hpf, only 23.8% of high power fields were diagnostic (see Table 2.1).

Remarkably, Figure 2.1c shows that many of the esophageal cross-sections contain eosinophil infiltrates that appear to follow Gaussian distributions. The apparently random location of the infiltrate peaks and their Gaussian shaped distributions suggest that eosinophil infiltrates are triggered at specific localized points within the esophagus presumably by localized release of chemoattractants at "point sources." (We note that, due to separation between adjacent sections, the evidence presented in these cross-sections cannot eliminate the possibility of line sources or linear foci of point sources aligned along the esophageal axis [15].)

The degree of eosinophil infiltration is shown as a function of the epithelial perimeter position in Figure 2.2. The total circumference of the esophageal luminal

epithelium ranged from 24.8 mm to 63.2 mm. Within both esophagectomy segments, the extent of infiltration appears to generally increase with perimeter or circumference.

The spatial heterogeneity in Figure 2.1 suggests that site selection for tissue acquisition may be critical [6]. Current biopsy protocols recommend obtaining five biopsies. In addition, biopsies should be obtained from both the proximal and distal esophagus. To predict the optimal sampling protocol, we performed a Monte Carlo simulation to mimic biopsy collection practices [14]. Three distinct sampling procedures were simulated, namely, random sampling across the entire esophagus, at a particular esophageal depth, and within equal length perimeter sectors (such as 4 quadrant locations) at one specific esophageal depth (see Figure 2.3). To take into consideration the differing intensities of eosinophilic infiltration in individual EoE patients, spatial heterogeneity in eosinophil infiltration was introduced by selecting random high power fields from the three lowest-density cross-sections, the three highest-density cross-sections, and from all 17 of the cross-sections. The lowest density cross-sections were taken to represent EoE patients with less robust eosinophil infiltrates, while the high density sampling represents EoE patients with more obvious disease manifestations. For each of the 9 scenarios (3 densities by 3 sampling protocols), 10,000 endoscopies were simulated, each with 2-40 biopsies per endoscopy. The number of biopsies that ensures a 95% or 99% confidence interval for EoE diagnosis is reported in Table 2.3.

The simulations indicate that the probability of detecting EoE ($\geq$1 biopsy with $\geq$15eos/hpf) in a single upper endoscopy with 4-5 biopsies ranges from 62% to ~100%, depending on eosinophil density [6, 7]. Table 2.3 shows that sampling purely randomly

across all sections or within equal length sectors appears to provide better detection than random sampling within circumferential sections (i.e., at a single esophageal depth). However, in all but the highest density infiltrates, sampling within equal length sectors would require removal of over half of the epithelium at that esophageal depth, leaving random sampling at multiple esophageal depths as the most feasible and informative sampling procedure.

Remarkably, in this specimen, a 95% confidence interval for EoE detection requires at least 12 biopsies for all but the highest eosinophil densities. This is in reasonable agreement with the conclusion of Gonsalves, et al., who examined very high density sections and found 4-5 biopsies per endoscopy to be sufficient. Previous work, however, has only considered probability of detection and not confidence of detection. The former represents only the mean, which may be associated with significant variation that only confidence interval analysis includes (σ/μ regularly exceeded 0.2). For example, five biopsies selected purely at random return a 96.4% probability of detecting EoE ($\geq$15 eos/hpf in $\geq$1 biopsy), but the corresponding standard deviation is 18.6%, leading to a confidence interval of only 59.9%. Only by increasing the number of biopsies to 12 does the confidence interval rise to 95% for the typical eosinophil densities of this patient.

We also note that in many cases, increasing the number of biopsies by only one or two increases the confidence interval (CI) from 95% to 99%. A 95% confidence interval in this context translates into one in twenty patients with a potential misdiagnosis. However, the increased probability of accurate detection for 5% of

patients must be balanced against the additional risk endured by the 95% of the patient population for whom an extra sample provides limited insight.

Table 2.4 indicates the probability that two consecutive endoscopies with either 5 (consensus criterion) or 8 (research criterion) biopsies will correctly diagnose the patient at three eosinophil densities. Five biopsies from an area of low-density eosinophil infiltration will yield a false negative 50.9% in at least one of the endoscopies in a *known* EoE patient. However, with more biopsies or higher eosinophil densities, this risk falls dramatically to 1.1-8.3%. The risk becomes negligible at high eosinophil density. The probability of an initial diagnosis of EoE followed by a misdiagnosis of EoE remission or that sampling errors will lead to an initial misdiagnosis of no EoE that will only be corrected with the second endoscopy are numerically identical as high as 20.9%, though with more biopsies or higher eosinophil densities, this risk can fall dramatically to 0.5-4.2% with average levels of infiltration and also become negligible at high eosinophil density.

2.5 Discussion

This study addresses a fundamental gap in our knowledge regarding eosinophil infiltration in EoE by spatially mapping the distribution of eosinophil density derived from a several centimeter long esophagectomy specimen from a patient with known eosinophilic esophagitis. The resulting distributions demonstrate significant variability in eosinophil density. Diagnostic areas or patches bearing $\geq$15 eosinophils/hpf are separated by regions with low to negligible (nondiagnostic) eosinophil density spanning

<0.5 mm to >38 mm (see Figure 2.1c and Table 2.2). Because endoscopic biopsies typically sample only 2 mm of tissue, eosinophil peak infiltrates may be easily missed.

From this distinct data set, we used a statistical (Monte Carlo) simulation to predict the number of biopsies required for EoE diagnosis based on the underlying eosinophil density [14]. For the current clinical practice of 4-5 biopsies, the simulations indicate a 62% to ~100% probability of detecting EoE (≥1 biopsy with ≥15 eosinophils/hpf). This variability was not anticipated by Gonsalves, et al., who found 1 biopsy with a criterion of ≥15 eos/HPF to be a 55% sensitive indicator of EoE and suggested that 5 biopsies are sufficient for essentially 100% EoE detection.[6] At least part of the difference may arise from the much higher eosinophil densities observed in their studies (median of 107 eos/hpf where 1 hpf=0.15 mm^2 versus our average of 14.8 eos/hpf, commensurate with our high density variant). More stringent criteria for disease diagnosis (e.g., ≥20 eosinophils/hpf) increase the number of biopsies that must be collected.

In this patient, approximately 30% of the esophageal epithelium contained a "diagnostic" eosinophil density of ≥15 eosinophils/hpf. In order to achieve a 95% confidence interval for EoE detection, this patient would typically require at least 12 biopsies at endoscopy (see Table 2.3). The extreme variability of eosinophil density in only this patient suggests that other patients may have equally patchy eosinophil distributions, and suggests that the clinical recommendations for EoE diagnosis may need to be reevaluated.

Our data also suggest a significant probability that a second endoscopy with biopsy may report resolution of pathologic esophageal eosinophilia, when in fact

disease remains. Based on this specimen, the probability of misdiagnosis based on sampling error alone is as high as 20.7% at the lower eosinophil infiltration density (see Table 2.4), a very real possibility for some patients. This means that as many as 20.7% of these patients initially diagnosed with EoE would appear to have disease resolution upon repeat biopsy, but in reality have persistent EoE. Placebo responses (seen in up to 9% of patients) reported in previous trials may result from inadequate sampling techniques alone and not actual disease resolution [16]. Others have reported that symptoms do not appear to correlate with disease activity, but this conclusion also derives from assessments of small numbers of potentially nonrepresentative biopsies collected blindly from within the adult esophagus [11,17]. Indeed, based on the perimeters or circumference for this patient, five 1 mm-3 mm biopsies represent only 0.02%- 0.71% of the esophageal lumen, and 8 biopsies represent only 0.04%-1.14% of the lumenal surface area of a 20 cm-25 cm adult esophagus.

We recognize that our study has limitations. Our data are derived from a single EoE patient and do not represent random population sampling from a broad EoE patient population. Additionally, this patient had esophageal adenocarcinoma, presumably arising from Barrett's esophagus in the setting of gastroesophageal reflux disease (GERD) [18]. The presence of additional pathology injects some uncertainty into the data, especially in the distal esophagus (segment 2), near the site of adenocarcinoma. Some of the eosinophilic infiltrates could potentially be secondary to gastroesophageal reflux or could represent a reaction to the tumor (e.g., tumor protrusion could moderate food bolus migration rates allowing for extra "contact time"). However, this patient had known eosinophilic esophagitis for several years, was treated with high-dose protein

pump inhibitor (PPI) therapy, and the histological features in his esophagus are strongly consistent with residual EoE rather than GERD or tumor reaction. In addition, we also studied tissue from the more proximal portion of the esophagectomy specimen, which was uninvolved by adenocarcinoma. Despite the potential disadvantages of using a specimen with other pathologic findings, this is a unique opportunity for the study of EoE. Prior reports of esophagectomy specimens from EoE patients are exceedingly rare, since the EoE population is typically young and healthy [12, 19]. Previous reports of esophagectomies either do not fulfill the criteria for EoE because eosinophils were only found in the muscularis propria and not in mucosal biopsies [19] or describe histologic findings only in 2 short lines [12]. To our knowledge, ours is the first and only study to systematically perform eosinophil counts on multiple full circumference sections of an EoE specimen. In addition, we have used these data in a mathematical model to predict the numbers of biopsies required for EoE diagnosis in tissue with varying eosinophil density. While our results are derived from a single EoE patient and other patients/phenotypes may differ in their eosinophil distributions, we believe that some of these results can be applied to other EoE patients. Our mathematical model calculated the probability of obtaining a diagnostic tissue specimen in areas of high, medium, and low eosinophil densities. Presumably, these findings could be extrapolated to different EoE patients, some of whom may present with very low or high eosinophil densities.

These spatial distributions also provide new insights that may inform studies into the etiology and pathogenesis of EoE. Specifically, this patient's eosinophil densities appear to follow Gaussian distributions, arguing that a "point of stimulus" may stimulate eosinophil infiltration at specific areas within the esophagus [15]. We caution,

however, that the centers of eosinophil infiltration cannot be determined from these cross-sections for much the same reason as marching along a straight line through the mountains does not necessarily determine the height of the tallest peak. The summit location must be triangulated, and there is insufficient information in these 20 sections alone to locate the true "peaks." While the typical Gaussian distribution of dense eosinophilia spans only 1.1-2.5 mm (at base), the separation between cross-sections is approximately 1.6-5.4 mm. This precludes us from precisely aligning peaks within adjacent sections.

Finally, as esophagectomies are not routinely available in EoE, this analysis strongly indicates the need for improved imaging of eosinophil infiltration patterns *in vivo* to accurately diagnose and understand this disease. This suggestion is in strong accord with a recent challenge issued by the American Partnership for Eosinophilic Disorders (APFED), who called for development of more informative and less invasive imaging of EoE patients. This study suggests that more intensive biopsy sampling may lead to greater diagnostic accuracy, and provide additional insight into the disease, particularly in the early stages where eosinophil infiltration densities may be more modest but when the patient may also benefit most from measured interventions.

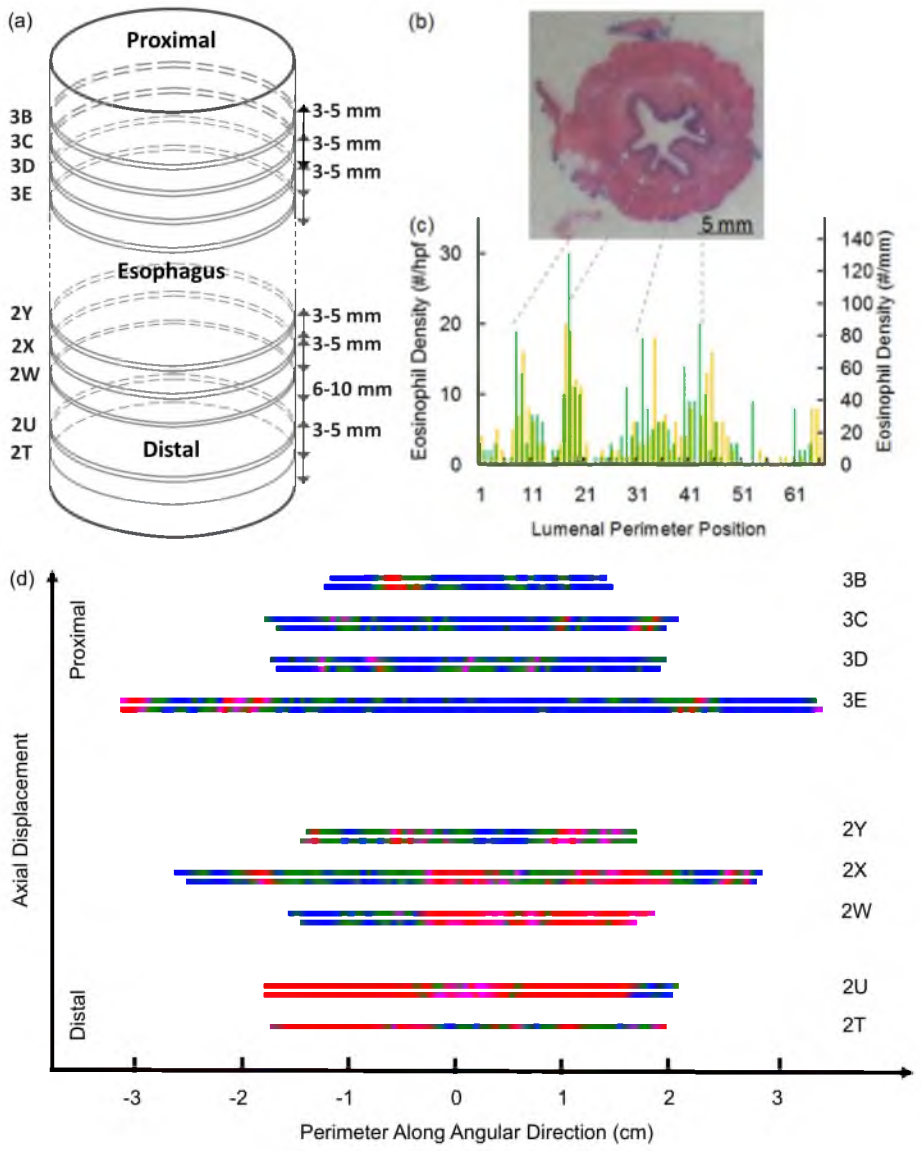

Figure 2.1. Histology, mapping, and data analysis. (a) Sequential ordering of sections within the esophagectomy. Distances between sections are not to scale but approximate. Two tissues slices separated by approximately 3-5 μm were cut for most sections. (b) Digital image of representative H&E stained esophageal section 3D. (c) Representative eosinophil density (in eos/hpf and eos/mm^2) as a function of lumenal perimeter position in terms of microscopy sites for section 3D. (d) Eosinophil density map as a function of both lumenal perimeter (in cm) and axial location (not to scale) at various densities of ≤3 eosinophils/hpf or less (blue), 4-14 eosinophils/hpf (green), 15-19 eosinophils/hpf (pink), and ≥20 eosinophils/hpf (red).

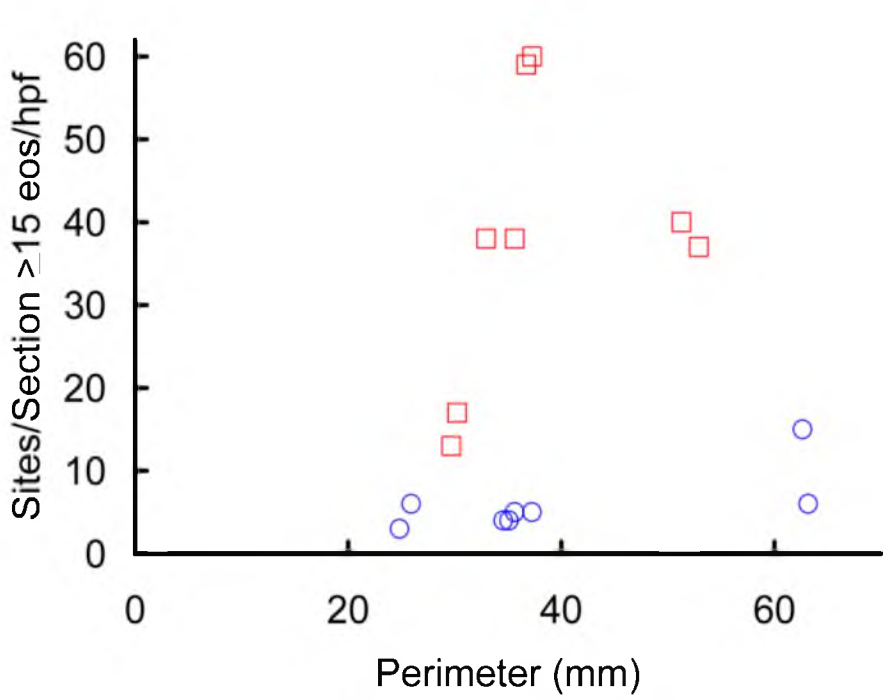

Figure 2.2. Number of sites with eosinophil density of ≥15 eosinophils/hpf versus length of epithelial perimeter for proximal sections 3B-3E (circles) and distal esophageal sections 2T-2Y (squares).

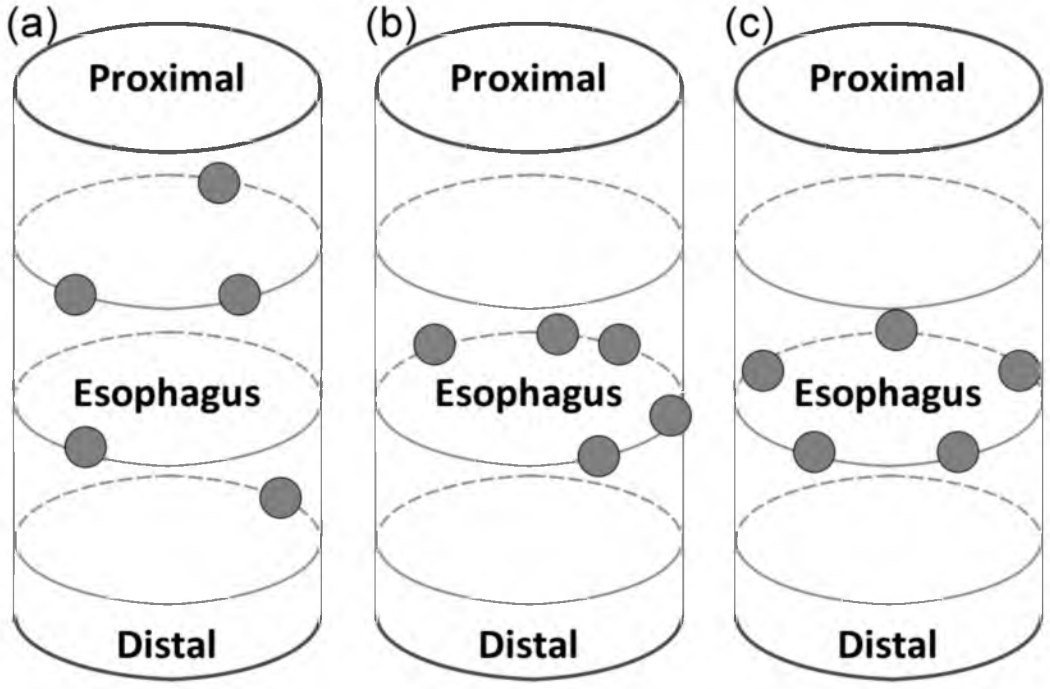

Figure 2.3. Three sampling patterns simulated including (a) random sampling across the entire esophagus, (b) at a particular esophageal depth, and (c) within equal length perimeter sectors at one specific esophageal depth. Each panel represents the location of 5 biopsies in the large grey dots (not to scale).

Table 2.1. Section attributes from proximal to distal.

Section Number	# of Sites or hpf/ Section	Perimeter (mm)[+]	Equivalent Diameter (cm)[+]	Sites ≥15 eos/hpf [++]	Percent of Sites ≥15 eos/hpf	Sites ≥20 eos/hpf [+++]	Percent of Sites ≥20 eos/hpf
3B	46	24.8	0.79	3	6.5%	3	6.5%
3B	48	25.9	0.83	6	12.5%	5	10.4%
3C	69	37.3	1.19	5	7.2%	3	4.3%
3C	65	35.1	1.12	4	6.2%	3	4.6%
3D	66	35.6	1.13	5	7.6%	1	1.5%
3D	64	34.6	1.10	4	6.3%	2	3.1%
3E	116	62.6	1.99	15	12.9%	8	6.9%
3E	117	63.2	2.01	6	5.1%	5	4.3%
2Y	55	29.7	0.95	13	23.6%	7	12.7%
2Y	56	30.2	0.96	17	30.4%	8	14.3%
2X	98	52.9	1.68	37	37.8%	25	25.5%
2X	95	51.3	1.63	40	42.1%	26	27.4%
2W	56	30.2	0.96	33	58.9%	24	42.9%
2W	61	32.9	1.05	38	62.3%	32	52.5%
2U	69	37.3	1.19	60	87.0%	55	79.7%
2U	68	36.7	1.17	59	86.8%	53	77.9%
2T	66	35.6	1.13	38	57.6%	29	43.9%
Totals:	1215			383	31.5%	289	23.8%

[+]Perimeter=# of sites x field of view (0.54 mm); equivalent diameter=perimeter/π.
[++] 15 eos/hpf=Clinical diagnostic criteria for EoE.
[+++] 20 eos/hpf=Research purpose criteria.

Table 2.2. Measured Patch Lengths.

Lengths	Nondiagnostic Regions or Patches (mm)	Diagnostic Regions (mm)
Median	1.6	1.1
Average	5.4	2.5
Standard Deviation	7.5	3.8
Maximum	38.3	16.2
Minimum	<0.5	<0.5

Table 2.3. Required number of biopsies needed to obtain ≥1 biopsy containing ≥15 eosinophils/hpf at 95% and 99% confidence intervals.

	Across Entire Esophagus*		At 1 Esophageal Depth+		Within Sectors at 1 Esophageal Depth§	
	95% CI	99% CI	95% CI	99% CI	95% CI	99% CI
Three Low Density Sections	30	>40	36	>40	15	16
All Sections	12	13	34	>40	14	15
Three High Density Sections	4	5	5	6	2	2

*Simulated by randomly selecting sites from any of the 17 sections (see Fig. 3a).
+Simulated by randomly selecting sites from within any one section (see Fig. 3b).
§Simulated by first selecting a section, dividing the section into equal length sectors (e.g., quadrants for 4 biopsies) based on equal divisions of the perimeter, and then randomly selecting a site from within each sector (see Fig. 3c).

Table 2.4. Probability that repeat endoscopy with random biopsy will detect EoE in ≥1 biopsy (≥15 eosinophils/hpf or 65 eosinophils/mm^2) out of 5 or 8 biopsies/endoscopy.

	Biopsies	Miss-miss	Miss-hit	Hit-miss	Hit-hit
Three Low Density Sections[+]	5	9.4%	20.9%	20.7%	49.1%
All Sections	5	0.2%	3.9%	4.2%	91.8%
Three High Density Sections[§]	5	0.0%	0.0%	0.0%	~100%
Three Low Density Sections[+]	8	1.9%	12.5%	12.1%	73.5%
All Sections	8	0.0%	0.6%	0.5%	98.9%
Three High Density Sections[§]	8	0.0%	0.0%	0.0%	~100%

*Percentages may not sum to 100.0% due to rounding uncertainty.
[+]Representing patients with a lower infiltration of eosinophils.
[§]Representing patients with a large, robust eosinophil infiltrates.

2.6 References

1. Gupta SK, Fitzgerald JF, Kondratyuk T, et al. Cytokine expression in normal and inflamed esophageal mucosa: a study into the pathogenesis of allergic eosinophilic esophagitis. J Pediatr Gastroenterol Nutr 2006;42:22-6.

2. Kephart GM, Alexander JA, Arora AS, et al. Marked deposition of eosinophil-derived neurotoxin in adult patients with eosinophilic esophagitis. Am J Gastroenterol 2010;105:298-307.

3. Straumann A, Bauer M, Fischer B, et al. Idiopathic eosinophilic esophagitis is associated with a T(H)2-type allergic inflammatory response. J Allergy Clin Immunol 2001;108:954-61.

4. Straumann A, Spichtin HP, Grize L, et al. Natural history of primary eosinophilic esophagitis: a follow-up of 30 adult patients for up to 11.5 years. Gastroenterology 2003;125:1660-9.

5. Furuta GT, Liacouras CA, Collins MH, et al. Eosinophilic esophagitis in children and adults: a systematic review and consensus recommendations for diagnosis and treatment. Gastroenterology 2007;133:1342-63.

6. Gonsalves N, Policarpio-Nicolas M, Zhang Q, et al. Histopathologic variability and endoscopic correlates in adults with eosinophilic esophagitis. Gastrointest Endosc 2006;64:313-9.

7. Shah A, Kagalwalla AF, N. G, et al. Histopathologic variability in children with eosinophilic esophagitis. Am J Gastroenterol. 2009;104:716-721.

8. Dellon ES, Aderoju A, Woosley JT, et al. Variability in diagnostic criteria for eosinophilic esophagitis: a systematic review. Am J Gastroenterol 2007;102:2300-13.

9. Komanduri S, Swanson G, Keefer L, et al. Use of a new jumbo forceps improves tissue acquisition of Barrett's esophagus surveillance biopsies. Gastrointest Endosc 2009;70:1072-8 e1.

10. Mackenzie SH, Go M, Chadwick B, et al. Eosinophilic oesophagitis in patients presenting with dysphagia--a prospective analysis. Aliment Pharmacol Ther 2008;28:1140-6.

11. Pentiuk S, Putnam PE, Collins MH, et al. Dissociation between symptoms and histological severity in pediatric eosinophilic esophagitis. J Pediatr Gastroenterol Nutr 2009;48:152-60.

12. Riou PJ, Nicholson AG, Pastorino U. Esophageal rupture in a patient with idiopathic eosinophilic esophagitis. Ann Thorac Surg 1996;62:1854-6.

13. Wang KK, Sampliner RE. Updated guidelines 2008 for the diagnosis, surveillance and therapy of Barrett's esophagus. Am J Gastroenterol 2008;103:788-97.

14. Pease LF. Optimizing the yield and selectivity of high purity nanoparticle clusters. Journal of Nanoparticle Research 2011;DOI: 10.1007/s11051-010-9974-6:in press.

15. Cussler EL. Diffusion: Mass Transfer in Fluid Systems. Cambridge: Cambridge University Press, 2009.

16. Konikoff MR, Noel RJ, Blanchard C, et al. A randomized, double-blind, placebo-controlled trial of fluticasone propionate for pediatric eosinophilic esophagitis. Gastroenterology 2006;131:1381-91.

17. Potter JW, Saeian K, Staff D, et al. Eosinophilic esophagitis in adults: an emerging problem with unique esophageal features. Gastrointest Endosc 2004;59:355-61.

18. Spechler SJ, Genta RM, Souza RF. Thoughts on the complex relationship between gastroesophageal reflux disease and eosinophilic esophagitis. Am J Gastroenterol 2007;102:1301-6.

19. Stevoff C, Rao S, Parsons W, et al. EUS and histopathologic correlates in eosinophilic esophagitis. Gastrointest Endosc 2001;54:373-7.

CHAPTER 3

EOSINOPHIL DEGRANULATION PATTERNS IN EOSINOPHILIC ESOPHAGITIS: AN ELECTRON MICROSCOPY STUDY[1]

3.1 Abstract

In eosinophilic esophagitis (EoE), eosinophil granulocytes accumulate and release granule proteins onto esophageal epithelium. However, little is understood about the mechanism of eosinophil degranulation in EoE. To determine and quantify eosinophil degranulation patterns, we studied esophageal biopsy specimens obtained at endoscopy from both proximal and distal esophagi of 9 randomly selected patients with EoE (3 female, 6 male). The specimens were fixed in glutaraldehyde, embedded in Epon, sectioned, and imaged by transmission electron microscopy. Eosinophils and their granules were identified by their distinctive morphology, and all eosinophils and granules were imaged. A total of 1672 images from 18 esophageal specimen blocks were evaluated and graded. Eosinophils were categorized based on membrane integrity and by cytoplasmic vesiculation as evidence of piecemeal degranulation. Granules were categorized based on reversal of staining (eosinophil granule core lightening) and other features including location within and outside of cells and membrane integrity. The

[1] The material presented in this chapter has been submitted to Journal of Allergy and Clinical Immunology (JACI).

results revealed that greater than 98% of eosinophils infiltrating the esophagus in EoE demonstrate morphological abnormalities ranging from granule changes with reversal of staining to marked cytoplasmic vesiculation to loss of membrane integrity with cytolytic disruption and release of intact, membrane-bound granules into the tissues. Approximately 81% of eosinophils showed membrane disruption. Extracellular granules were abundant in at least 70% of the images and about 50% of these granules showed reversal of staining. Based on the prominence of tubulovesicular development, piecemeal degranulation appears closely related to the other morphological changes in eosinophils in EoE. These findings reveal that eosinophils in EoE esophageal biopsy specimens are abnormal with greater than 80% showing cytolysis, and, therefore, that evaluation by light microscopy after hematoxylin and eosin (H&E) staining may not accurately reflect eosinophil numbers or involvement.

3.2 Introduction

Eosinophilic esophagitis (EoE) is an increasingly common disease characterized by eosinophil invasion of the esophageal mucosa, where eosinophil granulocytes (a type of white blood cell) accumulate and are activated. Activated eosinophils release granule proteins into both epithelial and sub-mucosal layers [1-4]. Evidence of eosinophil activation includes expression of membrane markers, formation of cytoplasmic vesicles, and changes in eosinophil granules with loss of electron density of the granule cores [5]. In EoE, eosinophil granule proteins including major basic protein 1, eosinophil derived neurotoxin (also known as Ribonuclease2), eosinophil peroxidase, and eosinophil cationic protein (also known as Ribonuclease3) are localized on esophageal epithelial

cells [4, 6]. Remarkably, eosinophil derived neurotoxin is extensively deposited on the diseased esophagus implying eosinophil activation and release of eosinophil derived neurotoxin from its storage site in the granule matrix [4]. However, the mechanisms responsible for eosinophil activation and the process by which granule proteins are deposited in the disease-affected esophagus remain incompletely described.

Secretion of eosinophil granule proteins occurs by eosinophil cytolysis and release of intact granules, which then liberate granule proteins, or by piecemeal degranulation ("piece by piece" release of eosinophils granule contents), a unique secretory process characterized by transport of vesicles to the cell surface [7, 8]. Tubulovesicular carriers, referred to as sombrero vesicles because they resemble the well-known Mexican hat, have been identified as playing a key role for transporting eosinophil proteins from granules to the plasma membrane for extracellular release [8]. Therefore, loss of membrane integrity is associated with cytolysis, and the presence of cytoplasmic cytoplasmic vesiculation, including sombrero vesicles, is taken as evidence of piecemeal degranulation

Here we identified and quantified eosinophil degranulation patterns by transmission electron microscopy in esophageal biopsy specimens from patients with EoE. The patterns were classified and graded according to cell membrane integrity, cytoplasmic vesiculation, granule morphology with respect to core staining and granule membrane integrity, and the occurrence of extracellular granules.

3.3 Materials and Methods

3.3.1 Patients. Nine patients (3 female, 6 male) were randomly selected from 20 patients participating in a study of omalizumab treatment in EoE (IRB 0013623; A Pilot Study of the Treatment of Eosinophilic Esophagitis With Omalizumab, ClinicalTrials.gov Identifier: NCT00123630). All of these patients satisfied diagnostic criteria for EoE [3]. Esophageal biopsy specimens were obtained during endoscopy concurrently for histology and for transmission electron microscopy at baseline before entering the study. Maximum esophageal eosinophil counts derived from examination after staining formalin-fixed biopsy specimens with hematoxylin and eosin (H&E) for individual patients are included in Table 3.1 (referred to in Results, below). All patients had at least 15 eosinophils per high power field (hpf) at 400X magnification in at least one biopsy specimen after high dose acid suppression therapy (twice daily proton pump inhibitor) for 8 weeks and before commencing treatment with omalizumab (or placebo control).

3.3.2 Electron microscopy. Tissue specimens were fixed in 2.5% glutaraldehyde, postfixed in 4% osmium tetroxide, dehydrated in graded ethanol, and stained with uranyl acetate and Reynolds lead citrate. A total of 18 tissue blocks, one biopsy specimen from proximal and distal esophagus from each of the 9 patients, were sectioned. Thin sections (90 μm thick) from each block were mounted on separate electron microscopy grids and then examined by transmission electron microscopy (Hitachi H7100, Gatan digital camera). For each section, the operator systematically scanned across the grid left to right and top to bottom at 2000 X magnification and photographed every eosinophil and all granules, both intracellular and extracellular,

identified based on the distinctive morphology of the cells and granules, particularly the characteristic cytoplasmic granule cores. The tissue sections from the distal and proximal esophagus specimens from each patient were evaluated together.

3.3.3 Eosinophil classification. A total of 1672 images were acquired during the grid scans, and all were examined and graded. Three graders (HS, LHH, and GJG) individually and independently inspected each image. Averages of the three graders are reported. (Detailed averages and standard deviations of 1672 electron photomicrographs graded by three individuals are provided in Appendix C.) Eosinophils and their granules in the images were evaluated based on cell membrane integrity, occurrence of cytoplasmic vesiculation recording the specific presence of sombrero vesicles, granule morphology, and occurrence of extracellular granules. Eosinophils that were only partially captured within an image were not graded.

Figures 3.1-3.5 show a gallery of findings in the images analyzed that were defined and inventoried: 1. Normal eosinophil (without granule changes, no cytoplasmic vesiculation, and no cytoplasmic membrane disruption, Figure 3.1); 2. Intracellular eosinophil granules displaying reversal of staining (core relatively radiolucent compared to the matrix, Figure 3.2); 3. Prominent cytoplasmic vesiculation, including piecemeal degranulation (tubulovesicular development with sombrero vesicles, Figures 3.2, 3.3, and 3.4); 4. Occurrence of extracellular eosinophil granules (individual eosinophil granules or clusters of fewer than 5 eosinophil granules with loss of cell membrane and/or surrounding cytoplasm, Figure 3.5). Cytoplasmic membrane integrity was classified as intact (no membrane loss), mainly intact ($\leq$20% membrane loss), partially disrupted (>20% membrane loss), or fully disrupted (no recognizable

membrane). Each category was tabulated only once per image, although multiple categories could be marked for that image. For example, if in one electron micrograph, 10 free granules were present, 6 displaying reversal of staining and 4 without granule changes, each category (reversal of core staining and no granule changes) was counted once.

3.4 Results

We examined the ultrastructural appearance of eosinophils and their granules in esophageal biopsy specimens by transmission electron microscopy from 9 patients with EoE by examining 1672 electron microscopic images obtained from systematically scanning grids of tissue sections from the specimens. We observed a spectrum of morphologies ranging from rare intact eosinophils with appearances comparable to eosinophils in peripheral blood of healthy persons (Figure 3.1) [9], to many cells showing disruption and loss of cytoplasmic membranes (Figure 3.4), to prominent cytoplasmic changes (Figures 3.2 and 3.3), including cytoplasmic vesiculation, especially with sombrero vesicles, and granules showing reversal of core staining (Figure 3.2) and to individual extracellular eosinophil granules scattered in the intercellular spaces among esophageal epithelial cells (Figure 3.5). We scored each image for the presence of eosinophils and extracellular granules; 809 of the images showed one or more eosinophils, defined as at least 5 eosinophil granules in a cluster and in close proximity regardless of membrane integrity, and 1185 images showed extracellular granules, defined by characteristic core morphology with fewer than 5 clustered in an area of the image. We further categorized eosinophils as to their specific

features including whether they had intact or disrupted cell membranes, by the presence of cytoplasmic vesicles including sombrero vesicles, because these have been identified in association with eosinophil piecemeal degranulation [8], and, for the intracellular granules, similar to the extracellular granules, by granule core morphology, particularly whether the granules showed reversal of core staining.

In the 1672 electron micrographic images, 900 eosinophils were recognized; the overall distribution of findings in these 900 eosinophils is represented in the Venn diagram in Figure 3.6 including overlap when more than one finding was observed. Of the 900 eosinophils, 80.6% showed loss of membrane integrity, varying from ≤20% loss to total loss of cytoplasmic membrane. Of the 80.6% eosinophils with loss of membrane integrity, 43% had fully disrupted cytoplasmic membranes. Considering cytoplasmic changes within the eosinophils, we found that most of the eosinophils, 91.6%, displayed increased cytoplasmic vesiculation, with the presence of sombrero vesicles in greater than 50%; sombrero vesicles could not always be identified definitively in the eosinophils with vesiculation, in part, likely because the sections were thin and may not have included identifying features and likely because the extent of the vesiculation in some of the cells obfuscated the defining appearance of sombrero vesicles. Most of the 900 eosinophils, 88%, demonstrated granule changes, especially reversal of core staining. Most of the eosinophils examined in the images displayed more than one of the categorized features; for example, as diagramed in Figure 3.6, 70.3% of the 900 eosinophils showed loss of membrane integrity, cytoplasmic vesiculation including with sombrero vesicles, and reversal of granule core staining. Other overlapping features are detailed in the legend to Figure 3.6. Very few of the eosinophils (1.3%) appeared

normal (not on diagram) with intact membranes and no evidence of cytoplasmic vesiculation or granule changes.

We observed a surprising frequency of extracellular eosinophil granules in these esophageal specimens. As noted above, in 1672 electron photomicrographs, 1185 images (71%) showed eosinophil granules, recognizable by their characteristic morphology, clearly outside of cells (Figure 3.5). From the 1185 images of free granules, 48% showed abnormalities with loss of core density and/or granule membrane loss. In many images, a single granule was present without other eosinophil remnants. In other images, isolated eosinophil granules were found with remnants of cell structures such as nuclear fragments. Many of the free granules were in fields largely devoid of other structures suggesting the presence of tissue edema, likely in dilated intercellular spaces.

Table 3.1 summarizes information individually for each patient and presents observations including the maximum eosinophil counts in esophageal biopsy specimens by H&E histology and average percentages of common findings in the images, that is, extracellular eosinophil granules (71% of images, 1185 of 1672 electron photomicrographic images) and eosinophils showing both reversal of granule core staining and cytoplasmic vesiculation including sombrero vesicles (83.2%, 749 of 900 eosinophils), and proportions of normal eosinophils. The total number of images graded for each patient and the total number of eosinophils (excluding the free granules) are charted. Note that the data are presented in percentage of total number of images graded per patient for the extracellular granules and in percentage of the total number of eosinophils identified per patient for the combined features of cytoplasmic vesiculation

and reversal of granule core staining and for normal eosinophils. The results show that the patients with the highest IgE levels (patients 3 and 7), also had high proportions of images with extracellular granules and normal eosinophils, although the normal eosinophil numbers are small. Patient 7, with an IgE level of 609 IU/mL, had the highest percentage of free granules (93.2%).

3.5 Discussion

The diseases in which eosinophil degranulation is prominent and the processes by which eosinophils release granule proteins into tissues have been studied for almost three decades. Identification and isolation of eosinophil granule proteins permitted development of antibodies to recognize the granule proteins in tissues and investigate their participation in disease [10]. One of the first studies was of tissues from patients dying of bronchial asthma. As expected, striking eosinophil infiltration was present, but unexpectedly, dramatic deposition of the eosinophil granule major basic protein 1 occurred on bronchial epithelium, in mucous plugs and in respiratory epithelium [11]. Subsequent studies have largely confirmed the remarkable occurrence of eosinophil granule protein deposition in affected tissues from a wide variety of diseases [12-23]. Perhaps this is most striking in atopic dermatitis (an inflammatory skin disorder) in which intact eosinophils are not or minimally increased, but affected skin shows striking deposition of eosinophil granule proteins [24].

Studies of the mechanisms of eosinophil degranulation in diseased tissues show two key modes of granule protein release. Electron microscopic evidence demonstrates that, with eosinophil activation, there is loss of the usual granule core electron density

indicating that the core protein, major basic protein 1 [25], has been released [26]. Electron microscopic evidence also demonstrates cytolytic changes in eosinophils and the accompanying presence of extracellular eosinophil granules with intact cores, often with reversal of granule core staining [27, 28]. *In vitro* studies have shown secretion of eosinophil granule proteins by vesicular transport and, in particular, in association with tubulovesicular development including sombrero vesicles [8]. Thus, two predominant mechanisms of eosinophil degranulation are known, cytolytic degranulation and piecemeal degranulation. Cytolytic degranulation is shown by disruption of the cell membrane and granules deposited outside of cells (typically associated with increased inflammatory actions of eosinophils), whereas piecemeal degranulation is associated with cytoplasmic vesiculation [8]. Analyses of tissues from patients with atopic dermatitis showed evidence of both cytolytic disruption of eosinophil membranes and extracellular granules [28]. A quantitative study of the mechanisms of eosinophil degranulation in nasal polyps found that approximately 33% of eosinophils had undergone cytolysis, whereas most eosinophils showed evidence of piecemeal degranulation [7].

In this study, we found that almost all of the eosinophils invading the esophagus in EoE showed changes of activation and degranulation with marked cytoplasmic vesiculation and varying degrees of membrane disruption. These changes were associated with the release of intact, membrane-bound granules into the tissues. The proportion of eosinophils with no or one change was remarkably small; 1.3% of eosinophils appeared normal without change; eosinophils with cytoplasmic vesiculation and no loss of membrane integrity or reversal of granule core staining comprised 1.7%;

eosinophils with reversal of granule core staining and no loss of membrane integrity or cytoplasmic vesiculation comprised 2%; and eosinophils with disruption of membrane, no cytoplasmic vesiculation or reversal of granule core staining comprised 0.9%. Therefore, fewer than 6% of the eosinophils showed only one or none of the scored features and approximately 93% showed two or three of the features.

Figure 3.7 is a bar graph summarizing the distribution of features observed in the eosinophils in the biopsy specimens from the 9 patients with EoE based on the evidence that activated and degranulating eosinophils exhibit reversal of granule core staining and piecemeal degranulation. In comparison to the previous study showing the predominance of piecemeal degranulation over cytolysis [7], we observed that the majority of eosinophils, over 80%, undergoing piecemeal degranulation and reversal of granule core staining also showed cytolysis as evidenced by loss of cytoplasmic membrane integrity, 70.3% (see Figure 3.6). This finding suggests that cytoplasmic vesiculation leads to enhanced secretion and eosinophil cytolysis.

Another striking finding in these studies was the frequency of extracellular eosinophil granules in EoE tissues indicating that cytolysis results in liberation of granules into extracellular sites. Studies of isolated eosinophil granules have demonstrated that extracellular granules retain secretory activity and, thus, have the ability to secrete individual granule proteins into tissues after stimulation [29]. Notably, prior studies demonstrated that striking eosinophil granule protein deposition occurs in EoE [4, 6]. The compilation of findings in this electron microscopic study along with the existing understanding of eosinophil activity provides strong evidence of eosinophil

activation with degranulation in EoE tissues including deposition of cytotoxic granule proteins.

The findings reported in this study further indicate that a large proportion of eosinophils in EoE biopsy specimens enumerated by light microscopy after H&E staining are undergoing cytolysis leading to release of granules and granule proteins onto esophageal tissues. The finding that approximately 80% of recognizable eosinophils by electron microscopy in biopsies from patients with EoE are undergoing cytolysis suggests that most of eosinophils counted by pathologists using light microscopy are, in fact, already showing membrane disruption and, thus, classifiable as dying cells. Along with the observations that striking eosinophil granule protein deposition occurs in EoE tissues, these observations provide compelling evidence that the full gamut of pro-inflammatory activities of the granule proteins is unleashed onto the epithelial cells. Moreover, it seems likely that eosinophil participation in EoE is only partly recognized by enumerating eosinophils. The possibility exists that, in some cases, the process of eosinophil cytolysis and loss of morphology is sufficiently advanced that few, if any, intact cells are recognizable. In these cases, one would overlook a diagnostic criterion for EoE when the effects of eosinophil inflammation are maximal. Overall, our findings imply that localization of eosinophil granule proteins, using immunostaining, for example for major basic protein 1 or cytochemical localization for eosinophil peroxidase, may be a better indicator of disease activity than counting of intact, and dying, eosinophils.

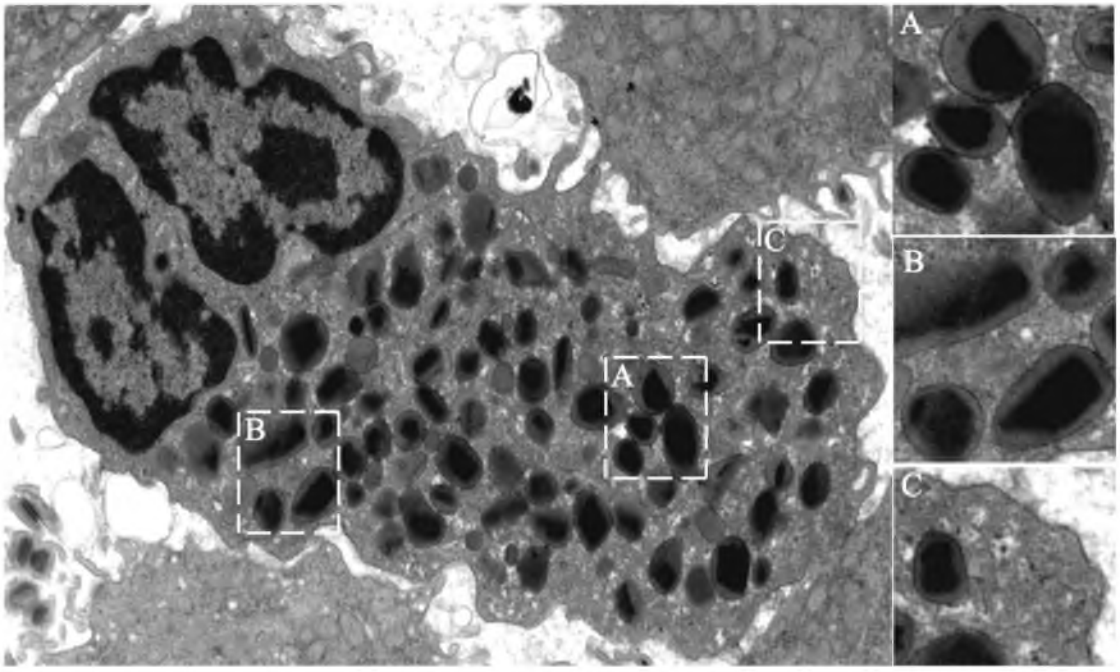

Figure 3.1. Eosinophil with normal granules, no evidence of cytoplasmic vesiculation, including sombrero vesicles and fully intact cytoplasmic membrane. A, B, and C show individual intact membrane-bound, cytoplasmic granules.

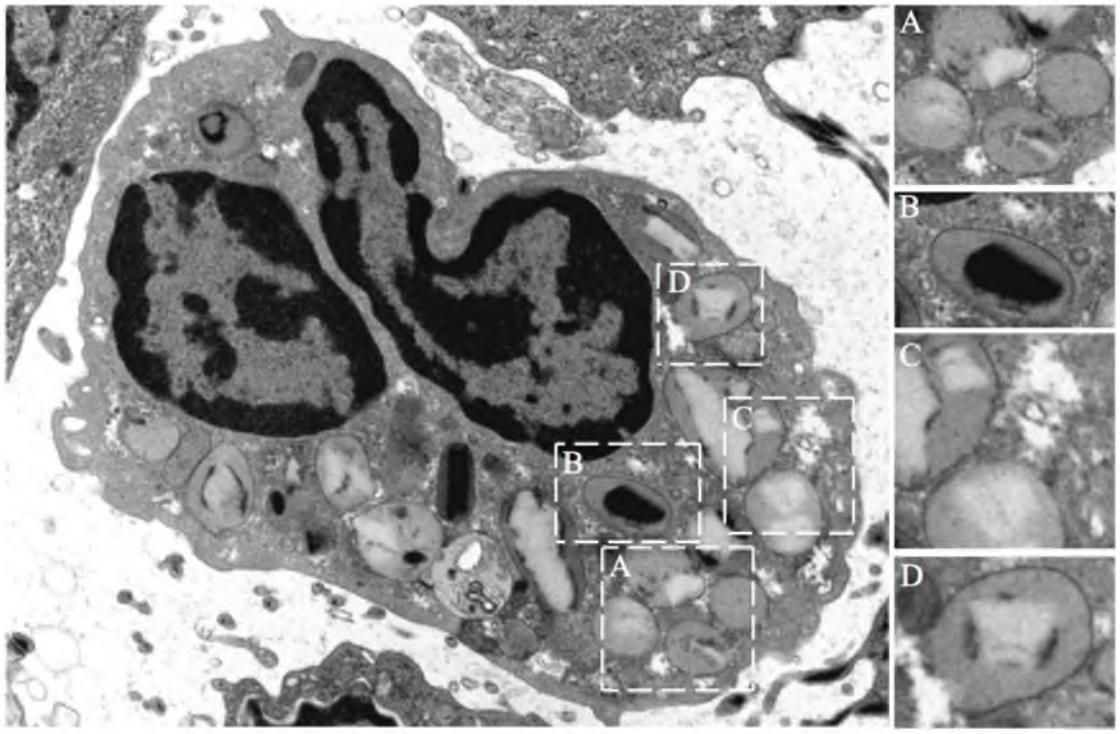

Figure 3.2. Eosinophil with intact cytoplasmic membrane showing reversal of granule core staining and cytoplasmic vesiculation. A, C, and D show reversal of granule core staining with radiolucent core areas. B shows an intact normal-appearing granule with an adjacent sombrero vesicle to the right.

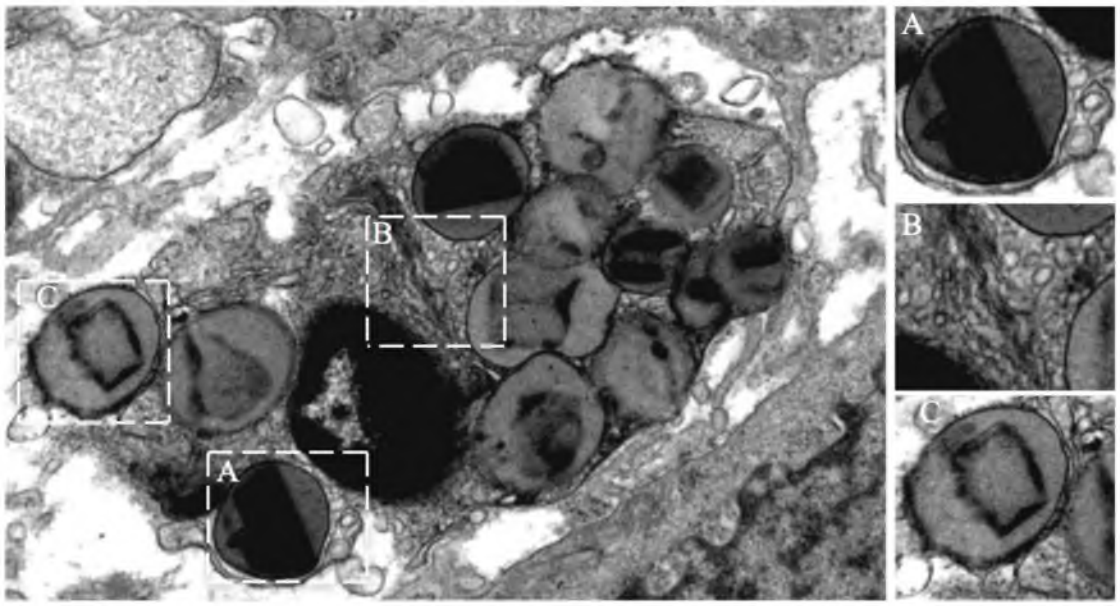

Figure 3.3. Eosinophil showing partial cytoplasmic membrane disruption, granules with reversal of core staining, overall increased cytoplasmic vesiculation with sombrero vesicles. A shows an intact granule and sombrero vesicles. B shows cytoplasmic vesicles. C shows a cytoplasmic granule with reversal of core staining.

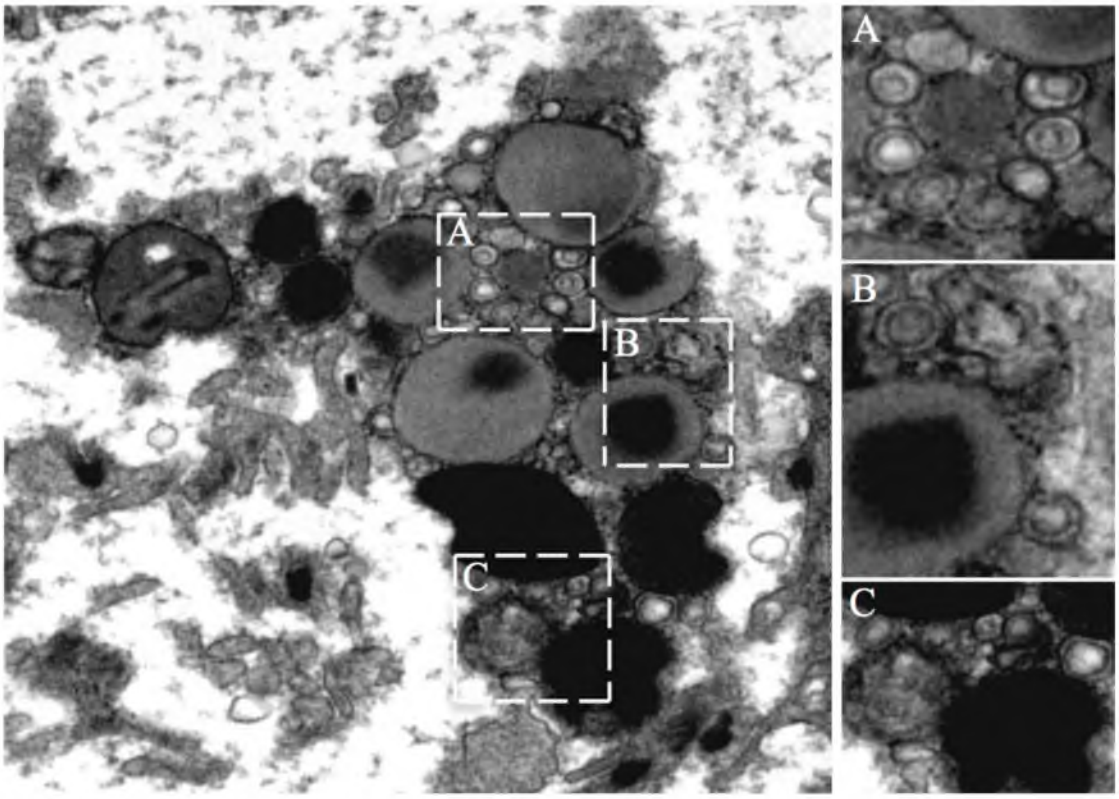

Figure 3.4. Eosinophil showing fully disrupted cell membrane and cytoplasmic vesiculation. A, B, and C show numerous sombrero vesicles.

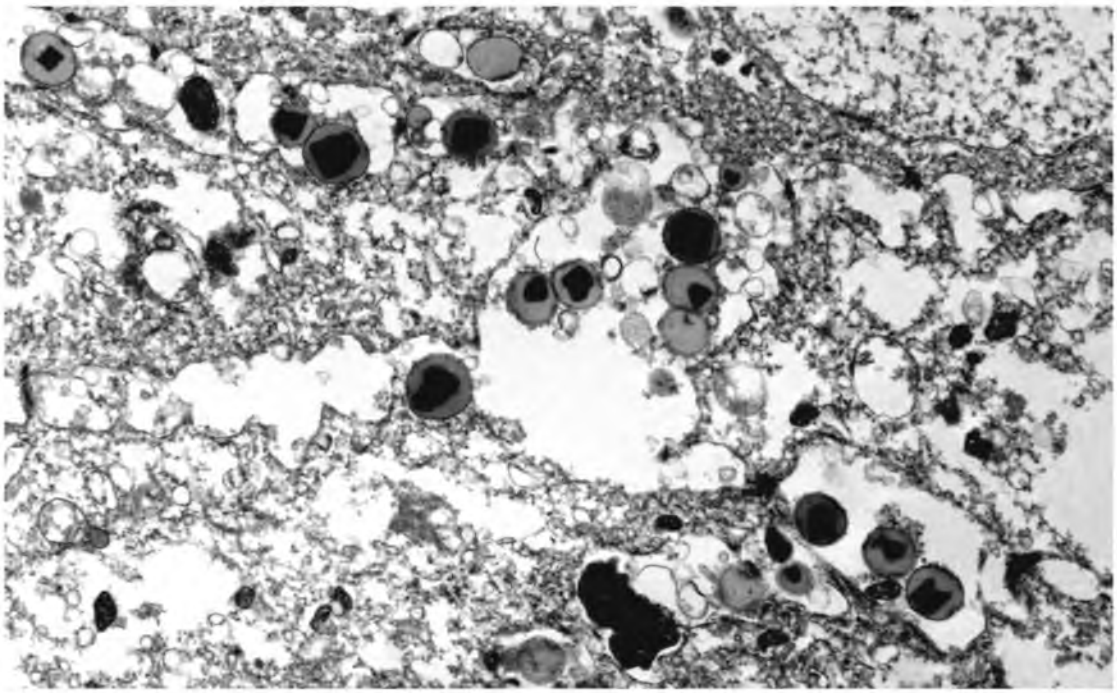

Figure 3.5. Eosinophil granules in epithelial intercellular spaces.

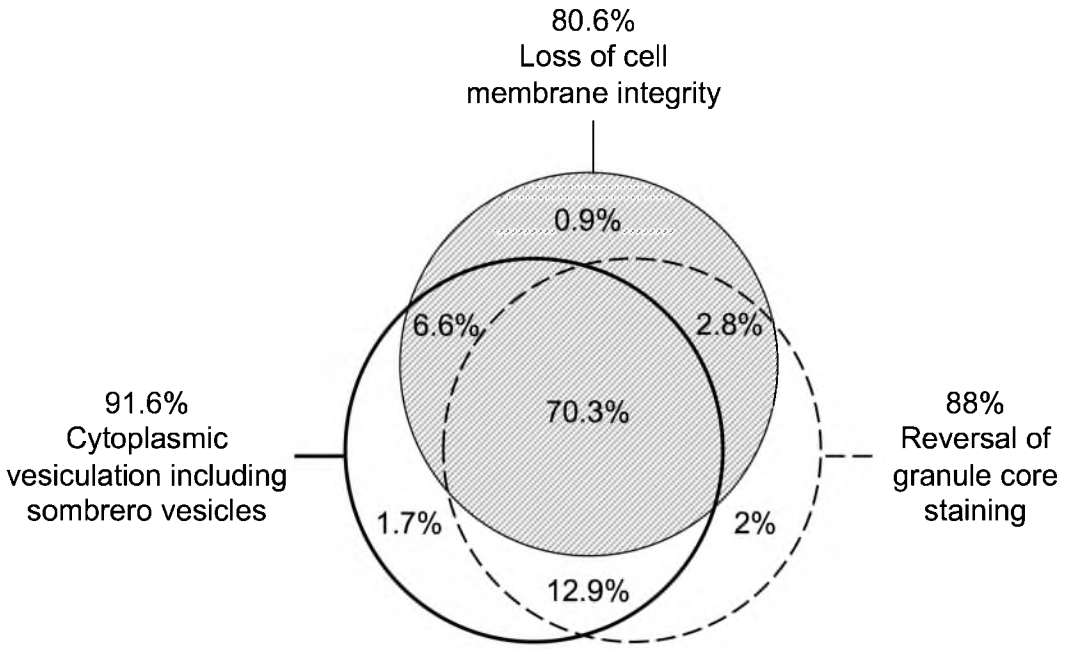

Figure 3.6. Venn diagram of the average percentage of findings in EoE esophageal eosinophils (n = 900 eosinophils) by transmission electron microscopy scored by 3 observers based on membrane integrity, cytoplasmic vesiculation including sombrero vesicles, and reversal of granule core staining. As represented here, 70.3% of the eosinophils showed all of the three features. Considering eosinophils with two features, 76.9% (70.3%+6.6%) showed loss of membrane integrity and cytoplasmic vesiculation including sombrero vesicles; 73.1% (70.3%+2.8%) showed loss of membrane integrity and reversal of granule core staining; and 83.2% (70.3%+12.9%) showed cytoplasmic vesiculation with sombrero vesicles and reversal of granule core staining. Relatively small proportions of the eosinophils demonstrated only one feature, 0.9% showed loss of membrane integrity alone, 1.7% showed cytoplasmic vesiculation with sombrero vesicles alone, and 2% with reversal of granule core staining alone. Only 1.5% of eosinophils showed cytoplasmic edema with no loss in membrane integrity and no evidence of cytoplasmic vesiculation or reversal of staining (not on diagram), and 1.3% of the eosinophils appeared as normal (intact) without the changes described above (not on diagram).

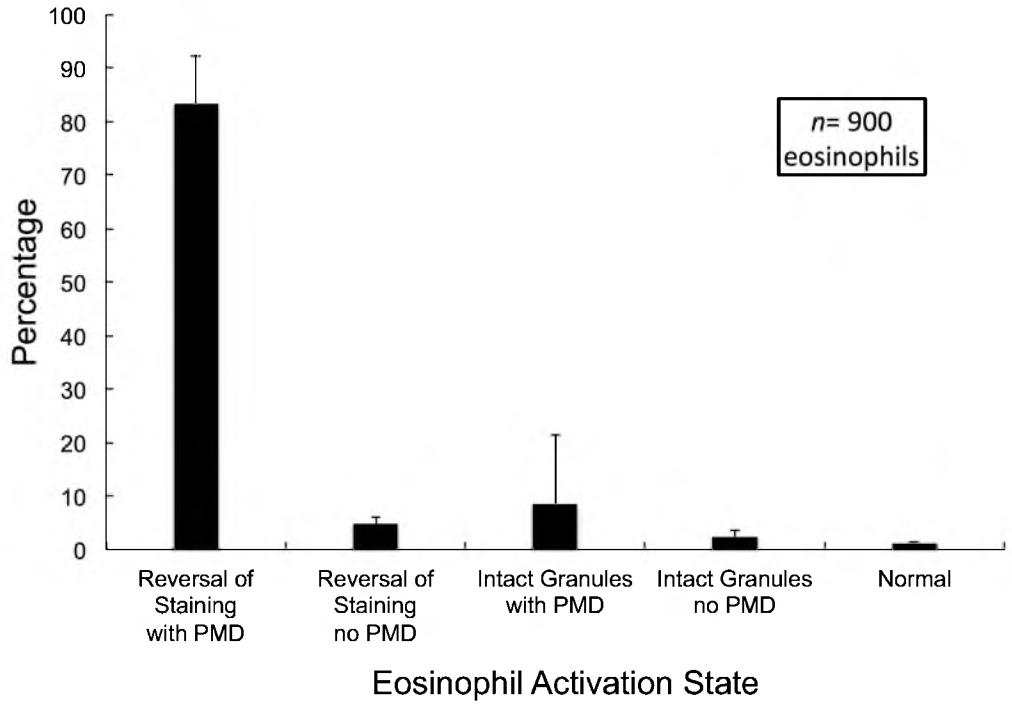

Figure 3.7. Percentage of eosinophils with cytoplasmic vesicles and granule abnormalities from electron microscopy of 9 EoE patients (PMD = piecemeal degranulation).

Table 3.1. Patient's age, gender, serum IgE level, maximum eosinophil (Eos) numbers by H&E histology of formalin-fixed esophageal biopsy specimens, number of electron micrographic images from examing esophageal biopsy specimen grids and number of eosinophils (excluding free granules) in the images, and average percentage of eosinophils showing piecemeal degranulation (PMD) and reversal of staining, and the average percentage of normal eosinophils.

Patient No.	Age / Gender	*IgE Level	Maximum Eos per hpf H&E	Number of Images / Number of Eos	Percent of Free Granules **	Percent of Eos Showing PMD and Reversal of Staining ***	Percent of Normal Eos ***
1	50 / M	116	28	253 / 120	76.4	84.5	0.0
2	28 / M	82	33	263 / 188	67.4	73.2	0.2
3	29 / M	554	28	226 / 92	74.3	79.3	4.0
4	44 / F	32	27	114 / 78	62.0	91.5	0.9
5	36 / F	171	30	169 / 131	55.8	78.4	2.0
6	23 / M	53	16	129 / 68	71.8	97.0	1.5
7	36 / F	609	30	185 / 33	93.2	72.7	7.1
8	29 / M	82	30	188 / 110	65.7	92.1	0.0
9	26 / F	35	47	145 / 80	65.3	89.6	0.8

* International units per mL.

** Calculated based on number of images showing free granules/total number of images x 100.

*** Calculated based on number of eosinophils showing these abnormalities/total number of eosinophils x 100.

hpf= high power field (400X magnification).

3.6 References

1. Straumann A, Spichtin HP, Grize L, Bucher KA, Beglinger C, Simon HU. Natural history of primary eosinophilic esophagitis: a follow-up of 30 adult patients for up to 11.5 years. Gastroenterology 2003; 125: 1660-69.

2. Furuta GT, Liacouras CA, Collins MH, Gupta SK, Justinich C, Putman PE, et al. Eosinophilic esophagitis in children and adults: a systematic review and consensus recommendations for diagnosis and treatment. Gastroenterology 2007; 133: 1342-63.

3. Liacouras CA, Furuta GT, Hirano I, Atkins D, Attwood SE, Bonis PA, et al. Eosinophilic esophagitis: updated consensus recommendations for children and adults. J Allergy Clin Immunol 2011; 128: 3-20 e26; quiz 21-22.

4. Kephart GM, Alexander JA, Arora AS,Romero Y, Smyrk TC, Talley NJ, et al. Marked deposition of eosinophil-derived neurotoxin in adult patients with eosinophilic esophagitis. Am J Gastroenterol 2010; 105: 298-307.

5. Justinich CJ, Ricci A, Jr., Kalafus DA, Treem WR, Hyams JS, Kreutzer DL. Activated eosinophils in esophagitis in children: a transmission electron microscopic study. J Pediatr Gastroenterol Nutr 1997; 25: 194-8.

6. Protheroe C, Woodruff SA, de Petris G, Mukkada V, Ochkur SI, Janarthanan S, et al. A novel histologic scoring system to evaluate mucosal biopsies from patients with eosinophilic esophagitis. Clin Gastroenterol Hepatol 2009; 7: 749-55.

7. Erjefalt JS, Andersson M, Greiff L, Krosgren M, Gizychi M, Jeffrey PK, et al. Cytolysis and piecemeal degranulation as distinct modes of activation of airway mucosal eosinophils. J Allergy Clin Immunol 1998; 102: 286-94.

8. Melo RC, Spencer LA, Perez SA, Neves JS, Bafford SP, Morgan ES, et al. Vesicle-mediated secretion of human eosinophil granule-derived major basic protein. Lab Invest 2009; 89: 769-81.

9. Gleich GJ, Zucker-Franklin D. Eosinophils. In: Zucker-Franklin D., Grossi CE, editors. Atlas of Blood Cells: Function and Pathology. Edi Ermes; 2003. p. 299-340.

10. Gleich GJ, Adolphson CR. The eosinophilic leukocyte: structure and function. Adv Immunol 1986; 39: 177-253

11. Filley WV, Holley KE, Kephart GM, Gleich GJ. Identification by immunofluorescence of eosinophil granule major basic protein in lung tissues of patients with bronchial asthma. Lancet 1982; 2: 11-16.

12. Kephart GM, Gleich GJ, Connor DH, Gibson DW, Ackerman SJ. Deposition of eosinophil granule major basic protein onto microfilariae of Onchocerca volvulus in the skin of patients treated with diethylcarbamazine. Lab Invest 1984; 50: 51-61.

13. Peters MS, Schroeter AL, Gleich GJ. Immunofluorescence identification of eosinophil granule major basic protein in the flame figures of Wells' syndrome. Br J Dermatol 1983; 109: 141-48.

14. Peters MS, Schroeter AL, Kephart GM, Gleich GJ. Localization of eosinophil granule major basic protein in chronic urticaria. J Invest Dermatol 1983; 81: 39-43.

15. Gleich GJ, Schroeter AL, Marcoux JP, Sachs MI, O'Connell EJ, Kohler PF. Episodic angioedema associated with eosinophilia. N Engl J Med 1984; 310: 1621-26.

16. Tai PC, Ackerman SJ, Spry CJ, Dunnette S, Olsen EG, Gleich GJ. Deposits of eosinophil granule proteins in cardiac tissues of patients with eosinophilic endomyocardial disease. Lancet 1987; 1: 643-47.

17. Harlin SL, Ansel DG, Lane SR, Myers J, Kephart GM, Gleich GJ. A clinical and pathologic study of chronic sinusitis: the role of the eosinophil. J Allergy Clin Immunol 1988; 81: 867-75.

18. Kephart GM, Andrade ZA, Gleich GJ. Localization of eosinophil major basic protein onto eggs of Schistosoma mansoni in human pathologic tissue. Am J Pathol 1988; 133: 389-96.

19. Hamann KJ, Kephart GM, Kazacos KR, Gleich GJ. Immunofluorescent localization of eosinophil granule major basic protein in fatal human cases of Baylisascaris procyonis infection. Am J Trop Med Hyg 1989; 40: 291-97.

20. Hertzman PA, Blevins WL, Mayer J, Greenfield B, Ting M, Gleich GJ. Association of the eosinophilia-myalgia syndrome with the ingestion of tryptophan. N Engl J Med 1990; 322: 869-73.

21. Songsiridej V, Peters MS, Dor PJ, Ackerman SJ, Gleich GJ, Busse WW. Facial edema and eosinophilia. Evidence for eosinophil degranulation. Ann Intern Med 1985; 103: 503-6.

22. Leiferman KM, Fujisawa T, Gray BH, Gray BH, Gleich GJ. Extracellular deposition of eosinophil and neutrophil granule proteins in the IgE-mediated cutaneous late phase reaction. Lab Invest 1990; 62: 579-89.

23. Noguchi H, Kephart GM, Colby TV, Gleich GJ. Tissue eosinophilia and eosinophil degranulation in syndromes associated with fibrosis. Am J Pathol 1992; 140: 521-28.

24. Leiferman KM, Ackerman SJ, Sampson HA, Haugen HS, Venencie PY, Gleich GJ. Dermal deposition of eosinophil-granule major basic protein in atopic dermatitis. Comparison with onchocerciasis. N Engl J Med 1985; 313: 282-85.

25. Peters MS, Rodriguez M, Gleich GJ. Localization of human eosinophil granule major basic protein, eosinophil cationic protein, and eosinophil-derived neurotoxin by immunoelectron microscopy. Lab Invest 1986; 54: 656-62.

26. Dvorak AM. Ultrastructural evidence for release of major basic protein-containing crystalline cores of eosinophil granules in vivo: cytotoxic potential in Crohn's disease. J Immunol 1980; 125: 460-62.

27. Dvorak AM, Weller PF, Monahan-Earley RA, Letourneau L, Ackerman SJ. Ultrastructural localization of Charcot-Leyden crystal protein (lysophospholipase) and peroxidase in macrophages, eosinophils, and extracellular matrix of the skin in the hypereosinophilic syndrome. Lab Invest 1990; 62: 590-607.

28. Cheng JF, Ott NL, Peterson EA, George TJ, Hukee MJ, Gleich GJ, et al. Dermal eosinophils in atopic dermatitis undergo cytolytic degeneration. J Allergy Clin Immunol 1997; 99: 683-92.

29. Neves JS, Perez SA, Spencer LA, Melo RC, Reynolds L, Ghiran I, et al. Eosinophil granules function extracellularly as receptor-mediated secretory organelles. Proc Natl Acad Sci U S A 2008; 105: 18478-83.

CHAPTER 4

^{99M}TECHNETIUM-LABELED HEPARIN: A NEW APPROACH TO DETECTION OF EOSINOPHILIC ESOPHAGITIS-ASSOCIATED INFLAMMATION[1]

4.1 Abstract

Here we identify and test an innovative imaging strategy to detect inflammation in eosinophilic esophagitis (EoE). As eosinophils degranulate, they deposit markedly basic proteins including major basic protein (MBP-1) not normally present in the esophagus. Here we evaluate binding of a radiolabeled anionic probe to these proteins in diseased esophageal tissue. We exposed biopsy specimens from EoE patients to heparin labeled with technetium 99m (^{99m}Tc). We found significant binding of ^{99m}Tc-heparin to eosinophil enriched tissues using a single photon emission computed tomography (SPECT) instrument. These findings identify ^{99m}Tc-heparin as a potential probe for investigation of eosinophil driven inflammation associated with EoE.

[1] The material presented in this chapter has been accepted in Journal of Allergy and Clinical Immunology (JACI). 2013. Epub a head of print. Reprinted and adapted with permission from Elsevier.

4.2 Introduction

In EoE, eosinophils infiltrate the esophagus, where they degranulate, releasing cytotoxic granule proteins, including MBP-1. However, the variability of eosinophil involvement presents a diagnostic challenge to the gastroenterologist as current diagnosis requires invasive esophagogastroduodenoscopy (EGD) with a minimum of 5 biopsies, representing less than 0.7% of the esophageal surface. The disease is known to be patchy, which may result in underdiagnosis, particularly for mild to moderately involved patients [1, 2]. To understand this disease, improved, preferably noninvasive, methods to characterize the severity of eosinophil-associated inflammation are required.

We propose a novel strategy to localize cationic eosinophil granule proteins using anionic heparin radiolabeled with ^{99m}Tc. Proteins deposited in the esophagus after eosinophil degranulation, such as MBP-1, are primary candidates, because they are absent in the normal esophagus. Here we hypothesize that ^{99m}Tc-heparin binds avidly to cationic eosinophil granule proteins, including MBP-1, and can be used to determine the presence of eosinophil products in the diseased esophagus using SPECT imaging [3]. Previous studies have shown that MBP-1 is deposited in the esophageal tissues and is available for binding [4, 5]. Heparin is a promising candidate because it has a very high negative charge density (MBP-1 has a correspondingly high density of positively charged moieties) and is not absorbed from the GI tract [6-8].

4.3 Materials and Methods

Solutions of stannous chloride (40 mg/mL, Sigma 243523) were prepared in deionized water under flowing nitrogen. A 0.5 mL aliquot was filtered and mixed with

1.00 mL NaCl (1.00 M) plus 150 mg of preservative free heparin (10,000 IU/mL, APP Pharmaceuticals, NDC 63323-543-02). Approximately 100 mCi of freshly eluted ^{99m}Tc was added and mixed for 30 minutes at room temperature. Aliquots containing approximately 10 mCi of ^{99m}Tc and 20 mg of heparin were removed for tissue experiments. The labeling efficiency, measured by paper chromatography Whatman # 31 with acetone, showed more than 98% binding of heparin to ^{99m}Tc. Radiolabeled heparin was also analyzed by Sephadex G25 column chromatography (HiTrap 5 mL desalting columns, GE healthcare, 17140801) with 0.15 M NaCl as the elution buffer, and 1.0 mL fractions were collected. Radioactivity eluted at fraction 4 (free ^{99m}Tc elutes at fraction 13), demonstrating that all of the ^{99m}Tc eluted at the void volume and confirming that there is no unbound ^{99m}Tc in the radiolabeled heparin. The stability of ^{99m}Tc-heparin in an acidic environment was tested by diluting in artificial gastric juice (Carolina Biological Supply Company, Burlington, NC, 864603) and showing that its properties were unaltered using both paper chromatography and Sephadex G25.

Esophageal biopsies were collected from normal subjects and patients participating in a prior elemental diet study (IRB 00040035 University of Utah) and kept frozen at -70°C. Biopsies from each patient were selected for histological analysis for eosinophil density or radiolabeling. Biopsies from normal subjects and EoE patients who resolved their esophageal eosinophilia under the elemental diet (hence the designation “resolved”) were chosen as negative controls. Tissues from normal, resolved EoE, and active EoE patients were incubated with the ^{99m}Tc-heparin, washed in buffered saline, and imaged using SPECT.

The activity of radiolabeled biopsy tissues was measured using a dose calibrator (Capintec model CRC-15R). Two-dimensional planar static images of the radiolabeled biopsies were obtained using the Ecam SPECT instrument (Siemens). The images were acquired for 3 minutes each using a 1.0 magnification, 256 by 256 matrix size. Correlation between eosinophil densities and SPECT counts obtained by 2D imaging were evaluated by Spearman rank correlation analysis. The cutoff SPECT intensity between active (e.g., ≥15 eosinophils per high power field (hpf), equivalent to ≥68 eosinophils/mm^2) and resolved (e.g., <15 eosinophils/hpf) EoE cases was determined by minimizing the difference between Gaussian fits. SPECT intensities above the cutoff were compared to those below using a Student *t* test. Data were fit with power law, exponential, and second order polynomial correlations. The power law fit displayed the highest r^2 value and was used to determine the eosinophil density corresponding to each cutoff.

4.4 Results

Table 4.1 presents the SPECT counts of each biopsy, summarizing its radioactivity and eosinophil density. Histopathological analyses confirmed that only samples 1-5 had eosinophil levels ≥15 eosinophils/high power field (hpf). The images (Figure 4.1) suggest that active EoE cases can be differentiated from resolved EoE (EoE patients treated) cases using this technique. Indeed, the Spearman rank correlation analysis finds a monotonic correlation between eosinophil density and SPECT count (r=0.67; p<0.05). Remarkably, even though the eosinophil densities are derived from the same patient but not from the same biopsy specimen used for SPECT imaging,

nevertheless, tissues from inflamed patients displayed significant binding to ^{99m}Tc-heparin that correlates with eosinophil density.

Using 15 eosinophils as the threshold for inflammation suggests a cutoff in SPECT intensity of 39000. However, this is not a clean cut off because sample 5, which has an eosinophil density of 21 eosinophils/hpf, lies below the cutoff. The alternative is to recognize that sample 6 has 10 eosinophils, which may be associated with significant MBP-1 release. Grouping samples 1-6 as inflamed and samples 7-8 as uninflamed finds a cutoff in SPECT intensity of 22400. The corresponding eosinophil density obtained via a power law fit is 2.6 eosinophils/hpf, indicating the sensitivity of this assay for eosinophil granule products.

4.5 Discussion

These proof-of-principle experiments clearly demonstrate that, first, heparin can be labeled with ^{99m}Tc in the presence of fresh stannous chloride without any chelating agent. Second, eosinophil density correlates with ^{99m}Tc emission as measured both in a well counter and by SPECT. Third, eosinophil enriched tissues can be distinguished from eosinophil poor tissues using ^{99m}Tc-heparin conjugate and SPECT quantitation (The correlation between the activity and SPECT intensity is further demonstrated in Appendix D). Yet, the analysis finds that 15 eosinophils/hpf may not be the best cutoff to distinguish granule protein deposition. For example, our analysis finds significant SPECT counts at 10 eosinophils/hpf (see sample 6 in Table 4.1). Some variation around the nominal cutoff of 15 eosinophils/hpf is not unexpected because eosinophil presentation in EoE is known to be patchy, the eosinophil density and SPECT count are

not from identical biopsies but from the same patient, and some eosinophils may have degranulated completely leaving only the MBP-1 signature [2]. While the full set of all proteins that bind ^{99m}Tc-heparin remains unclear, we assume they are likely derived from eosinophils because of the cationicity of the eosinophil granule proteins and their known abilities to bind heparin. Other products derived from mast cells, such as mast cell tryptase, may also bind ^{99m}Tc-heparin because tryptase is known to bind to heparin [9,10]. However, prior studies discourage belief that tryptase deposition is wide spread [11].

This is the first and only study to experimentally evaluate radiolabeled contrast agents for detection of EoE-associated inflammation. Further studies are underway to rigorously validate this technique as an assay for eosinophil involvement and to evaluate oral administration of ^{99m}Tc-heparin in the presence of a mucosal layer and esophageal peristalsis. Although radioactivity offers considerable sensitivity as demonstrated, the binding of the heparin conjugate to the eosinophil's granule proteins will likely depend on the esophageal residence time (or passage rate), which will have an impact on the sensitivity of the assay. However, we believe that the current findings are important because they provide a new avenue for quantification of inflammation. If successful, this strategy will provide unprecedented insight into the specific involvement of eosinophils and their granule proteins within the esophagus of EoE patients, which will create improved opportunities to understand the disease pathogenesis and treatment efficacy.

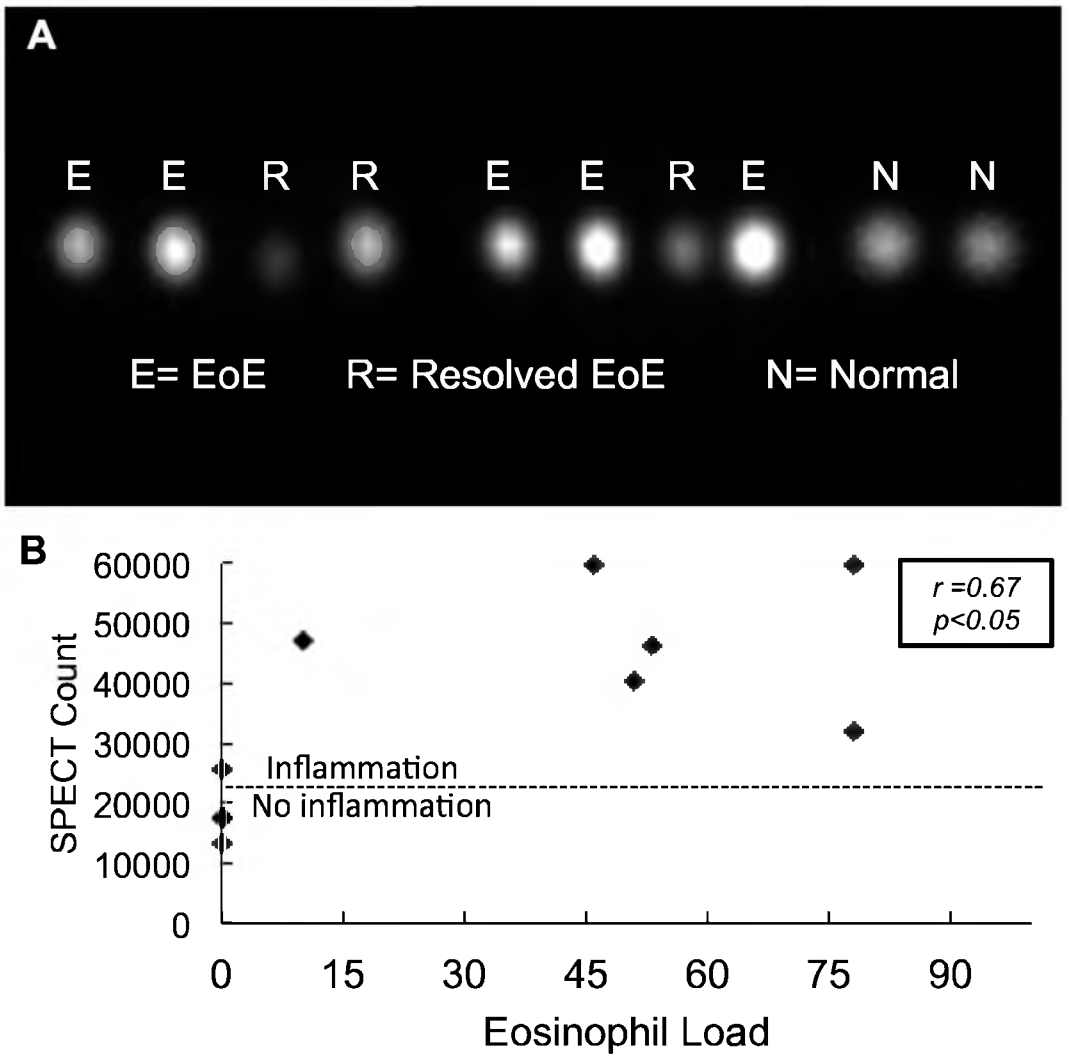

Figure 4.1. Experimental results. (a) 2D planar SPECT image of biopsies from normal, active EoE, and resolved EoE patients. From right the samples are from patient number: 5, 3, 7, 6, 4, 2, 8, 1, 9, and 10 in Table 4.1, respectively. Multiple SPECT images collected on multiple days were spliced together to make panel a (the four samples on the right, the four in the middle, and the two on the right were taken on different days). (b) SPECT count of biopsies as a function of eosinophil loads from the same patient.

Table 4.1. Radioactivity measurements, histological data, and the SPECT count of EoE versus control samples. Eosinophil load is based on 10 microscopy fields of view at 400X magnification.

Sample Number	Disease State	Eosinophil Loads	Activity μCi	SPECT Count
1	Active EoE	78	122.5	59634
2	Active EoE	51	87.1	40474
3	Active EoE	53	75.7	46457
4	Active EoE	46	98.1	59923
5	Active EoE	78	52.4	31780
6	Resolved EoE	10	100	47048
7	Resolved EoE	0	19.9	13202
8	Resolved EoE	0	27.7	17518
9	Normal	0	21.4	17740
10	Normal	0	41.3	25766

4.6 References

1. Gonsalves N, Policarpio-Nicolas M, Zhang Q, Rao MS, Hirani I. Histopathologic variability and endoscopic correlates in adults with eosinophilic esophagitis. GastrointestEndosc. 2006;64:313-9.

2. Saffari H, Peterson KA, Fang JC, Teman C, Gleich GJ, Pease LF. Patchy eosinophil distributions in an esophagectomy specimen from a patient with eosinophilic esophagitis: Implications for endoscopic biopsy. J Allergy Clin. Immunol. 2012;130:798-800.

3. Swaminathan GJ, Myszka DG, Katsamba PS, Ohunki LE, Gleich GJ, Acharya KR. Eosinophil-granule major basic protein, a C-type lectin, binds heparin. Biochemistry. 2006;44:14152-8.

4. Kephart GM, Alexander JA, Arora AS, Romero Y, Smyrk TC, Talley NJ, Kita H. Marked deposition of eosinophil-derived neurotoxin in adult patients with eosinophilic esophagitis. Am J Gastroenterol. 2010;105:298-307.

5. Talley NJ, Kephart GM, McGovern TW, Carpenter HA, Gleich GJ. Deposition of eosinophil granule major basic protein in eosinophilic gastroenteritis and celiac disease. Gastroenterology. 1992;103:137-45.

6. Hirash J, Warkentin TE, Shaughnessy SG, Anand SS, Halperin JL, Raschke R, Granger C, Ohman EM, Dalen JE. Heparin and low-molecular-weight heparin: mechanisms of action, pharmacokinetics, dosing, monitoring, efficacy, and safety. Chest. 2001;119:64S-94S.

7. Laforest MD, Colas-Linhart N, Guiraud-Vitaux F, Bok B, Bara L, Samama M, Marin J, Imbault F, Uzan A. Pharmacokinetics and biodistribution of technetium 99m labelled standard heparin and a low molecular weight heparin (enoxaparin) after intravenous injection in normal volunteers. Br J Haematol. 1991;77:201-208.

8. Kulkami PV, Parkey RW, Wilson JE 3rd, Lewis SE, Buja LM, Bonte FJ, Willerson JT. Modified technetium-99m heparin for the imaging of acute experimental myocardial infarcts. J Nucl Med. 1980;21:117-21.

9. Johnson DA, Barton GJ. Mast cell tryptases: examination of unusual characterisitcs by multiple sequence alignment and molecular modeling. Protein Sci. 1992;1:370-377.

10. Swaminathan, GJ, Myszka DG, Katsamba PS, Ohnuki LE, Gleich GJ, Acharya KR. Eosinophil-granule major basic protein, a C-type lectin, binds heparin. Biochemistry, 2005.;44(43):14152-8.

11. Perez GL, Peters MS< Reda AM, Butterfield JH, Peterson EA, Leiferman KM. Mast cells, neutrophils, and eosinophils in prurigo nodularis. Arch Dermatol. 1993;129:861-5.

12. Wang Y, Liu X, Hnatowich DJ. An improved synthesis of NHS-MAG3 for conjugation and radiolabeling of biomolecules with (99m) Tc at room temperature. Nat. Protoco. 2007;2(4):972-8.

CHAPTER 5

BIODISTRIBUTION AND DOSE ASSESSMENT OF ORALLY ADMINISTERED ^{99M}TC-HEPARIN IN MICE: A CONTRAST AGENT FOR EOSINOPHILIC ESOPHAGITIS ASSOCIATED INFLAMMATION[1]

5.1 Abstract

^{99m}Tc-heparin is a targeted contrast agent to identify localized inflammation in eosinophilic esophagitis (EoE), because the markedly basic eosinophil granule proteins, such as major basic protein 1 (MBP-1), that are deposited in inflamed regions of the esophagus and other gastrointestinal (GI) organs bind strongly to heparin. Here we evaluate the distribution of ^{99m}Tc-heparin administered orally to mice (C57-BL/6). ^{99m}Tc-heparin (0.5 mCi/mouse, 1.5 mg) was administered by oral gavage. Organ specific distributions and dosimetry were evaluated at 0.75, 1.5, 3, 6, 18, and 30 hours after administration. The results show that ^{99m}Tc-heparin is not absorbed significantly through the gastrointestinal (GI) tract into other bodily tissues. The highest observed activity occurred mainly in stomach, small intestine, and colon. These findings suggest

[1] The materials provided in this chapter have been submitted to Journal of Nuclear Medicine and Biology.

that ^{99m}Tc-heparin will be well tolerated in patients and initiate a new avenue for clinical detection of eosinophil-associated inflammation in the GI tract.

5.2 Introduction

Eosinophilic esophagitis (EoE) is an inflammatory disease characterized by infiltration of eosinophils into the esophagus and has become increasingly prominent over the past two decades [1-4]. This disease, which commonly affects children, adolescents, and young adults, induces difficult or painful swallowing (dysphagia) and food impaction necessitating emergency intervention [5,6]. In such cases, esophagogastroduodenoscopy (EGD) must be performed, in which a fiber optic tube is inserted into the upper gastrointestinal tract, to remove the obstruction.

The diagnosis of EoE is made by obtaining a medical history of dysphagia and performing EGD to obtain esophageal biopsies. The disease affects the esophagus in a spotty manner, such that 5 or preferably more biopsies should be obtained [6]. Biopsies are examined by a pathologist, and inflammation associated with 15 or greater eosinophils per high power field satisfies current diagnostic guidelines. However, treatment is challenging partly because of the variation in the degree of eosinophil infiltration within the esophagus, leading to possible underdiagnosis if the tissue is sampled insufficiently [6-8]. Also, patients may require 10-20 procedures to accurately determine the triggers to their disease, although such procedures are invasive and require anesthesia [9,10].

In EoE, eosinophils release their distinctive, markedly cationic granule proteins into the tissues of the affected esophagus. The primary proteins comprising eosinophil

granules include major basic protein (MBP-1), eosinophil derived neurotoxin (EDN, also known as Ribonuclease2), eosinophil peroxidase (EPO), and eosinophil cationic protein (ECP, also known as Ribonuclease3), and all of these proteins are cytostimulatory and cytotoxic [11-13]. Certain of the eosinophil granule proteins, such as MBP-1 and EPO, are among the most basic proteins in the body with isoelectric points approaching 12 [14]. Heparin, naturally present in the body, is a highly sulfated, polydisperse, linear polysaccharide and the most acidic polysaccharide in the human body [14]. Heparin is widely used as a clinical agent and is only biologically active when given by intravenous and subcutaneous routes, for prevention and treatment of thromboembolic disorders [16-18].

Realizing that these markedly basic proteins deposit in the inflamed esophagus, we previously demonstrated that localized inflammation can be detected by incubation of ^{99m}Tc-heparin [19]. We showed that heparin binds strongly to MBP-1 and found significant binding of ^{99m}Tc-heparin to eosinophil enriched tissues using single photon emission computed tomography (SPECT) [19,20]. These findings identify ^{99m}Tc-heparin as a potential probe to investigate eosinophil driven inflammation associated with EoE and, indeed, of the full gastrointestinal tract.

In the current study, we hypothesized that ^{99m}Tc-heparin remains in the GI tract and is not appreciably absorbed. This is important because limiting the biodistribution of the radionuclide to the GI tract attenuates the radiation risk profile. ^{99m}Tc-heparin was administered to healthy mice by oral gavage. Qualitative SPECT data and quantitative organ biodistributions were obtained to estimate the radiation dosimetry of ^{99m}Tc-heparin. We assayed for radioactivity in each organ of the gut, liver, lung, spleen,

kidney and other organs within a 30-hour period after the agent was administered. These data enable future studies exploring clinically the usefulness of ^{99m}Tc-heparin to detect EoE associated inflammation.

5.3 Material and Methods

5.3.1 Preparation of ^{99m}Tc-heparin. ^{99m}Tc-heparin was prepared by diluting stannous chloride (5 mg/mL, Sigma 243523) in water under flowing nitrogen. A 0.10 mL sample was filtered and mixed with 15 mg of preservative free heparin (10,000 IU/mL, APP Pharmaceuticals, LLC). Approximately 185 MBq (5 mCi) of freshly eluted ^{99m}Tc was added and mixed for 15 minutes at room temperature. Aliquots, 100 μL, containing approximately 18 MBq (0.5 mCi) of ^{99m}Tc and 1.5 mg of heparin, were removed for oral administration to mice. Quality control was checked by paper chromatography (Whatman no. 31) with acetone following manufacturer's instructions.

5.3.2 Quantitative organ biodistribution. All animal experiments were performed in accordance with approved University of Utah Institutional Animal Care and Use Committee (IACUC) protocols (Protocol Number: 12-07018). ^{99m}Tc-heparin (approximately 18 MBq (0.5 mCi)/mouse, 1.5 mg) was administered orally to healthy female 13-20 weeks adult mice (C57BL/6, Charles River Laboratories International, Inc., average weight = 29.14 ± 1.5 g) by oral gavage under brief restraint using a straight 1.5 in., 20-gauge needle with a 1.25 mm ball tip. Three animals per group were euthanized with CO_2 at 45 minutes, 1.5, 3, 6, 18, and 30 hours. With care to avoid cross-contamination, whole organs, blood, and hind leg muscle samples were harvested within approximately 20 minutes, weighed, and counted for up to 2 minutes in a Captus

3000 well counter (Bicorn model 2MW2/2-X NaI drilled well crystal detector in a Canberra 727 well). The proximal large intestine was considered to include the cecum plus 2 cm of the distal bowel, while the remainder was considered distal large intestine. Larynx and thyroid were harvested and measured together. Results were expressed as the percentage injected dose per gram of harvested organ (%ID/g).

5.3.3 SPECT imaging. To obtain qualitative images of ^{99m}Tc activity, mice were anesthetized with isoflurane gas (5% induction, 1-2% maintenance, IMWI/VetOne, Meridian, ID, Cat# 501017) and positioned prone on the scanner bed 40 minutes prior to euthanasia. SPECT/CT images of mice were acquired using an Inveon trimodality PET/SPECT/CT scanner (Siemens Preclinical Solutions, Knoxville, TN). A sensor (Biovet, France) was used to monitor the respiration rate of mice under anesthesia. CT images were first acquired consisting of 220 degrees and 480 projections at each of 2 bed positions. The exposure time was 135 ms with a detector set to 80 kV peak and 500 μA. Data were reconstructed onto a 416×416×752 image matrix using the COBRA software package (Exxim Computing Corporation, Pleasanton, CA). The effective CT image pixel size was 97 μm. SPECT data were acquired immediately following the CT using a 2 mm single pinhole collimator with a detector radius of rotation at 35 mm. Images were acquired over 1.5 detector revolutions with 6° between each of 90 projections. A 90 mm bed travel was used. Each projection was acquired for 12 seconds, and the data were histogrammed with a 10% window centered at 140 keV. Reconstruction was performed using ordered subset expectation maximization 3D (OSEM3D) with 8 iterations and 6 subsets. Reconstructed images were analyzed and visualized using the Siemens Inveon Research Workplace (IRW) software.

5.3.4 Dosimetry calculation. The OLINDA/EXM dose estimation software was used to determine the effective doses and doses to individual organs via calculations and constants defined in the International Commission on Radiological Protection (ICRP) Publication 106 [21]. Residence times, τ, in the various organs were measured using trapezoidal averaging of the mean data for each time interval. The residence time of the nuclide is the cumulated activity in the source organ divided by the administered activity and is expressed in units of μCi-h/μCi.

Extrapolation of mouse data to human was accomplished using a well-established organ weighting scheme [22],

$$\left(\frac{\%IA}{organ}\right)_{human} = \left(\frac{\%IA}{g_{organ}}\right)_{mouse} x \ (kg_{Total\ Body})_{mouse} \ x \ \left(\frac{g_{organ}}{kg_{Total\ Body}}\right)_{human} \quad (5.1)$$

where ($\%IA/g_{organ}$) is percent injected activity per gram of organ. Each mouse organ was weighed and the total body mass of each mouse was used to extrapolate the mouse data to human. Average human organ and total body masses were used based on data in ICRP 23 and other published sources [23,24].

5.4 Results and Discussion

Here we evaluate the hypothesis that ^{99m}Tc-heparin remains in the GI tract using quantitative organ biodistributions. To estimate radiation dosimetry, 18 mice received orally administered ^{99m}Tc-heparin and were sacrificed at six times (3 mice/time). Data at each time show recovery of 89-99% of the administered material and 99% of the material measured immediately prior to sacrifice.

Figure 5.1 shows the biodistribution of ^{99m}Tc-heparin acquired at time of harvest as measured by well counting. Forty-five minutes after oral administration, the stomach and small intestines account for the majority of the ^{99m}Tc-heparin. The proximal large intestine shows the highest uptake 1.5 hours after oral administration. The majority of activity after 6 hours of incubation of ^{99m}Tc-heparin appears in the distal large intestine. Little uptake appears in the esophagus, lung, and thyroid. The very modest uptake in the lung and esophagus may be due to esophageal reflux associated with oral gavage. All other organs show negligible uptake at all time points, indicating that ^{99m}Tc-heparin is not a significant contributor to organ and effective dose outside the GI tract. Indeed, over 98% of the accumulated activity resides in the GI tract alone.

To visually track the localization of radiolabeled dose in mice, SPECT/CT images were taken 40 minutes prior to euthanasia. Figure 5.2 shows the SPECT/CT images acquired at 3, 6, 18, and 30 hours after oral administration of ^{99m}Tc-heparin. At 3 and 6 hours post administration, the majority of activity remains mostly in the GI tract, particularly in the stomach and intestines. Negligible localization appears in the liver, kidney, and lungs, indicating that ^{99m}Tc-heparin neither absorbs significantly through the GI tract nor circulates in the blood stream. The radioactivity is negligible in all of the organs at longer time points (18, 30 hours), confirming that ^{99m}Tc-heparin is not absorbed.

Figure 5.3 shows the average net activity (μCi) at each time interval represented as the number of disintegrations per unit of administered activity (μCi-h/μCi) in each source organ. The stomach and small intestines show the highest initial uptakes followed by gradual decreases. Uptake by the proximal and distal intestine gradually

increases over 3 and 6 hours, respectively, and then decreases thereafter. Little radioactivity is observed in the esophagus, lung, and thyroid, and negligible activity appears elsewhere.

Table 5.1 shows estimated residence times in humans from orally administered ^{99m}Tc-heparin. Equation 5.1 provides the scaling necessary to convert the mouse measured average accumulated activities into human equivalents by source organ. The table lists these results in descending order based on the dose to the organ.

OLINDA/EXM dose estimation software estimates the total effective dose for humans. The results for a standard adult are shown in Table 5.2. Approximately 74% of the contribution to the effective dose derives from the organs in the GI tract. For example, the doses to the ovaries and bone marrow result from the accumulated activity of other organs (i.e., irradiation from accumulated activity in surrounding organs), because accumulated activity in these organs was not specifically measured.

Given that greater than 98% of the accumulated activity appears in the GI tract and the contribution to the effective dose from these organs accounts for approximately 75% of the dose, additional resolution of the observed uncertainties is unlikely to result in more than a 25% change in the estimated dose to human subjects. Potential improvements to the experimental process include improving the collection fraction and better accounting for dose in organs receiving less than 2% of the total accumulated activity, but such improvements will likely have only a small to negligible effect on the estimates of effective dose.

5.5 Conclusions

These proof-of-principle experiments clearly show that ^{99m}Tc-heparin remains in GI tract. Indeed, ^{99m}Tc-heparin was not absorbed significantly into other bodily tissues. Furthermore, because heparin and short-lived ^{99m}Tc have long been used in clinical medicine, we believe that the conjugates will be well tolerated in our patients. These findings are important because they initiate a new avenue for clinical detection of eosinophil-associated inflammation.

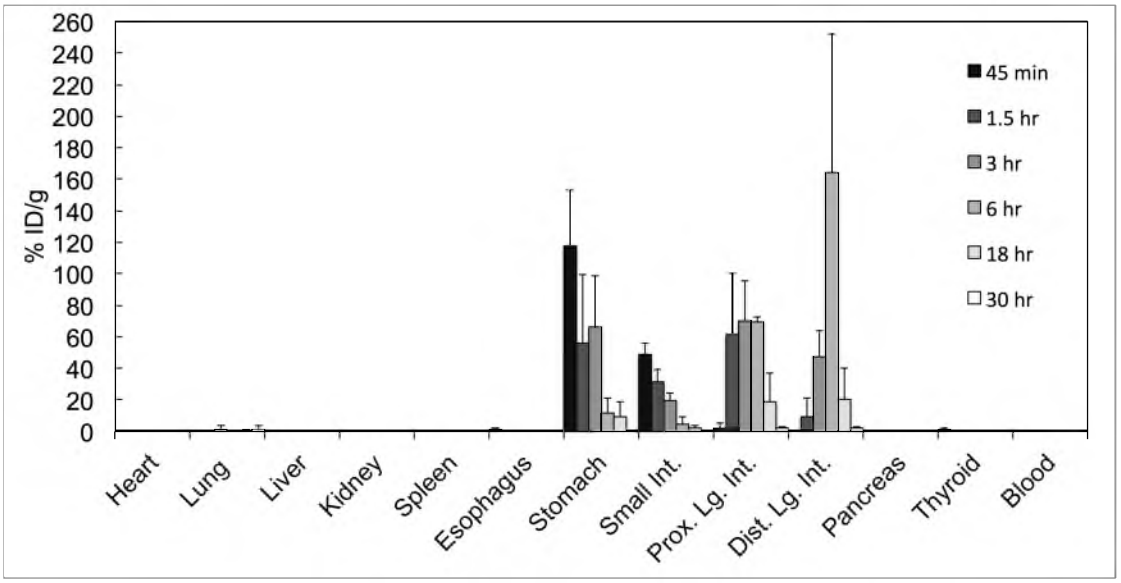

Figure 5.1. Biodistribution of ^{99m}Tc-heparin in collected organs as measured using a well counter at different times. Arithmetic means and standard deviations of %ID/g are corrected for physical decay of the isotope. In=Intestine, Lg=Large, Prox=Proximal, Dist=Distal.

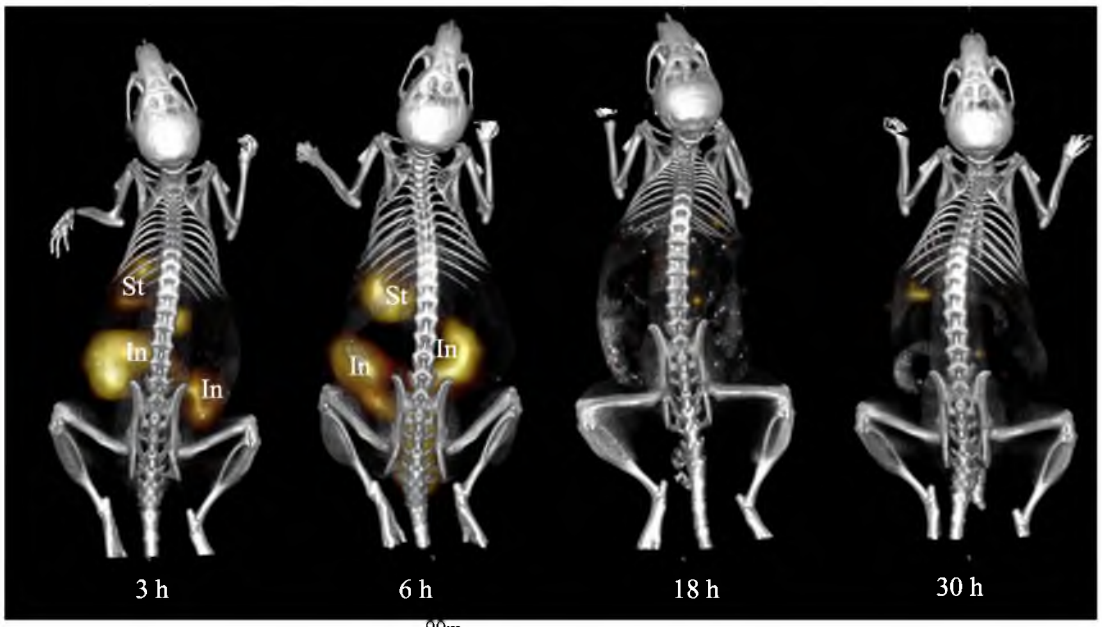

Figure 5.2. SPECT/CT images of ^{99m}Tc-heparin orally administered to mice at 3, 6, 18, and 30 hours. St=stomach, In=Intestines. SPECT/CT intensity were optimized separately in each image and set higher at later time points to reveal locations of radioactivity. The optimization is based off of revealing locations of radioactivity. We started by applying based off of the inflection point of the histogram being set to max, then adjusting mildly further reducing the max given the lack of signal. The bed, anesthesia nose cone, and monitoring lines were selectively removed from the images to enhance visibility.

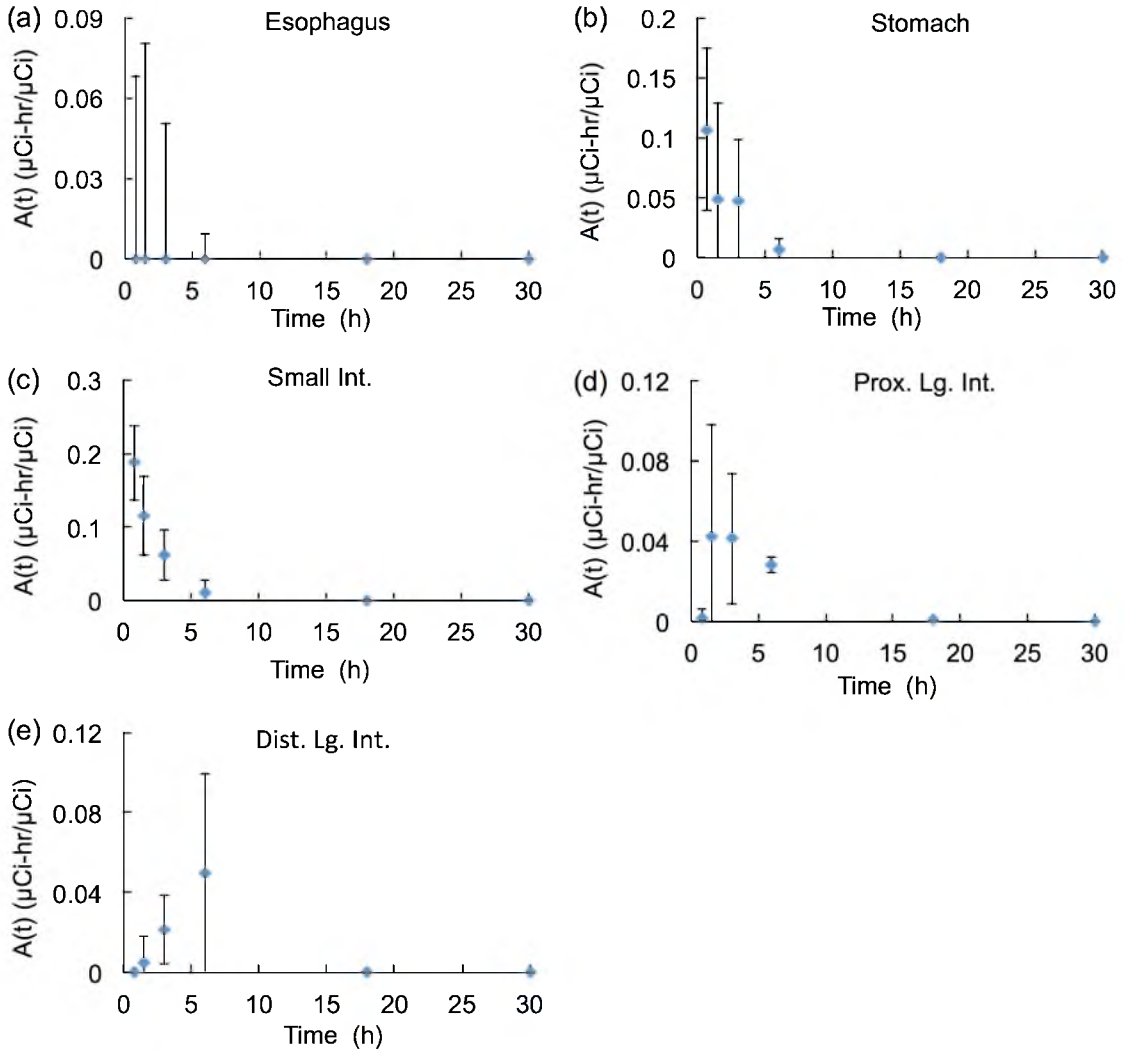

Figure 5.3. Average (and 95% confidence interval) net activity (μCi) of GI tract organs (a) esophagus, (b) stomach, (c) small intestine, (d) proximal large intestine, and (e) distal large intestine at each time interval (0.75, 1.5, 3, 6, 18, and 30 hours) expressed as residence time, τ (μCi-h/μCi).

Table 5.1. Estimated residence times in humans.

Organ	A (μCi-h/μCi)	Fraction of Total
Dist. Lg. In.	0.4355	0.2916
Small Int.	0.4226	0.2829
Prox. Lg. In.	0.3602	0.2411
Stomach	0.2541	0.1701
Lung	0.02012	0.01347
Urine	$3.830 \cdot 10^{-4}$	$2.564 \cdot 10^{-4}$
Liver	$2.708 \cdot 10^{-4}$	$1.813 \cdot 10^{-4}$
Esophagus	$2.359 \cdot 10^{-4}$	$1.579 \cdot 10^{-4}$
Larynx/Thyroid	$1.381 \cdot 10^{-4}$	$9.248 \cdot 10^{-5}$
Bladder	$9.002 \cdot 10^{-5}$	$6.026 \cdot 10^{-5}$
Kidney	$7.918 \cdot 10^{-5}$	$5.300 \cdot 10^{-5}$
Heart	$4.281 \cdot 10^{-5}$	$2.866 \cdot 10^{-5}$
Trachea	$3.724 \cdot 10^{-5}$	$2.493 \cdot 10^{-5}$
Pancreas	$2.300 \cdot 10^{-5}$	$1.540 \cdot 10^{-5}$
Spleen	$1.452 \cdot 10^{-5}$	$9.719 \cdot 10^{-6}$
Testicles	$1.206 \cdot 10^{-6}$	$8.072 \cdot 10^{-7}$
Thymus	$6.022 \cdot 10^{-7}$	$4.032 \cdot 10^{-7}$
Gall Bladder	$5.582 \cdot 10^{-7}$	$3.737 \cdot 10^{-7}$

Table 5.2. OLINDA estimates for a standard adult human using estimated residence times.

	mGy/MBq	Fraction of Total Dose
Lower Large Intestine Wall	$2.46 \cdot 10^{-3}$	0.512
Stomach Wall	$1.04 \cdot 10^{-3}$	0.217
Ovaries	$8.87 \cdot 10^{-4}$	0.0185
Red Marrow	$1.02 \cdot 10^{-4}$	0.0212
Upper Large IntestineWall	$6.83 \cdot 10^{-5}$	0.0142
Urinary Bladder Wall	$6.64 \cdot 10^{-5}$	0.0138
Lungs	$4.92 \cdot 10^{-5}$	0.0102
Small Intestine	$4.68 \cdot 10^{-5}$	$9.75 \cdot 10^{-3}$
Liver	$2.99 \cdot 10^{-5}$	$6.23 \cdot 10^{-3}$
Uterus	$1.32 \cdot 10^{-5}$	$2.75 \cdot 10^{-3}$
Pancreas	$8.27 \cdot 10^{-6}$	$1.72 \cdot 10^{-3}$
Osteogenic Cells	$7.83 \cdot 10^{-6}$	$1.63 \cdot 10^{-3}$
Spleen	$5.61 \cdot 10^{-6}$	$1.17 \cdot 10^{-3}$
Kidneys	$4.84 \cdot 10^{-6}$	$1.01 \cdot 10^{-3}$
Breasts	$4.73 \cdot 10^{-6}$	$9.85 \cdot 10^{-4}$
Muscle	$3.00 \cdot 10^{-6}$	$6.25 \cdot 10^{-4}$
Adrenals	$2.70 \cdot 10^{-6}$	$5.62 \cdot 10^{-4}$
Skin	$1.77 \cdot 10^{-6}$	$3.69 \cdot 10^{-4}$
Thyroid	$5.46 \cdot 10^{-7}$	$1.14 \cdot 10^{-4}$
Thymus	$3.60 \cdot 10^{-7}$	$7.50 \cdot 10^{-5}$
Brain	$5.45 \cdot 10^{-9}$	$1.13 \cdot 10^{-6}$
Gallbladder Wall	$<1 \cdot 10^{-10}$	$<1 \cdot 10^{-10}$
Heart Wall	$<1 \cdot 10^{-10}$	$<1 \cdot 10^{-10}$
Testes	$<1 \cdot 10^{-10}$	$<1 \cdot 10^{-10}$
Effective Dose (mSv/MBq)	$4.81 \cdot 10^{-3}$	

5.6 References

1. Straumann A, Spichtin HP, Grize L, Bucher KA, Beglinger C, Simon HU. Natural history of primary eosinophilic esophagitis: a follow-up of 30 adult patients for up to 11.5 years. *Gastroenterol.* 2003;125:1660-1669.

2. Furuta GT, Liacouras CA, Collins MH, et al. Eosinophilic esophagitis in children and adults: a systematic review and consensus recommendations for diagnosis and treatment. *Gastroenterol.* 2007;133:1342-1363.

3. Liacouras CA, Furuta GT, Hirano I, et al. Eosinophilic Esophagitis: Updated Consensus Recommendations for children and adults. *J. Allergy Clin. Immunol.* 2011;128:3-20.

4. Gupta SK, Fitzgerald JF, Kondratyuk T, HogenEsch H. Cytokine expression in normal and inflamed esophageal mucosa: a study into the pathogenesis of allergic eosinophilic esophagitis. *J. Pediatr. Gastroenterol. Nutr.* 2006;42:22-26.

5. Attwood, SE, Smyrk TC, Demeester TR, Jones JB. Esophageal eosinophilia with dysphagia. A distinct clinicopathologic syndrome. *Dig. Dis. Sci.* 1993. 38:109-116.

6. Saffari H, Peterson KA, Fang JC, Teman C, Gleich GJ, Pease LF. Patchy eosinophil distributions in an esophagectomy specimen from a patient with eosinophilic esophagitis: Implications for endoscopic biopsy. *J. Allergy Clin. Immunol.* 2012;130:798-800.

7. Gonsalves N, Policarpio-Nicolas M, Zhang Q, Rao MS, Hirano I. Histopathology variability and endoscopic correlates in adults with eosinophilic esophagitis. Gastrointest Endosc 2006;64:313-319.

8. Pasha, SF, DiBaise JK, Kim HJ, et al. Patient characteristics, clinical, endoscopic, and histologic findings in adult eosinophilic esophagitis: a case series and systematic review of the medical literature. *Dis. Esophagus*, 2007;20: 311-319.

9. Shah A, Kagalwalla AF, Gonsalves N, Melin-Aldana H, Li BU, Hirano I. Histopathologic variability in children with eosinophilic esophagitis. *Am. J. Gastroenterol.* 2009;104:716-721.

10. Dellon ES, Aderoju A, Woosley JT, Sandler RS, Shaheen NJ. Variability in diagnostic criteria for eosinophilic esophagitis: a systematic review. *Am. J. Gastroenterol.* 2007;102:2300-2313.

11. Kephart GM, Alexander JA, Arora AS, et al. Marked deposition of eosinophil-derived neurotoxin in adult patients with eosinophilic esophagitis. *Am. J. Gastroenterol.* 2010; 105: 298-307.

12. Justinich CJ, Ricci A, Jr., Kalafus DA, et al. Activated eosinophils in esophagitis in children: a transmission electron microscopic study. *J. Pediatr. Gastroenterol. Nutr.* 1997; 25: 194-198.

13. Protheroe C, Woodruff SA, de Petris G, *et al.* A novel histologic scoring system to evaluate mucosal biopsies from patients with eosinophilic esophagitis. *Clin Gastroenterol.. Hepatol* 2009;7:749-755 e711.

14. Plager DA, Stuart S, Gleich GJ. Human eosinophil granule major basic protein and its novel homolog. *Allergy*. 1998;53:33-40.

15. Hirsh J, Warkentin TE, Shaughnessy SG, et al. Heparin and low-molecular-weight heparin: mechanisms of action, pharmacokinetics, dosing, monitoring, efficacy, and safety. *Chest*. 2001;119:64S-94S.

16. Laforest MD, Colas-Linhart N, Guiraud-Vitaux F, et al. Pharmacokinetics and biodistribution of technetium 99m labelled standard heparin and a low molecular weight heparin (enoxaparin) after intravenous injection in normal volunteers. *Br. J. Haematol.* 1991;77:201-208.

17. Kulkarni PV, Parkey RW, et al. Modified technetium-99m heparin for the imaging of acute experimental myocardial infarcts. *J. Nucl. Med.* 1980;21:117-21.

18. Kulkarni PV, Parkey RW, Buja LM, Wilson JE 3rd, Bonte FJ, Willerson JT. Technetium Labeled Heparin: Preliminary Report of a New Radiopharmaceutical with Potential for Imaging Damaged Coronary Arteries and Myocardium. *J. Nucl. Med.* 1978;19:810-815.

19. Saffari H, Krstyen JJ, Gonzalez C, et al. ^{99m}Technetium-labeled heparin: a new approach to detection of eosinophilic esophagitis-associated inflammation. *J. Allergy Clin. Immunol.* 2013. In press.

20. Swaminathan GJ, Myszka DG, Katsamba PS, Ohunki LE, Gleich GJ, Acharya KR. Eosinophil-granule major basic protein, a C-type lectin, binds heparin. *Biochemistry*. 2006;44:14152-8.

21. ICRP, 2008. Radiation Dose to Patients from Radiopharmaceuticals - Addendum 3 to ICRP Publication 53. ICRP Publication 106. Ann. ICRP 38 (1-2).

22. Kirschner A, Ice R, Beierwaltes W. Radiation dosimetry of 131I-19-iodocholesterol: the pitfalls of using tissue concentration data, the author's reply. *J. Nucl. Med.* 1975;16:248-249.

23. International Commission on Radiological Protection. Report on the Task Group on Reference Man. ICRP Publication 23, Pergamon Press, New York, 1975.

24. Stabin MG, JA Siegel. Physical models and dose factors for use in internal dose assessment. *Health Physics.* 2003;85:294-310.

CHAPTER 6

^{99M}TC-HEPARIN: KINETICS OF BINDING

6.1 Abstract

Due to the ability of heparin binding to eosinophilic granule proteins, such as major basic protein (MBP-1), ^{99m}Tc-heparin can be used as an imaging contrast agent to detect inflammation and eosinophil granule proteins deposition in eosinophilic esophagitis (EoE). Here we evaluate the kinetics of binding of ^{99m}Tc-heparin to non-human primate tissue (*ex vivo* monkey esophagus) and model the amount of binding to the esophageal wall versus drinking times and flow rates. This information will inform ^{99m}Tc-heparin administration protocols, optimize the imaging intensity corresponding to the bound material to the esophageal wall, and lead to better detection of eosinophil granule proteins density in EoE patients.

6.2 Experimental Values for Rate Constants

To model the swallowing of ^{99m}Tc-heparin to the esophageal wall, we need to first experimentally determine the "on" and "off" rate constants of the radiolabeled conjugate to the esophageal wall.

6.2.1 Experimentally determined "on" rate constant. To calculate the on-rate constant, k_{on}, the radiolabeled heparin was incubated with biopsy-sized monkey

esophageal tissue treated overnight with MBP-1. Intact frozen monkey esophagi were provided from CA National Primate Research Center, UC Davis. The monkey esophagi were thawed and washed several times with Ringer's solution (Sigma-Aldrich K4002) and the fats were removed carefully prior to the experiment. The monkey esophagus was opened up, and the epithelium layer (soft tissue in white color) was carefully separated from the deeper tissue (muscle layer, dark red color tissue) using small scissors and forceps. The epithelium layer was then cut in approximately equal size biopsies (approximately 2 mm by 2 mm). The tissue samples were incubated overnight with approximately 0.2 mg/mL MBP-1 solution (made freshly from stock solution in 1X PBS before use). The next day, the samples were taken to Intermountain Radiopharmacy. Freshly prepared ^{99m}Tc-heparin (approximately 15 mg heparin, 10 mCi ^{99m}Tc, see Material and Methods section of Chapter 4 for details) was used. The tissue radioactivity was measured using a dose calibrator (Capintec model CRC-15R) after incubation with ^{99m}Tc-heparin for 10, 30, 60, and 90 minutes. For each time point, two experiments were conducted, and the average activity after two quick washes in 1X PBS was reported. The result in Figure 6.1a shows that the reaction follows a first order reaction $dA/dt=k_{on}A$, or $\mathrm{Ln}(A/A_o)=k_{on}(t-t_o)$. This can be rearranged into the equation of a line on a log-linear plot ($\mathrm{Ln}(A)=k_{on}t+[\mathrm{Ln}(A_o)-k_{on}t_o,]$). The slope of the semi-log plot of activity versus time gives us the value for k_{on} (see Figure 6.1b). Rate constant k_{on} in our experiments is 0.0149 1/min (range: 0.0052 to 0.035 1/min). This means that the characteristic on time ($=1/k_{on}$) is 67.1 min (range: 28 to 192 min).

6.2.2 Experimentally determined "off" rate constant. The radiolabeled heparin was incubated with biopsy-sized monkey esophageal tissue treated overnight with

MBP-1 (solution concentration of approximately 0.2 mg/mL, details mentioned above). The following day, at the Intermountain Radiopharmacy (IRP) at University of Utah, ^{99m}Tc-heparin was incubated for 20 minutes with the MBP-1 treated monkey esophagus samples. The tissue was then washed every 2 minutes for a period 64 minutes in 1X PBS and the radioactivity was measured using a dose calibrator (Capintec model CRC-15R). The experiment was done in triplicate and the average radioactivity over time was reported. As shown in Figure 6.2a, the reaction follows a first order reaction. The slope of the semi-log plot of activity versus time gives us the value for off-rate constant, k_{off}, (see Figure 6.2b). The experimental value for off-rate constant k_{off} is 0.0146 1/min (range: 0.004 to 0.03 1/min).

The binding ratio (K_{ratio}) is defined as,

$$K_{ratio} = \frac{k_{off}}{k_{on}}, \tag{6.1}$$

which is approximately 1, with the range of 0.1 (K_{ratio}^{min}) to 5.8 (K_{ratio}^{max}).

6.3 Modeling the Swallowing of ^{99m}Tc-heparin

The swallowing process can be modeled by

$$\frac{\partial C_f}{\partial t} = D\nabla^2 C_f - k_{on} C_f + k_{off} C_b \tag{6.2}$$

$$\frac{\partial C_b}{\partial t} = k_{on} C_f - k_{off} C_b, \tag{6.3}$$

where

C_f = Free radiolabeled conjugate at the esophageal wall (decay not included),

C_b = Bound radiolabeled conjugate at the esophageal wall (decay not included), and

D = Diffusion coefficient.

The first term on the left side of Equation 6.2 is the accumulation of free (unbound) radiolabeled conjugate. The terms on the right side of Equation 6.2 are the diffusion term and source terms (consumption and the production term), respectively. In this study, the bound material correlates with the amount of MBP-1 deposition in diseased esophagi. For Equation 6.3, the left-hand side is the accumulation of bound material, which is equal to the production and the consumption term, respectively, on the right-hand side of the equation. Adding Equations 6.2 and 6.3 together, the total rate of change of bound and free material is equal to diffusion of free (unbound) material to the esophageal wall.

To solve the swallowing process numerically, the equations are scaled with scaled variables given in Equation 6.4. The reaction time scale, i.e., $1/k_{on}$, is used for characteristic time scale.

$$\bar{C}_f = \frac{C_f}{C_{f_0}}, \quad \bar{C}_b = \frac{C_b}{C_{f_0}}, \quad \bar{t} = \frac{t}{t^*} = k_{on}t, \quad \bar{x} = \frac{x}{R} \tag{6.4}$$

with

$$C_{f0}\left(\frac{1}{mL}\right) = \frac{1}{Q\left(\frac{mL}{min}\right).t_d(min)}, \tag{6.5}$$

where, R is the thickness of mucosa layer (3 mm), approximated from the esophagectomy sample (details given in Chapter 2), Q is the volumetric flow rate (the rate of the material flow through the esophagus), and t_d is the drinking time.

The Damköhler number (Da) is the ratio of diffusion time scale to reaction time scale, which is defined as

$$Da = \frac{Diffusion\ time\ scale}{Reaction\ time\ scale} = k_{on}\ \frac{R^2}{D}. \tag{6.6}$$

The diffusion coefficient (D) is calculated by the Stoke-Einstein equation for water properties at 20°C (room temperature at which the experimental values of rate constant were calculated). This assumption is more accurate for diseased esophagus, where there is an increase in extracellular spaces and the junctions between cells are not as tight as in normal tissue (see the increase in intercellular spaces in electron microscopy figures in Chapter 3).

By substituting Equation 6.4 and using Damköhler number, the scaled form of Equations 6.2 and 6.3 become

$$\frac{\partial \bar{C}_f}{\partial \bar{t}} = \frac{1}{Da}\ \nabla^2 \bar{C}_f - \bar{C}_f + K_{ratio}\bar{C}_b \tag{6.7}$$

$$\frac{\partial \bar{C}_f}{\partial \bar{t}} = \bar{C}_f - K_{ratio}\bar{C}_b \tag{6.8}$$

Since, the radioactivity of materials decay over time, the activity of bound and free radiolabeled conjugate in Equations 6.7 and 6.8 will follow a decay function

$$\bar{C}_{f_{decayed}} = \bar{C}_f \, e^{\frac{-Ln(2)}{t_{\frac{1}{2}}}t} \text{ and } \bar{C}_{b_{decayed}} = \bar{C}_b \, e^{\frac{-Ln(2)}{t_{\frac{1}{2}}}t}, \quad (6.9)$$

where, $t_{1/2}$= Technetium-99m half life ~ 6 hours.

Therefore the new-scaled equations, which include the radioactivity decay over time are given in Equation 6.10 and 6.11. Note that from hereafter the scaled bound and free material includes the decay factor and the subscript "decayed" is eliminated for simplicity.

$$\frac{\partial \bar{C}_f}{\partial \bar{t}} = \frac{1}{Da}\nabla^2 \bar{C}_f - \left(1 + \frac{Ln(2)}{t_{\frac{1}{2}}}\right)\bar{C}_f + K_{ratio}\,\bar{C}_b \quad (6.10)$$

$$\frac{\partial \bar{C}_b}{\partial \bar{t}} = \bar{C}_f - \left(K_{ratio} + \frac{Ln(2)}{t_{\frac{1}{2}}}\right)\bar{C}_b \quad (6.11)$$

The scaled initial value and boundary conditions (B.C) are:

$$\begin{aligned} &\bar{C}_b \text{ and } \bar{C}_f = 0 && @\ \bar{x} = 1 \\ &\bar{C}_f = 1 && 0 \le \frac{t}{t_d} \le 1 \\ &\bar{C}_f = 0 && \frac{t}{t_d} > 1 \\ &\bar{C}_b \text{ and } \bar{C}_f = 0 && @\ t = 0 \end{aligned}$$

The total bound radiolabeled conjugate (C_b^{total}) and the total free radiolabeled conjugate (C_f^{total}) were calculated as a function of depth in the tissue of the esophageal wall by solving the equations above.

$$C_b{}^{total} = \int_0^R C_b\, dx\ ,\ C_f{}^{total} = \int_0^R C_f\, dx \tag{6.12}$$

Four integral domains were selected to calculate the total bound and free radiolabeled conjugate: (1) 0 to 0.1 mm (the lumen surface and the depth of 10 cells with the assumption of each cell being ~ 0.01 mm, respectively); (2) 0 to 0.2 mm (depth of ~ 20 cells); (3) 0 to 0.3 mm (depth of ~ 30 cells); and (4) the total esophageal depth of ~ 3 mm. The ratio of C_b^{total} to C_f^{total} was also calculated. In order to distinguish the bounded conjugate from free (unbound conjugate), the ratio of C_b^{total} to C_f^{total} should remain higher than 3 (≥75% of the intensity is from binding of radiolabeled material to eosinophilic granule proteins). The equations were solved for clinical relevant drinking time of 5, 15, and 30 minutes with a flow rate of 1 mL per minute (low enough to avoid bolus flow which drives material past the esophagus without significant binding time), and the time for imaging the esophagus was estimated based on $C_b^{total}/C_f^{total}>3$ (see Figures 6.3-6.8). Results are reported without scaling. Note that the *y*-axes in Figure 6.3-6.9 are converted to 1/mL such that one can multiply the initial activity to estimate the amount of bound/free material in activity/mL units (a standard protocol in medicinal physics).

The results from 5, 15, and 30 minutes drinking time with flow rate of 1 millimeter per minute suggest that the imaging window starts after 10 minutes to ensure

the ratio of total binding to free conjugate be higher than 3, for the first 0.1 mm in depth of esophageal tissue.

The results also depend on the variability in the kinetic rate constants. To evaluate the effect of kinetic rate constant, the equations were numerically solved at the lowest and highest value of K_{ratio} (0.1 and 5.8, respectively) and the C_b^{total} , C_f^{total}, and C_b^{total}/C_f^{total} were estimated at constant drinking time of 15 minutes (clinically relevant value) and flow rate of 1 mL/min (see Figures 6.9-6.12). The results clearly show that the amount of bound material increases significantly, by a factor of at least three, at low K_{ratio} (=0.1, see Figure 6.9). The ratio of C_b^{total}/C_f^{total} increases remarkably (>20 after 20 minutes, and increases to >100 in an hour), which promises good imaging quality. Conversely, at maximum K_{ratio} (=5.8), the C_b^{total}/C_f^{total} never reaches the value of 3, because the amount of bound material decreases dramatically by approximately 10 fold (see Figure 6.5 and 6.11). These findings are very helpful to estimate the esophagus-imaging window in EoE patients.

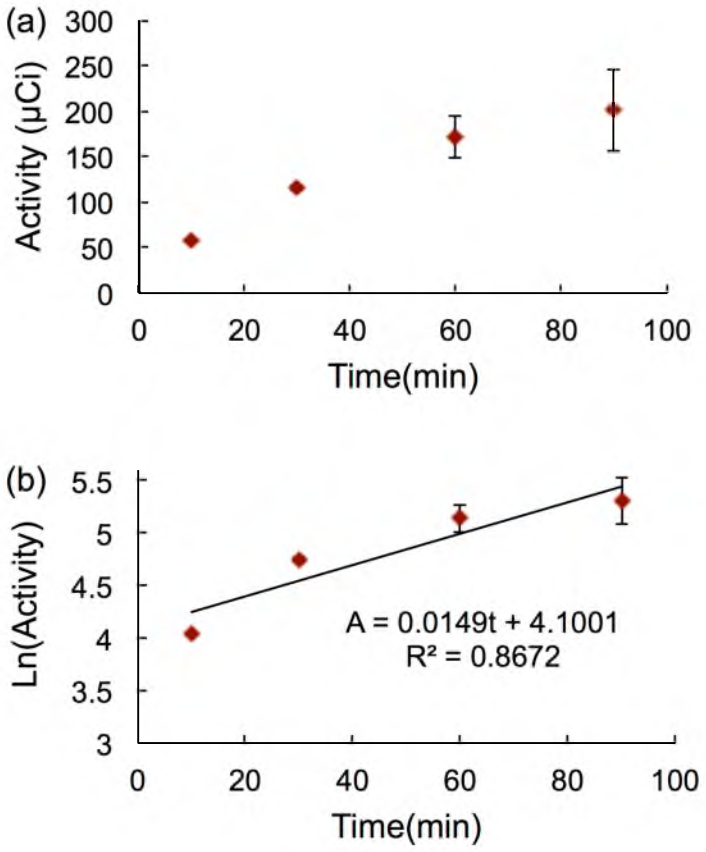

Figure 6.1. Biopsy-sized monkey esophageal tissue treated with MBP-1, incubated with radiolabeled heparin at different times. Rate constant k_{on} in our experiments is 0.0149 1/min (range: 0.0052 to 0.035 1/min). This means that the characteristic on time (=1/k_{on}) is 67.1 min.

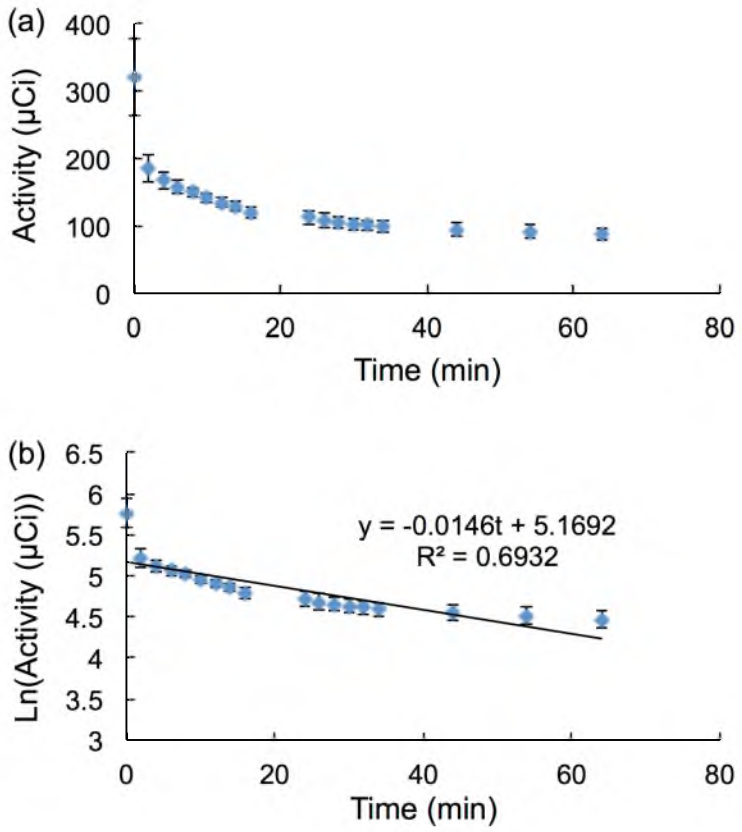

Figure 6.2. Biopsy-sized monkey esophageal tissue treated with MBP-1, incubated with radiolabeled heparin at different times. Rate constant k_{off} in our experiments is 0.0146 1/min (range: 0.004 to 0.03 1/min). This means that the characteristic on time (=1/k_{off}) is 68.5 min.

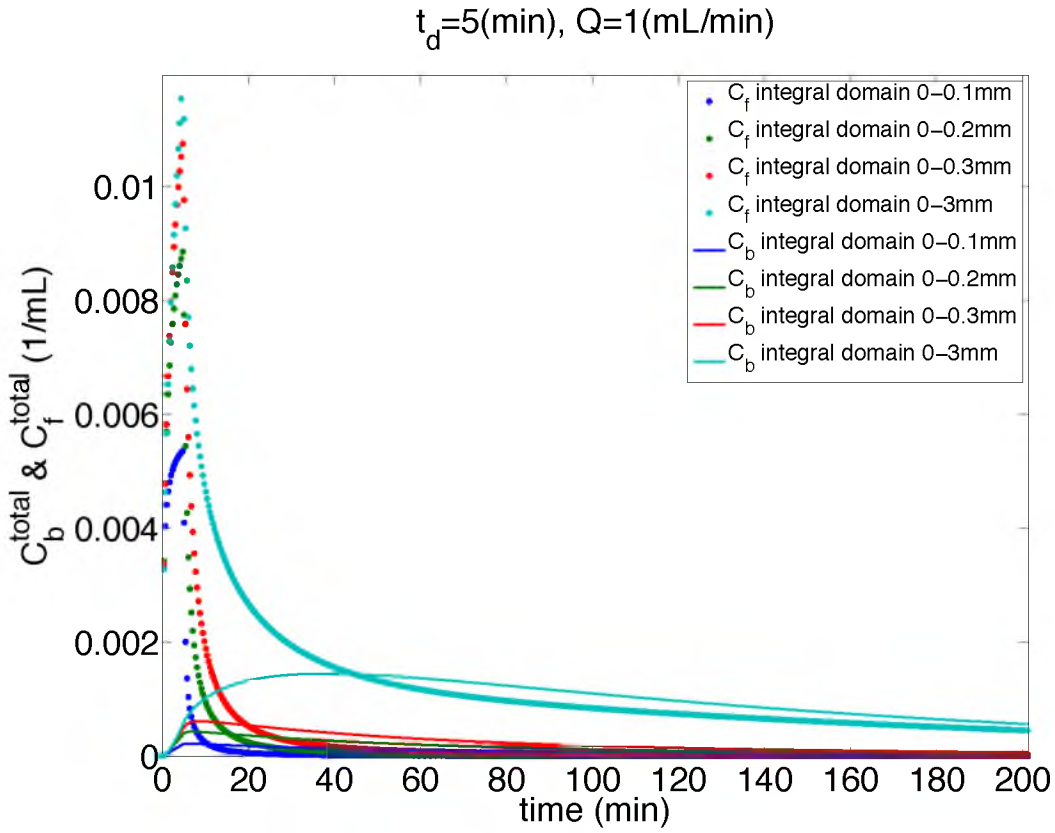

Figure 6.3. Total bound radiolabeled and total free radiolabeled material as a function of time at different integral domain (0.1 mm=10 cell thickness, 0.2 mm=20 cell thickness, 0.3 mm=300 cell thickness, and full 3 mm esophageal thickness. The simulation is based on K_{ratio}=1, drinking time=5 min, and volumetric flow of 1 mL/min.

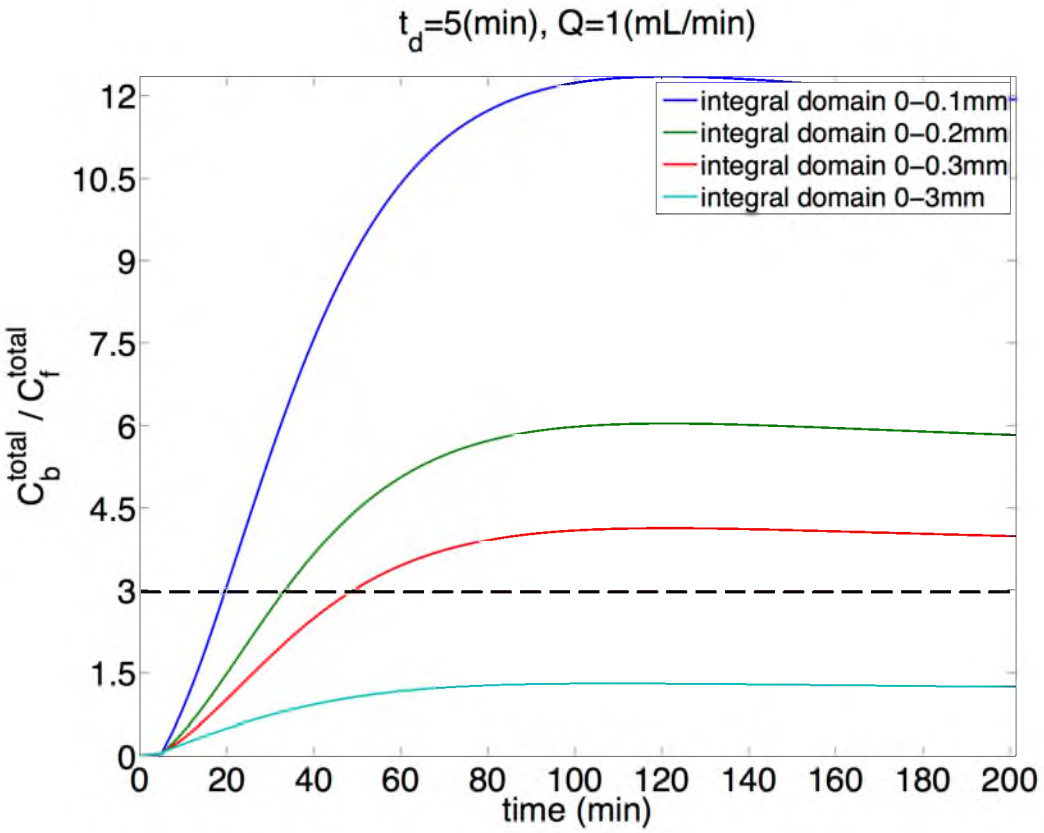

Figure 6.4. Ratio of bound radiolabeled to free radiolabeled material as a function of time at different integral domain (0.1 mm=10 cell thickness, 0.2 mm=20 cell thickness, 0.3 mm=300 cell thickness, and full 3 mm esophageal thickness. The simulation is based on K_{ratio}=1, drinking time=5 min, and volumetric flow of 1 mL/min. The horizontal dash line indicates the lower limit of detection (ratio>3).

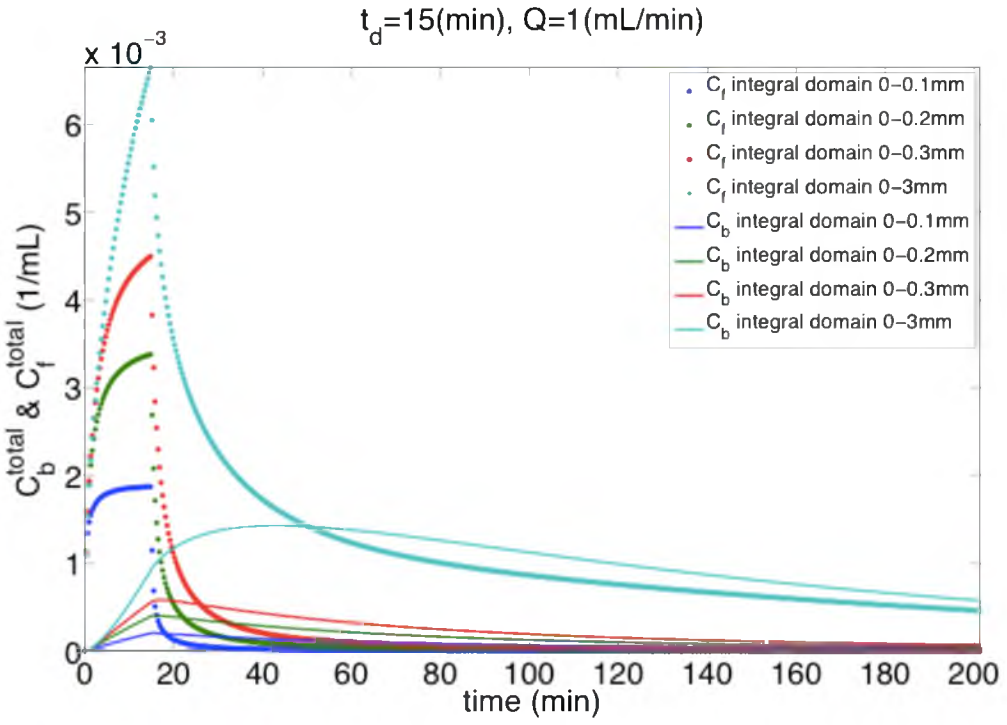

Figure 6.5. Total bound radiolabeled and total free radiolabeled material as a function of time at different integral domain (0.1 mm=10 cell thickness, 0.2 mm=20 cell thickness, 0.3 mm=300 cell thickness, and full 3 mm esophageal thickness. The simulation is based on K_{ratio}=1, drinking time=15 min, and volumetric flow of 1 mL/min.

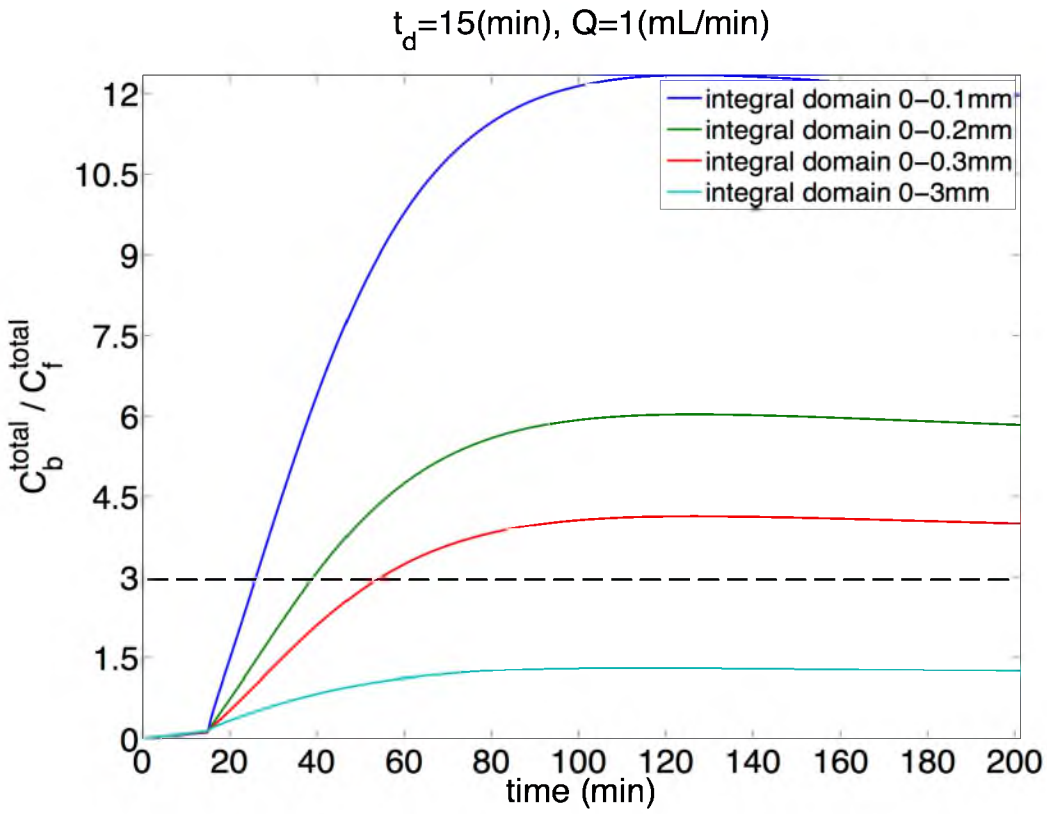

Figure 6.6. Ratio of bound radiolabeled to free radiolabeled material as a function of time at different integral domain (0.1 mm=10 cell thickness, 0.2 mm=20 cell thickness, 0.3 mm=300 cell thickness, and full 3 mm esophageal thickness. The simulation is based on K_{ratio}=1, drinking time=15 min, and volumetric flow of 1 mL/min. The horizontal dash line indicates the lower limit of detection (ratio>3).

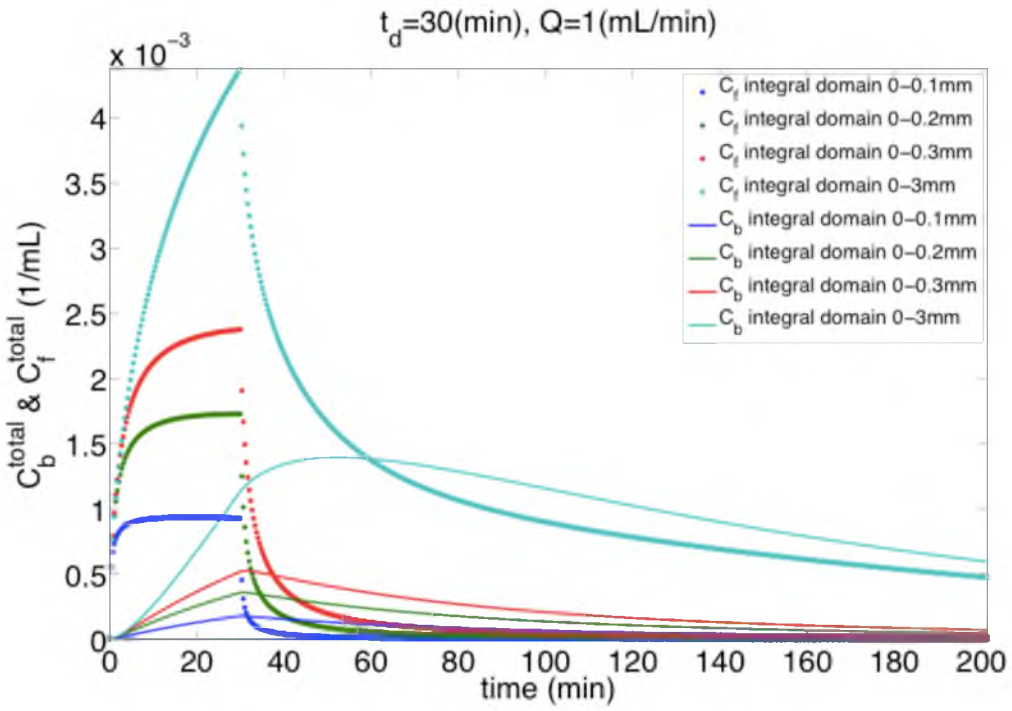

Figure 6.7. Total bound radiolabeled and total free radiolabeled material as a function of time at different integral domain (0.1 mm=10 cell thickness, 0.2 mm=20 cell thickness, 0.3 mm=300 cell thickness, and full 3 mm esophageal thickness. The simulation is based on K_{ratio}=1, drinking time=30 min, and volumetric flow of 1 mL/min.

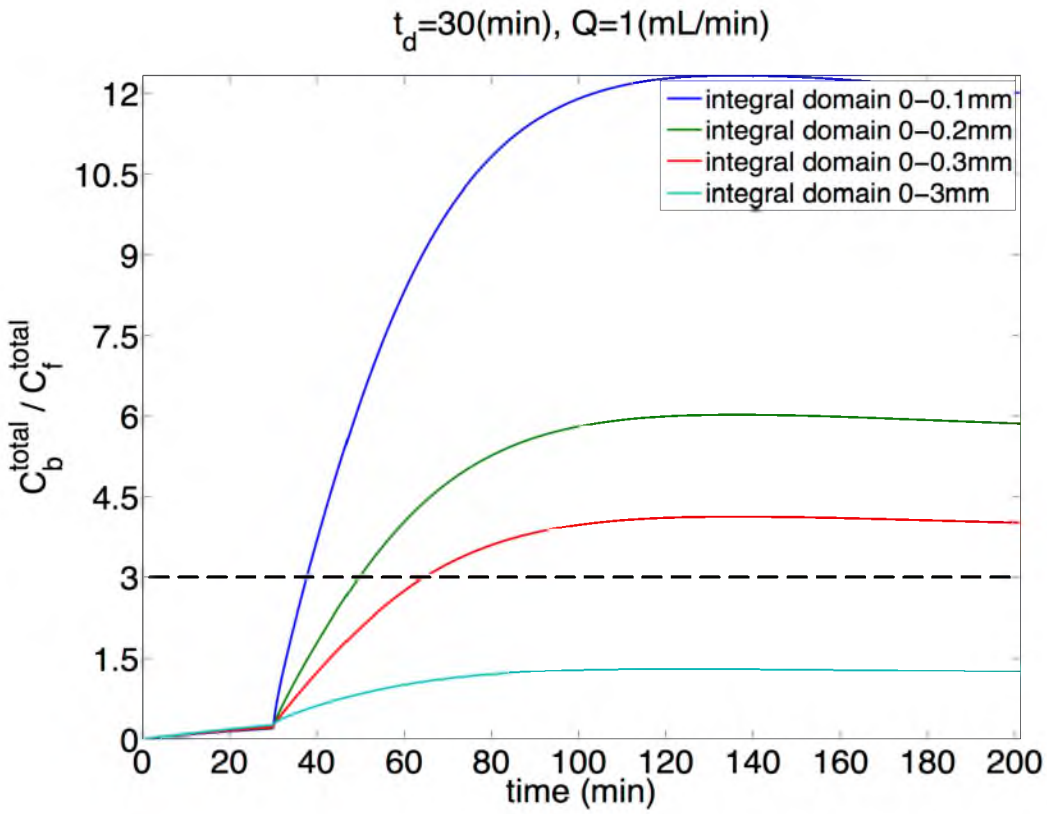

Figure 6.8. Ratio of bound radiolabeled to free radiolabeled material as a function of time at different integral domain (0.1 mm=10 cell thickness, 0.2 mm=20 cell thickness, 0.3 mm=300 cell thickness, and full 3 mm esophageal thickness. The simulation is based on K_{ratio}=1, drinking time=30 min, and volumetric flow of 1 mL/min. The horizontal dash line indicates the lower limit of detection (ratio>3).

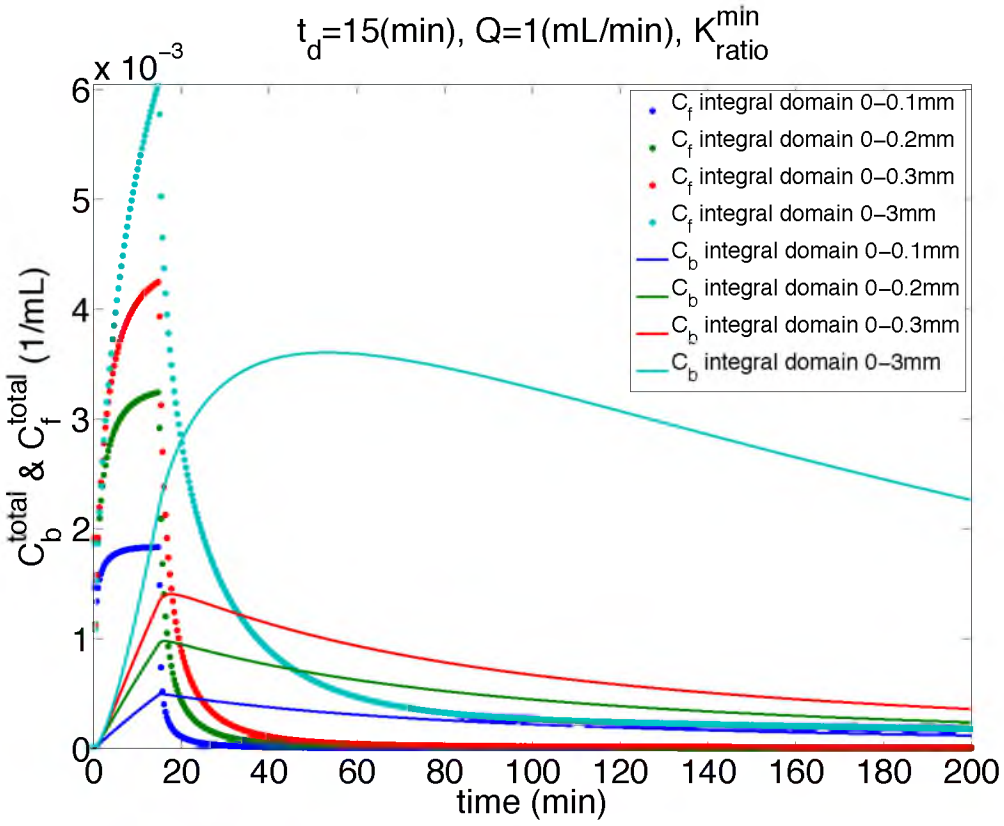

Figure 6.9. Total bound radiolabeled and total free radiolabeled material as a function of time at different integral domain (0.1 mm=10 cell thickness, 0.2 mm=20 cell thickness, 0.3 mm=300 cell thickness, and full 3 mm esophageal thickness. The simulation is based on $K_{ratio}=K^{min}=0.1$, drinking time=15 min, and volumetric flow of 1 mL/min.

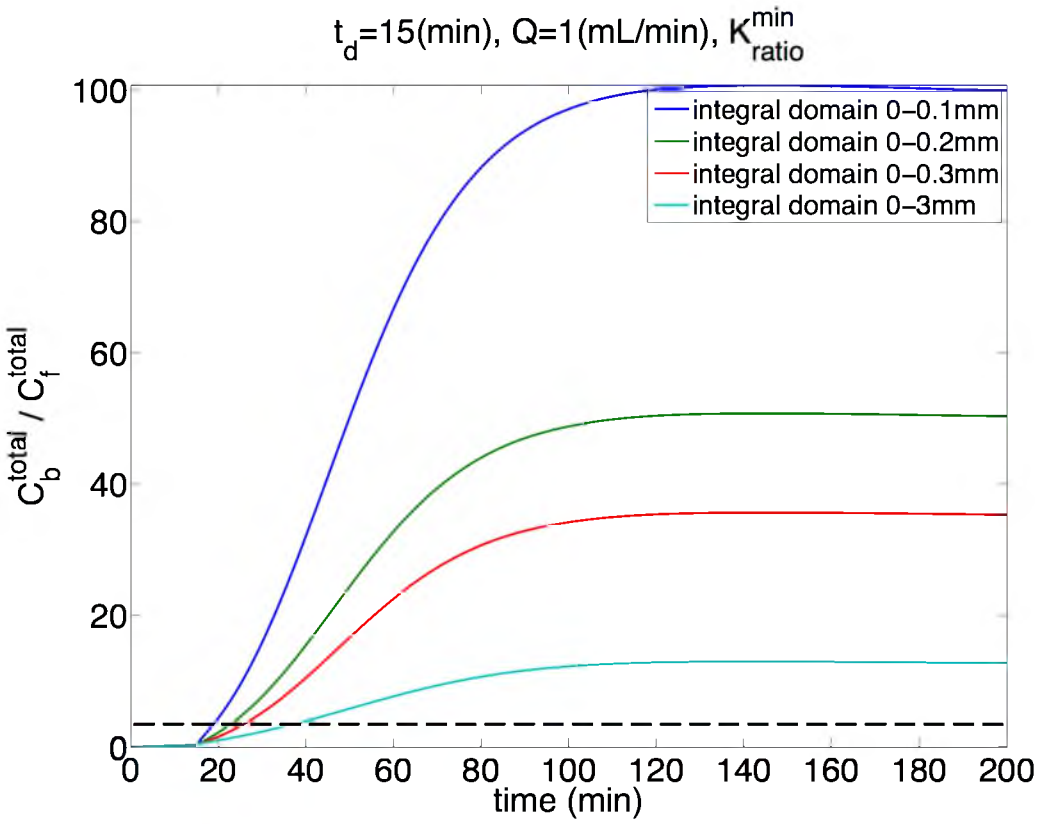

Figure 6.10. Ratio of bound radiolabeled to free radiolabeled material as a function of time at different integral domain (0.1 mm=10 cell thickness, 0.2 mm=20 cell thickness, 0.3 mm=300 cell thickness, and full 3 mm esophageal thickness. The simulation is based on K_{ratio}=K^{min}=0.1, drinking time=15 min, and volumetric flow of 1 mL/min. The horizontal dash line indicates the lower limit of detection (ratio>3).

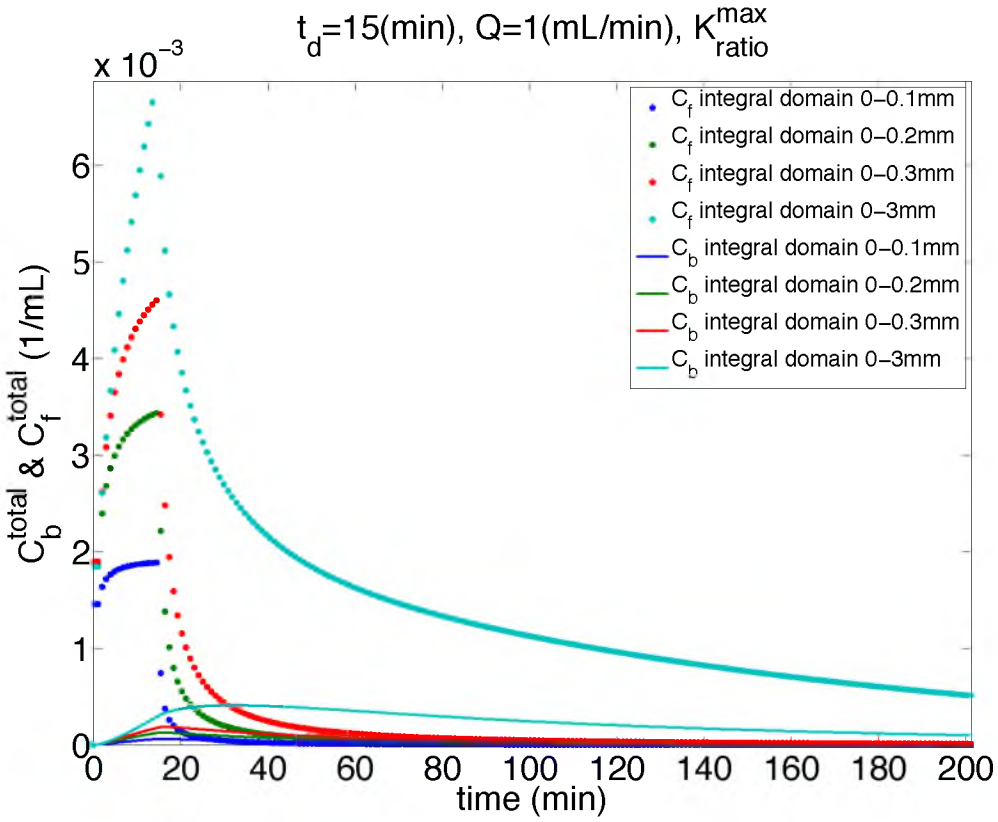

Figure 6.11. Total bound radiolabeled and total free radiolabeled material as a function of time at different integral domain (0.1 mm=10 cell thickness, 0.2 mm=20 cell thickness, 0.3 mm=300 cell thickness, and full 3 mm esophageal thickness. The simulation is based on $K_{ratio}=K^{max}=5.8$, drinking time=15 min, and volumetric flow of 1 mL/min.

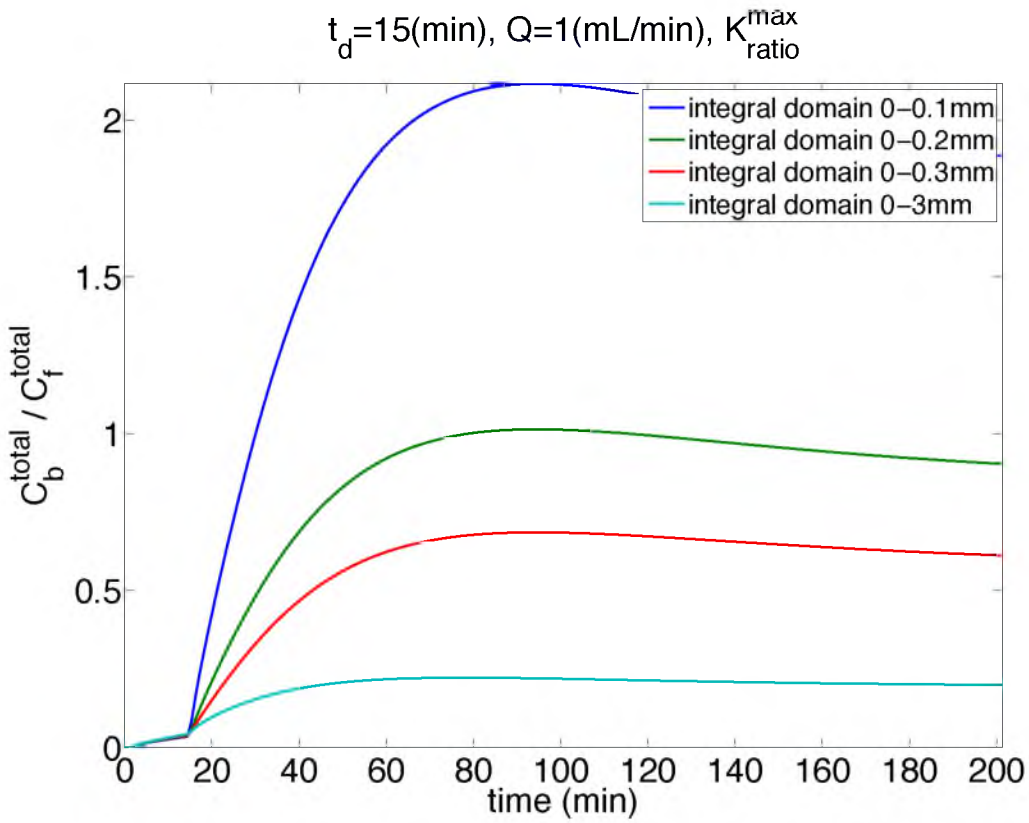

Figure 6.12. Ratio of bound radiolabeled to free radiolabeled material as a function of time at different integral domain (0.1 mm=10 cell thickness, 0.2 mm=20 cell thickness, 0.3 mm=300 cell thickness, and full 3 mm esophageal thickness. The simulation is based on $K_{ratio}=K^{max}=5.8$, drinking time=15 min, and volumetric flow of 1 mL/min.

CHAPTER 7

CONCLUSIONS

The general purpose of this project is to develop a minimally invasive technique to detect eosinophil-associated inflammation in eosinophilic esophagitis (EoE). Current diagnosis is to monitor the involvement through biopsy samples, which is invasive and may not fully represent the disease state. We hypothesized that ^{99m}Tc-heparin can be used as a radiolabeled agent to detect the eosinophil's proteins degranulation in the diseased esophagus. Our long-term plan is to have patients swallow the reagent and image its binding by single-photon emission computed tomography (SPECT) imaging.

To achieve our goal, we first studied the disease patchiness by mapping the eosinophils density of the esophagectomy sample from a known EoE patient and found that misdiagnosis may be possible by esophagogastroduodenoscopy (EGD), if not sampling adequately. Second, we studied degranulation patterns in EoE from 9 randomly selected patients and found that more than 80% of the eosinophils are undergoing cytolysis by releasing their markedly basic granule protein in the tissue. With the realization that these proteins are deposited in the inflamed esophagus, we further hypothesized that the eosinophils associated inflammation by detecting the granule proteins degranulation such as major basic protein (MBP-1), could be detected and localized by swallowing radiolabeled heparin. We radiolabeled heparin with

technetium-99m (^{99m}Tc-heparin) and tested the binding using both paper and column chromatography. The binding efficiency was more than 98% and stable for more than 10 hours (more details in Chapter 4), indicating that technetium binds strongly to heparin. We then tested the ability of ^{99m}Tc-heparin binding to cationic eosinophil granule proteins, and we found that ^{99m}Tc-heparin would bind to tissues coated with these eosinophil granule proteins. We also have been able to demonstrate that the radiolabeled heparin is able to bind *in vitro* to biopsies of the esophagus from patients with EoE using SPECT imaging. The animal study was done in healthy mice to evaluate the biodistribution of ^{99m}Tc-heparin administered orally. The results showed that the majority of the conjugate is not absorbed through the gastrointestinal tract. The human dosimetry was done based on the mice data and the radiation dose to each organ was estimated.

This work lays an important foundation for clinical trials of this reagent. Presently, our proposal to perform the first trials of this reagent in human subjects is under review by the Radioactive Drug Research Committee (RDRC) at University of Utah. We propose to do basic science research on humans to determine the distribution of the ^{99m}Tc-heparin and whether radiolabeled heparin localizes specifically to the esophagus of patients with eosinophilic esophagitis. We desire to test whether radiolabeled heparin will bind to the eosinophil's granule protein in eosinophilic esophagitis patients, because an animal model of eosinophilic esophagitis, which shows the striking deposition of eosinophil granule proteins remains unavailable. Furthermore, because heparin is a physiological substance that has long been used in clinical medicine, we believe that it will be well tolerated in our patients.

We believe that with radioimaging we can more fully appreciate the eosinophil involvement throughout the entire length of the esophagus by having the patients swallow a radiolabeled agent specific to eosinophil granule proteins. If successful, this will open a new avenue to clinically monitor the disease state and to better understand the disease pathogenesis.

APPENDIX A

ADDITIONAL INFORMATION: ESOPHAGECTOMY SECTIONS

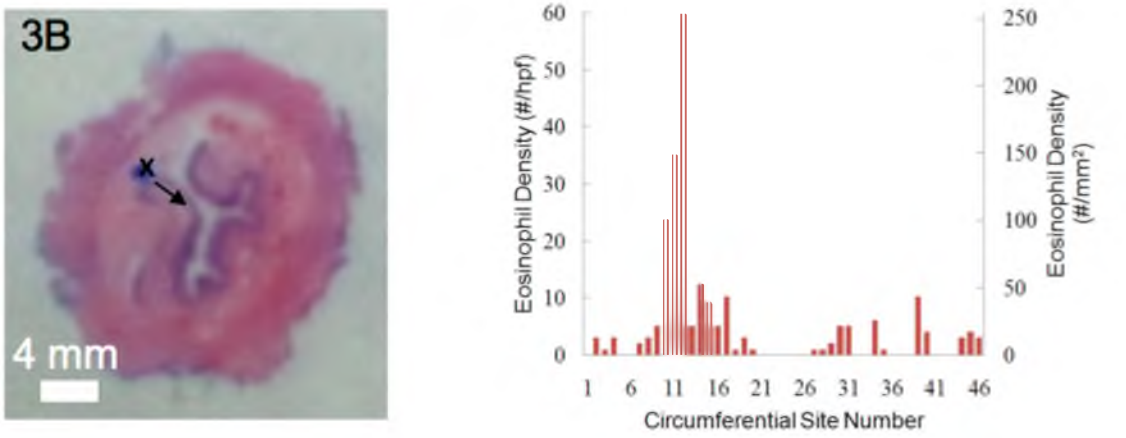

Figure A.1. Digital image of representative H&E stained esophageal section and eosinophil density (in eos/hpf and eos/mm^2) as a function of lumenal perimeter position in terms of microscopy sites for section 3B. The start point is shown by "x" marker following the direction with an "arrow" on the digital pictures.

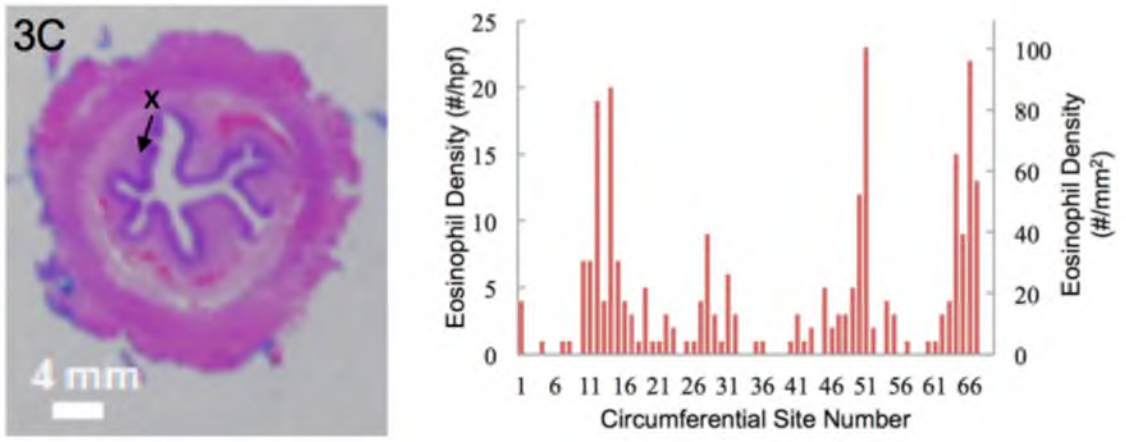

Figure A.2. Digital image of representative H&E stained esophageal section and eosinophil density (in eos/hpf and eos/mm^2) as a function of lumenal perimeter position in terms of microscopy sites for section 3C. The start point is shown by "x" marker following the direction with an "arrow" on the digital pictures.

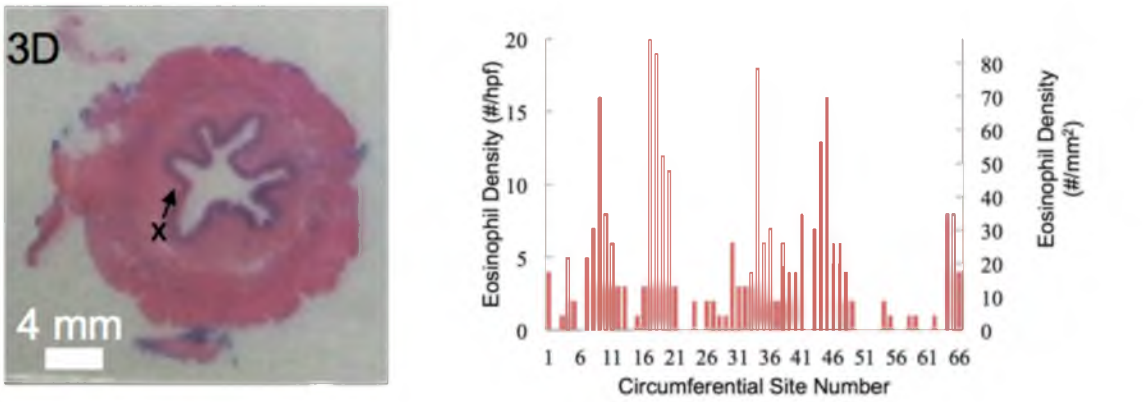

Figure A.3. Digital image of representative H&E stained esophageal section and eosinophil density (in eos/hpf and eos/mm^2) as a function of lumenal perimeter position in terms of microscopy sites for section 3D. The start point is shown by "x" marker following the direction with an "arrow" on the digital pictures.

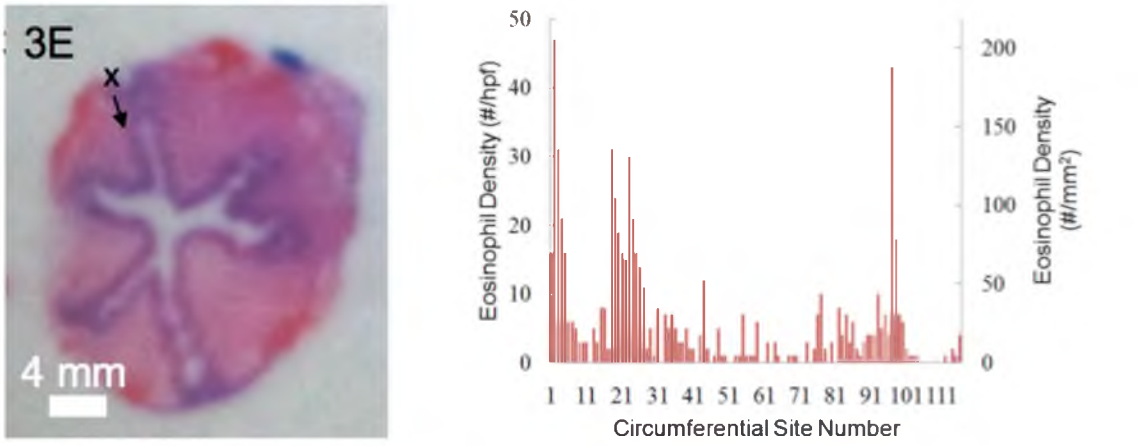

Figure A.4. Digital image of representative H&E stained esophageal section and eosinophil density (in eos/hpf and eos/mm^2) as a function of lumenal perimeter position in terms of microscopy sites for section 3E. The start point is shown by "x" marker following the direction with an "arrow" on the digital pictures.

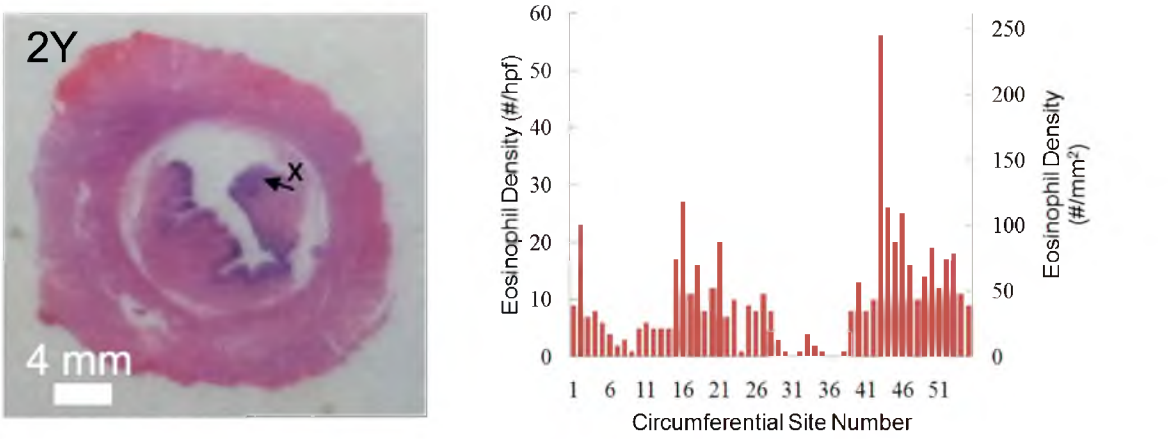

Figure A.5. Digital image of representative H&E stained esophageal section and eosinophil density (in eos/hpf and eos/mm^2) as a function of lumenal perimeter position in terms of microscopy sites for section 2Y. The start point is shown by "x" marker following the direction with an "arrow" on the digital pictures.

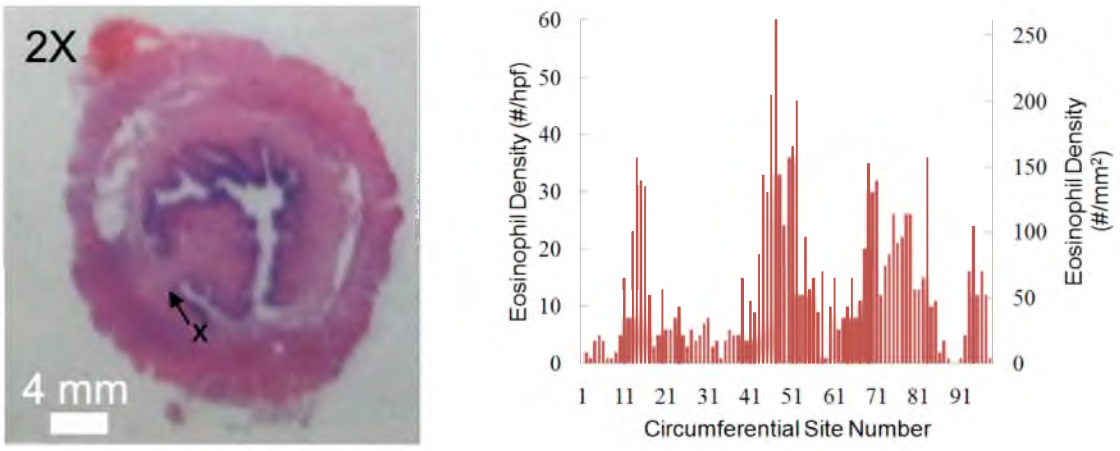

Figure A.6. Digital image of representative H&E stained esophageal section and eosinophil density (in eos/hpf and eos/mm^2) as a function of lumenal perimeter position in terms of microscopy sites for section 2X. The start point is shown by "x" marker following the direction with an "arrow" on the digital pictures.

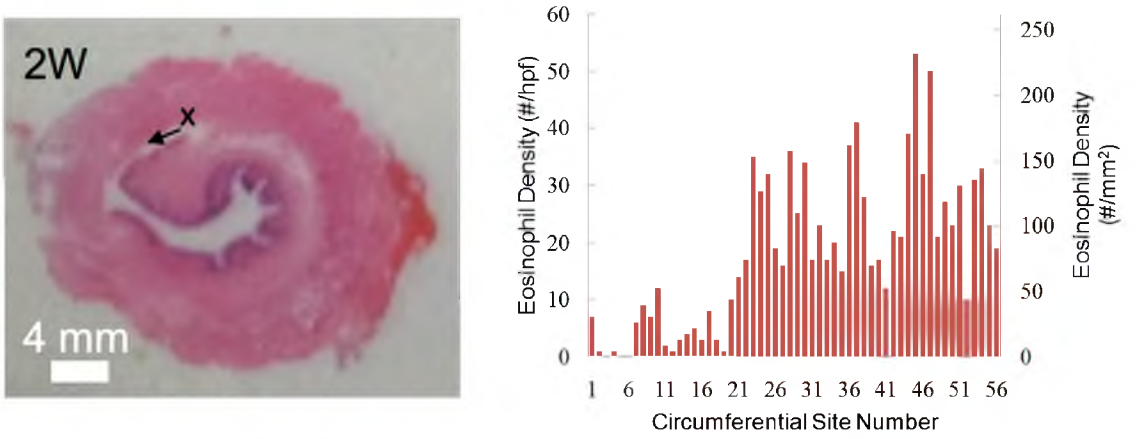

Figure A.7. Digital image of representative H&E stained esophageal section and eosinophil density (in eos/hpf and eos/mm^2) as a function of lumenal perimeter position in terms of microscopy sites for section 2W. The start point is shown by "x" marker following the direction with an "arrow" on the digital pictures.

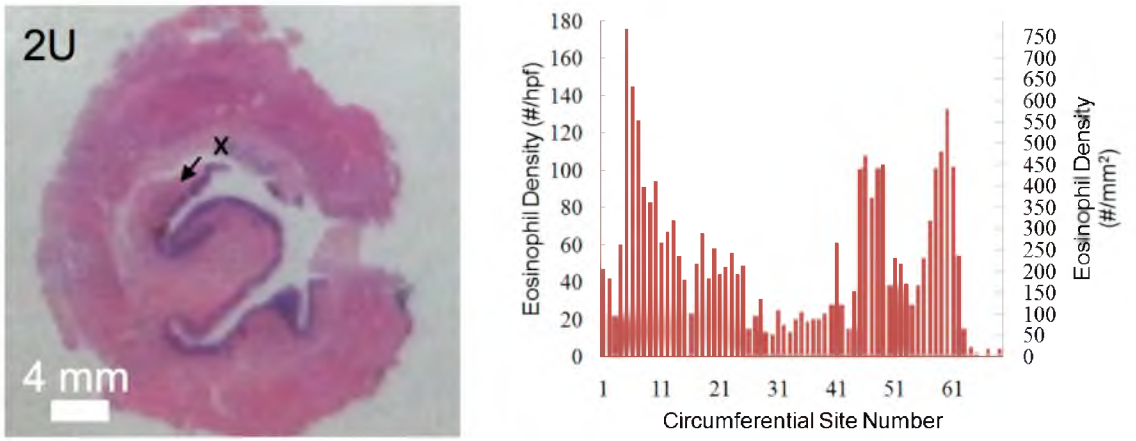

Figure A.8. Digital image of representative H&E stained esophageal section and eosinophil density (in eos/hpf and eos/mm^2) as a function of lumenal perimeter position in terms of microscopy sites for section 2U. The start point is shown by "x" marker following the direction with an "arrow" on the digital pictures.

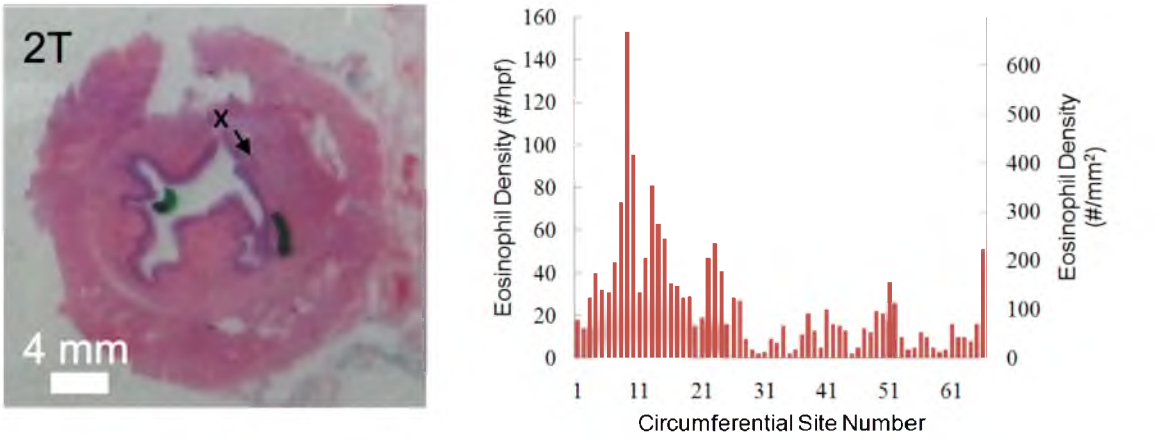

Figure A.9. Digital image of representative H&E stained esophageal section and eosinophil density (in eos/hpf and eos/mm^2) as a function of lumenal perimeter position in terms of microscopy sites for section 2T. The digital picture of slide 2T had two marking sites (not on the epithelium layer, i.e., the mapping region) upon receipt from the Department of Pathology. The start point is shown by "x" marker following the direction with an "arrow" on the digital pictures.

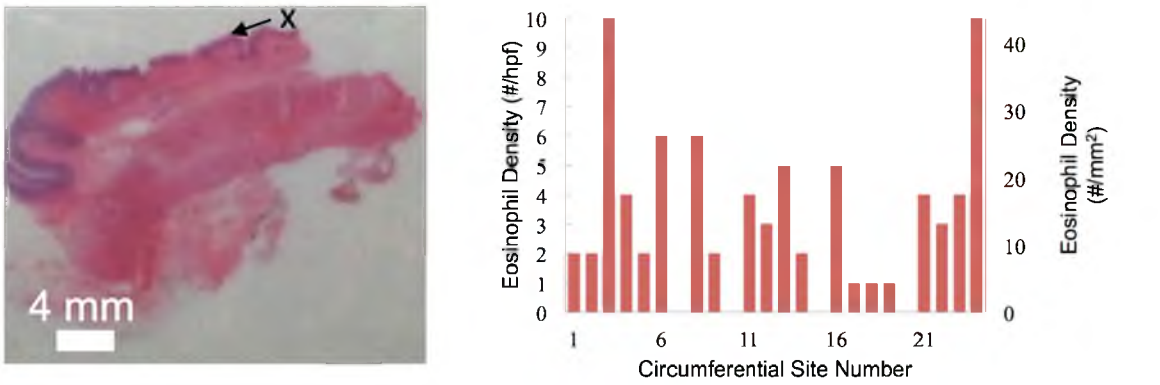

Figure A.10. Digital image of a longitudinal section representative H&E stained esophageal section and eosinophil density (in eos/hpf and eos/mm^2) as a function of lumenal perimeter position in terms of microscopy sites. The start point is shown by "x" marker following the direction with an "arrow" on the digital pictures.

APPENDIX B

ADDITIONAL DESCRIPTION OF THE SIMULATION PROTOCOL

A Monte Carlo simulation was coded in Visual Basic for Applications (VBA) in MS Excel 2003. The 2003 version was selected because it executes the code 20-30% faster than more recent versions. A key attribute of these simulations is that they directly use the recorded eosinophil densities collected above. The code randomly selects a row and column representing the eosinophil density from a worksheet in which all of the data are summarized. Each column represents a circumferential or longitudinal section of the esophagus. Each row represents a site for counting. If the density exceeds 15 eos/hpf, then the sites are designated as diseased. Four immediately adjacent sites constitute a biopsy because each biopsy typically spans approximately 2 mm and each site represents a 0.54 mm diameter field of view. To be representative of the clinical practice of reporting only peak eosinophil densities, if only one of the four sites within a biopsy exceeds 15 eos/hpf, then the entire biopsy is designated as diseased. The process is repeated two to forty times to represent multiple biopsy collection per endoscopy. The result of each endoscopy (1 for diseased and 0 for normal) is stored in an array. Ten thousand biopsies are collected for each condition. The average, μ, and standard deviation, σ, are calculated from the 10,000 entries in the array.

The simulation analyzed three sample patterns at three eosinophil site densities. The average eosinophil site density (30.2%) was simulated by allowing column selection from all available columns. The low eosinophil site density (5.7%) was simulated by allowing column selection from the three columns with the fewest number of sites with eosinophil densities exceeding 15 eos/hpf. The high eosinophil site density (79.3%) was simulated by allowing column selection from the three columns with the most number of sites with eosinophil densities exceeding 15 eos/hpf. Three sampling

patterns were also evaluated. Purely random sampling was imitated by using the Rnd functionality to randomly select both the allowed column and row for each biopsy. Random sampling from within a section was simulated by first designating a column corresponding to a section and then repeatedly and randomly selecting rows using the Rnd functionality in that column. Random sampling within a sector of a section was accomplished by first selecting one column for all biopsies in an endoscopy. The number of available sites (rows) was divided by the number of sites to determine which sites correspond to which sector. Random sampling within that narrow sector was then accomplished using the Rnd functionality. Since all sectors are of equal length a sector represents a fraction of the perimeter, which may or may not correspond with sectors defined by angle because the eosophageal lumen is not strictly circular. If four consecutive sites exceed the number of rows, sampling within a biopsy restarts at the top row, even for sector sampling. Only nonempty cells were employed.

APPENDIX C

ADDITIONAL INFORMATION: ELECTRON MICROSCOPY GRADINGS

Table C.1. The average (Avg) and standard deviation (Std) of 1672 electron photomicrographs (9 EoE patients, 900 eosinophils) graded by three individuals based on membrane integrity, evidence of cytoplasmic vesiculation including sombrero vesicles, granule morphology, and extracellular granule location. Cytoplasmic membrane integrity was classified as intact (no membrane loss), mainly intact (≤20% membrane loss), partially disrupted (>20% membrane loss), or fully disrupted (no recognizable membrane).

	Free Granules	Sombrero Vesicles	Cytoplasmic Vesiculation	Normal Eosinophils
Avg ± Std	1185 ± 68	641 ± 55	483 ± 66	11 ± 2

Eosinophils: Reversal of Staining (Cell Activation) with Piecemeal Degranulation				
	Intact Membrane	Mainly Intact Membrane	Partially Disrupted Membrane	Fully Disrupted Membrane
Avg ± Std	116 ± 34	124 ± 21	175 ± 42	334 ± 26

Eosinophils: Reversal of Staining (Cell Activation) without Piecemeal Degranulation				
	Intact Membrane	Mainly Intact Membrane	Partially Disrupted Membrane	Fully Disrupted Membrane
Avg ± Std	18 ± 7	4 ± 2	6 ± 3	15 ± 3

Eosinophils: Normal Granules with Piecemeal Degranulation				
	Intact Membrane	Mainly Intact Membrane	Partially Disrupted Membrane	Fully Disrupted Membrane
Avg ± Std	16 ± 20	18 ± 22	6 ± 7	36 ± 47

Eosinophils: Normal Granules without Piecemeal Degranulation				
	Intact Membrane	Mainly Intact Membrane	Partially Disrupted Membrane	Fully Disrupted Membrane
Avg ± Std	13 ± 4	6 ± 4	1 ± 0	2 ± 2

APPENDIX D

CALIBRATION CURVE: ACTIVITY VERSUS SPECT INTENSITY

In all experiments, the activity of radiolabeled biopsy tissues was measured using a dose calibrator (Capintec model CRC-15R). Two-dimensional planar static images of the radiolabeled biopsies were obtained using the Ecam SPECT instrument (Siemens). The calibration curve between the activity measurement and the SPECT intensity was checked at different days. Some variation from the linear curve of SPECT count versus activity can be because of the radioactivity decay, error in the activity measurement and SPECT count, time variation between each measurement, and the transportation of samples from Radiopharmacy to Nuclear Medicine.

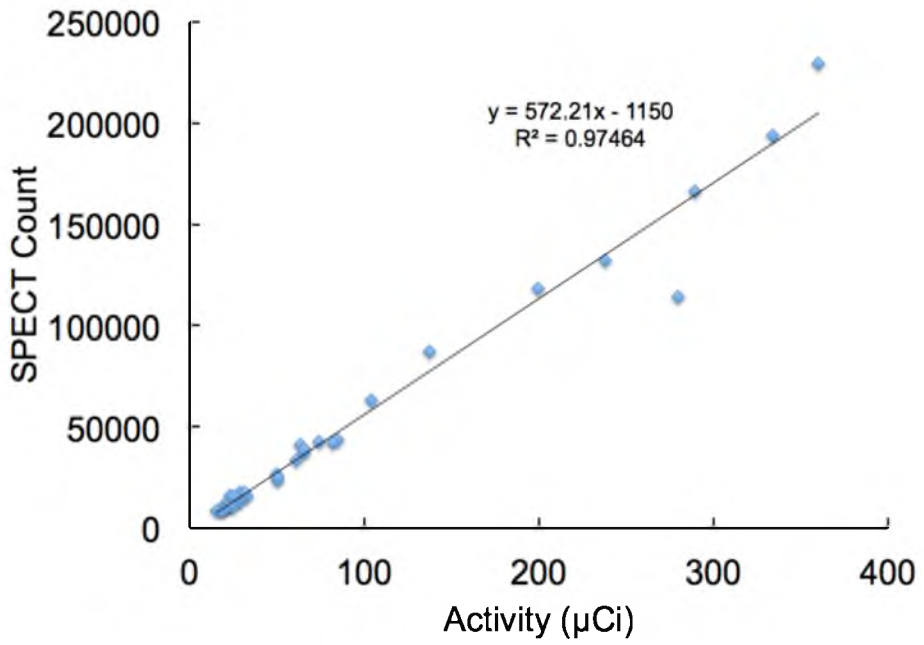

Figure D1. Correlation curve of activity measurement on *ex vivo* monkey esophageal tissue at the Intermountain Radiopharmacy and SPECT intensity at Nuclear Medicine, University of Utah.

APPENDIX E

ALTERNATIVE RADIOLABELED CANDIDATES

In addition to heparin, alternative radiolabeled chelating agents such as anti-MBP1 antibodies, polyanions (poly-glutamic acid and poly aspartic asid), SAGE polymers (semisynthetic glycosaminoglycan ethers, provided generously by Dr. Glenn Prestwich at the University of Utah), and enoxaparin (NDC 0075-0623) were also used to evaluate the hypothesis. In this appendix, the radiolabeling procedure and the limitations are briefly discussed.

Antibody Radiolabeling

A murine monoclonal anti-MBP (J13-6B6) supernatant synthesized previously by Gleich's lab was purified using MabTrap Kits (Sigma, 54842). The amount of antibody purified in each cycle was approximately 12 mg in 6 mL elution buffer. The purified anti-MBP antibody was then mixed with NHS-MAG3 (N-hydroxysuccinimidyl S-acetylmercaptoacetyltriglycinate) to the ratio of 1:15. After vortexing and incubating the mixture for 2 hours at room temperature, the solution was run through a G25 Sephadex column (GE healthcare, 11-0003-29) to separate the conjugated antibody-MAG3 complex from the free NHS-MAG3. The step-by-step protocol of chelating has been described in full detail by Wang, *et al.*, and the authors generously provided the chelator NHS-MAG3 [12]. The peak fractions were combined and stored at 4°C for radiolabeling experiment.

To label the antibody with Tc-99m, 600 μg of antiMBP antibody-MAG3 was mixed with 1 mL Tc-99m (200 mCi), 0.6 mL tartrate buffer, 0.2 mL fresh stannous chloride solution, and 1 mL 0.25 M ammonium acetate. The mixture was then applied on a G-25 desalting column (GE healthcare, 17-1408-1), and the radioactivity of the

fractions was measured using the calibrator available at the radiopharmacy facility. The maximum (highest) peak was then used for labeling monkey esophagi samples.

The binding affinity of radiolabeled antibody was also checked with a desalting column (see Figure E.1). With antibodies, a small second peak appeared in the activity measurements of eluted fractions, which means that the antibody was completely saturated with Tc-99m (peak at fraction 3) and the free Tc-99m eluted from the column at the second peak (fraction 11). As shown in Figure E.1, the peak in absorbance corresponds to the peak in radioactivity.

Plastic tubes (height: 4.8 cm, diameter: 0.4 cm, volume: 1.2 mL) were filled up with approximately 0.2 mg/mL MBP-1 solution (freshly prepared in 1X PBS) and was enclosed with parafilm and incubated overnight in a fridge at 4°C. A control sample was filled up with 1X PBS only. The following day, the samples were washed and incubated with peak fractions from the G-25 column (approximately 20 mCi ^{99m}Tc-antiMBP) for 3 hours. The samples were taken to Nuclear Medicine at University of Utah hospital and SPECT images were acquired. As shown in Figure E.2, the intensity of the treated sample is significantly higher than the control sample (not treated with MBP-1).

Although the binding of the ^{99m}Tc-antiMBP antibodies to the tissue is promising (see Figure E.2), there are several disadvantages of using the anti-MBP antibodies as the targeting candidate. First, the source of anti-MBP antibodies is very limited and expensive to reproduce. Second, numerous steps are needed to synthesize and purify the antibody and to use MAG3 as a chelating agent, leading to more complicated procedures than radiolabeling heparin. Third, the binding efficiency of the antibody is lower than of heparin due to the presence of free ^{99m}Tc.

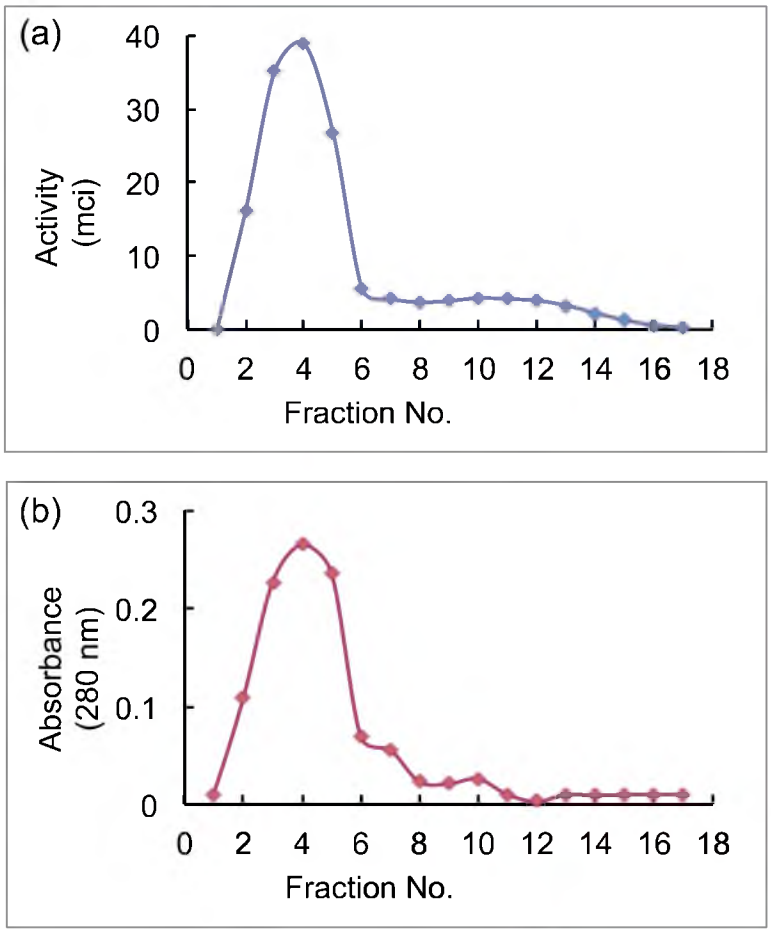

Figure E.1. Sample measurements. (a) Activity of ^{99m}Tc-antiMBP of fractions eluted from desalting column. (b) Absorbance at 280 nm for decayed ^{99m}Tc-antiMBP as a function of fractions eluted from column.

Figure E.2. SPECT image of plastic tube coated with and without MBP-1 (control), both incubated with ^{99m}Tc-antiMBP for an hour.

Polyanion Radiolabeling

To label the polyanions, the same procedure with heparin conjugation was used except that the heparin was substituted with polyanions (poly-glutamic acid and poly-aspartic acid). The repeatability of the labeling experiments was not achieved, because after mixing for 15 to 30 minutes with fresh (unfiltered) tin solution and adding the ^{99m}Tc, the solution precipitated and was no longer clear.

SAGE Polymer Radiolabeling

With SAGE polymers (semisynthetic glycosaminoglycan ethers, provided generously by Dr. Genn Prestwich at University of Utah), the solution started to precipitate after radiolabeling. Also, due to the limited access of SAGE polymers, and the availability of pharmaceutical grade heparin, further investigation on this particular polymer was not pursued.

Enoxaparin Radiolabeling

Enoxaparin is a low molecular weight heparin (5 kDa versus 15 – 30 kDa for the heparin explored elsewhere herein). Successful radiolabeling of enoxaparin was achieved and the labeling efficiency was the same as that of the higher molecular weight heparin indicated in Chapter 4. However, the binding affinity of enoxaparin to the eosinophil's granule proteins was lower than that of the higher molecular weight heparin